Rare B decays as a probe to beyond standard model physics

By

Rusa Mandal

PHYS10201204003

The Institute of Mathematical Sciences, Chennai

A thesis submitted to the

Board of Studies in Physical Sciences

In partial fulfillment of requirements

For the Degree of

DOCTOR OF PHILOSOPHY

of

HOMI BHABHA NATIONAL INSTITUTE

October, 2017

Homi Bhabha National Institute

Recommendations of the Viva Voce Board

As members of the Viva Voce Board, we certify that we have read the dissertation prepared by Rusa Mandal entitled " Rare B decays as a probe to beyond standard model physics" and recommend that it maybe accepted as fulfilling the dissertation requirement for the Degree of Doctor of Philosophy.

_____ Date:

Balachandran Sathiapalan (Chair)

_____ Date:

Rahul Sinha (Guide/Convener)

_____ Date:

Shrihari Gopalakrishnan

_____ Date:

D. Indumathi

_____ Date:

Purusattam Ray

_____ Date:

External Examiner

Final approval and acceptance of this dissertation is contingent upon the candidate's submission of the final copies of the dissertation to HBNI.

I hereby certify that I have read this dissertation prepared under my direction and recommend that it may be accepted as fulfilling the dissertation requirement.

Date:

Place: Guide

STATEMENT BY AUTHOR

This dissertation has been submitted in partial fulfillment of requirements for an advanced degree at Homi Bhabha National Institute (HBNI) and is deposited in the Library to be made available to borrowers under rules of the HBNI.

Brief quotations from this dissertation are allowable without special permission, provided that accurate acknowledgment of source is made. Requests for permission for extended quotation from or reproduction of this manuscript whole or in part may be granted by the Competent Authority of HBNI when in his or her judgment the proposed use of the material is in the interests of scholarship. In all other instances, however, permission must be obtained from the author.

Rusa Mandal

DECLARATION

I, hereby declare that the investigation presented in the thesis has been carried out by me. The work is original and has not been submitted earlier as a whole or in part for a degree / diploma at this or any other Institution / University.

Rusa Mandal

Dedicated to

My parents

It doesn't matter how beautiful your theory is, it doesn't matter how smart you are. If it doesn't agree with experiments, it's wrong. – Richard P. Feynman

ACKNOWLEDGMENTS

I would like to express my sincere gratitude to my advisor Prof. Rahul Sinha for valuable guidance, scholarly inputs, freedom for work and consistent encouragement I received throughout the research work. His deep insights on the subject phenomenology has enlightened me immensely. I am grateful for his encouragement to explore new topics and to present works at various national as well as international workshops/universities in my PhD life. I thank for the opportunity to work under the supervision of him, a person of amicable and positive disposition.

I would like to extend my gratitude to my collaborators Prof. Debajyoti Choudhury, Prof. Anirban Kundu and Prof. Thomas E. Browder for having the opportunity to work with you and getting in touch with your experienced and vast pool of knowledge. A sincere acknowledgment to Prof. Eung Jin Chun and Prof. Priyotosh Bandyopadhyay for helping me to learn completely new research subjects apart from my thesis work. The experience gained from these collaborative works has enlightened me to the broader prescriptive of High Energy Phenomenology. I thank Diganta for the nice collaboration in my first research paper. A very heartful thanks to my juniors as well as collaborators, Abinash and Anirban for always cherishing me with your amazing chats in last three years – no matter how simple/difficult the situation was!

I want to thank Prof. M. V. N. Murthy, Prof. Romesh Kaul, Prof. Ramesh Anishetty, Prof. Bala Sathiapalan, Prof. R. Shankar, Prof. Nemani Suryanarayana, Prof. Shrihari Gopalakrishna, Prof. Rajesh Ravindran for teaching me some wonderful courses. I also thank other members of my doctoral committee Prof. D. Indumathi, Prof. Purusattam Ray for the insightful suggestions and members of IMSc pheno group Prof. G. Rajasekaran, Prof. Nita Sinha and Prof. V. Ravindran for the discussions during weekly Pheno Lunch.

My sincere gratitude goes to past and current dean academic Prof. Ghanashyam Date and Prof. Sibasish Ghosh for being helpful in handling the HBNI official requirements. I am thankful to all my school teachers and university faculties for the inspiration to choose higher education, like PhD, in my career.

I also thank the research groups I have visited during my PhD – Institute Jožef Stefan, INFN Torino, University of Cincinnati, University of Kentucky, University of Illinois, Korea Institute for Advanced Study, Paul Scherrer Institute, University of Siegen where I had fruitful and enriching discussions.

It is my pleasure to thank all IMSc Official Staffs, Canteen Workers, Security Persons who have made such a comfortable and pleasant stay. A special regards to R. Indra, Vasan and Jahir for always providing immediate help.

I am thankful to the students and post-docs at IMSc: Abinash, Anirban, Aritra, Atanu, Dibyakrupa, Jahanur, Minati, Nirmalya, Pinaki, Prasanna, Rahul, Rajesh, Rana, Renjan, Ria, Sanjay, Soumya, Soumyadeep, Shibasis, Shilpa, Subhadeep, Taushif, Tanmay, Tanmoy, Tuhin and many others for the chance of discussing and learning physics.

Let me have the opportunity to thank the friends, with whom the life at IMSc has become so enjoyable, in a very short and incomplete list. The cooking at Thoraipakkam flats with energetic Subhadeep; gossiping and eating out in many different restaurants with enthusiastic Shilpa, Taushif, Rana, Pinaki, Jahanur; exploring best breakfast places at Chennai with Rajesh, Ramu and playing cricket, tennis with these people and other friends was really the amazing time of my life.

Finally I thank my parents for their continuous support and love throughout various phases of my life – *Baba* for being the best person to teach me, starting from Science to lessons on humanity, *Maa* for all her unconditional sacrifices, and my friend Pinaki for motivating me to pursue research and believing in me more than I do! Thank you all for always being there with me.

List of publications (included in this thesis)

1. **"Testing new physics effects in $B \to K^* \ell^+ \ell^-$"**

   Rusa Mandal, Rahul Sinha and Diganta Das

   Phys. Rev. D **90**, 096006 (2014)

   arXiv:1409.3088 [hep-ph]

2. **"Implications from $B \to K^* \ell^+ \ell^-$ observables using 3fb^{-1} of LHCb data"**

   Rusa Mandal and Rahul Sinha

   Phys. Rev. D **95**, 014026 (2017)

   arXiv:1506.04535 [hep-ph]

3. **"Minimal unified resolution to $R_{K^{(*)}}$ and $R(D^{(*)})$ anomalies with lepton mixing"**

   Debajyoti Choudhury, Anirban Kundu, Rusa Mandal and Rahul Sinha

   Phys. Rev. Lett. **119**, 151801 (2017)

   [arXiv:1706.08437 [hep-ph]]

List of publications (not included in this thesis)

1. **"Signal of right-handed currents using $B \to K^* \ell^+ \ell^-$ observables at the kinematic endpoint"**

   Anirban Karan, Rusa Mandal, Abinash kumar Nayak, Rahul Sinha and Thomas E. Browder

   Phys. Rev. D **95**, 114006 (2017)

   arXiv:1603.04355 [hep-ph]

2. **"Vacuum stability in extended standard model with leptoquark"**

   Priyotosh Bandyopadhyay and Rusa Mandal

   Phys. Rev. D **95**, 035007 (2017)

   arXiv:1609.03561 [hep-ph]

3. **"Implications of right-handed neutrinos in $B - L$ extended standard model with scalar dark matter"**

   Priyotosh Bandyopadhyay, Eung Jin Chun and Rusa Mandal

   Phys. Rev. D **97**, 015001 (2018)

   [arXiv:1707.00874 [hep-ph]]

4. **"Scalar dark matter in leptophilic two-higgs-doublet model"**

   Priyotosh Bandyopadhyay, Eung Jin Chun and Rusa Mandal

   Phys. Lett. B **779** (2018) 201-205

   [arXiv:1709.08581 [hep-ph]]

List of preprints (not included in this thesis)

1. **"$R_{K^{(*)}}$ and $R(D^{(*)})$ anomalies resolved with lepton mixing"**

   Debajyoti Choudhury, Anirban Kundu, Rusa Mandal and Rahul Sinha

   [arXiv:1712.01593 [hep-ph]]

2. **"Revisiting scalar leptoquark at the LHC"**

   Priyotosh Bandyopadhyay and Rusa Mandal

   [arXiv:1801.04253 [hep-ph]]

Seminars presented

1. **"Minimal unified resolution to B anomalies with lepton mixing"**, given at "SUSY 2017", Mumbai, India on December 12, 2017.

2. **"Minimal unified resolution to B anomalies with lepton mixing"**, given at "KIAS-KEK-NCTS joint workshop 2017", at "Korea Institute for Advanced Study", Seoul, South Korea on November 9, 2017.

3. **"Rare B decays and new physics"**, given at "University of Siegen,", Germany on September 13, 2017.

4. **"Rare B decays and new physics"**, given at "Paul Scherrer Institute, Villigen", Switzerland on September 7, 2017.

5. **"Right-handed currents in $B \to K^* \ell^+ \ell^-$"**, given at "Looking for BSM Physics" Bangalore, India on December 20, 2016.

6. **"Vacuum stability with leptoquark"**, given at "XXII DAE-BRNS High Energy Physics Symposium 2016" New Delhi, India on December 16, 2016.

7. **"Right-handed currents in $B \to K^* \ell^+ \ell^-$"**, given at "XXII DAE-BRNS High Energy Physics Symposium 2016" New Delhi, India on December 13, 2016.

8. **"Right-handed currents in $B \to K^* \ell^+ \ell^-$"**, given at "CKM Unitarity Triangle 2016", at "Tata Institute of Fundamental Research", Mumbai, India on November 28, 2016.

9. **"Vacuum stability with leptoquark"**, given at "Korea Institute for Advanced Study" Seoul, South Korea on November 3, 2016.

10. **"Signal of right-handed currents in the decay $B \to K^* \ell^+ \ell^-$"**, given at "KIAS-Durham-KEK-KIPMU joint workshop 2016", at "Korea Institute for Advanced Study" Seoul, South Korea on October 28, 2016.

11. **"Signal of right-handed currents in the decay $B \to K^* \ell^+ \ell^-$"**, given at "University of Illinois, Chicago", USA on August 26, 2016.

12. **"Signal of right-handed currents in the decay $B \to K^* \ell^+ \ell^-$"**, given at "University of Kentucky, Lexington", USA on August 25, 2016.

13. **"Signal of right-handed currents in the decay $B \to K^* \ell^+ \ell^-$"**, given at "University of Cincinnati", USA on August 23, 2016.

14. **"Implications from $B \to K^* \ell^+ \ell^-$ observables using 3fb^{-1} of LHCb data"**, given at "38th International Conference on High Energy Physics, Chicago", USA on August 6, 2016.

15. **"New physics searches for the decay $B \to K^* \ell^+ \ell^-$"**, given at Frontiers in High Energy Physics 2016 at "The Institute of Mathematical Sciences, Chennai" on March 22, 2016.

16. **"Theory status of the decay $B \to K^* \ell^+ \ell^-$"**, given via Skype at Workshop on High Energy Physics Phenomenology on December 9, 2015.

17. **"What can we learn from the decay $B \to K^* \ell^+ \ell^-$"**, given at " Istituto Nazionale di Fisica Nucleare Torino", Italy on July 2, 2015.

18. **"What can we learn from the decay $B \to K^* \ell^+ \ell^-$"**, given at "Institute Jožef Stefan", Slovenia on June 29, 2015.

19. **"Testing new physics effects in $B \to K^* \ell^+ \ell^-$"**, given at "XXI DAE-BRNS High Energy Physics Symposium 2014" at "Indian Institute of Technology, Guwahati" on December 11, 2014.

Conferences and workshops attended

1. **SUSY 2017**, held at Tata Institute of Fundamental Research, Mumbai, India from 11 – 15 December, 2017.

2. **KIAS-KEK-NCTS joint workshop 2017**, Korea Institute for Advanced Study, Seoul, South Korea from 6 – 10 November, 2017.

3. **CERN-Fermilab HCPSS 2017** held at CERN, Geneva, Switzerland from 28 August – 6 September, 2017.

4. **Looking for BSM Physics** held at Indian Institute of Science, Bangalore, India on from December 20 – 22, 2016.

5. **XXII DAE-BRNS High Energy Physics Symposium 2016** held at University of Delhi, New Delhi, India from December 12 – 16, 2016.

6. **CKM Unitarity Triangle 2016** , held at Tata Institute of Fundamental Research, Mumbai, India from November 28 – December 2, 2016.

7. **KIAS-Durham-KEK-KIPMU joint workshop 2016**, held at Korea Institute for Advanced Study, Seoul, South Korea from 24 – 28 October, 2016.

8. **11th Hadron Collider Physics Summer Schools** held at Fermi National Accelerator Laboratory, Batavia, USA from 11 – 20 August, 2016.

9. **38th International Conference on High Energy Physics, 2016** held at Chicago, USA from 3 – 10 August, 2016.

10. **Summer School on Particle Physics** held at International Centre for Theoretical Physics, Trieste Italy, from 15 – 26 June, 2015.

11. **XXI DAE-BRNS High Energy Physics Symposium 2014** held at Indian Institute of Technology, Guwahati from 8 – 12 December, 2014.

12. **Sangam @ HRI 2014: Instructional Workshop in Particle Physics** held at Harish-Chandra Research Institute, Allahabad, from 24 – 29 March 2014.

13. **XXVIII SERC Main School on Theoretical High Energy Physics** held at Indian Institute of Technology, Kanpur, between November 11 – 30, 2013.

14. **Frontiers of High Energy Physics IMSc Golden Jubilee Symposium** held at The Institute of Mathematical Sciences, Chennai between December 10 – 13, 2012.

ABSTRACT

The thesis predominantly deals with the rare decay $B \to K^* \ell^+ \ell^-$ where the full angular analysis of the final state gives rise to a multitude of observables. We show the most general parametric form of the amplitude in the standard model (SM) accounts almost all possible contributions within it, especially, the nonfactorizable contributions. The formalism results into a new relation involving all the CP conserving observables and is derived without any hadronic approximations within the SM. We use the formalism to extract the hadronic parameters which are involved in this decay mode from LHCb data. The values of form factors show significant discrepancies when compared with theoretical expectations and leads to a speculation of possible evidence of physics beyond the SM. The thesis also explains, in terms of a simple and compelling new physics scenario with only two new parameters, the discrepancies between the SM expectations and the data for the neutral-current observables $R_{K^{(*)}}$, as well as the charged-current observables $R(D^{(*)})$. While being consistent with all other data, this class of operators predicts some interesting signatures in the context of both B decays as well as high-energy collisions.

Contents

List of Figures

List of Tables

Synopsis

Motivation and Introduction

The standard model (SM) of particle physics is hugely recognized with the discovery of Higgs boson, the last remaining particle in the predicted list of the SM. However, there exist some clear indications that the SM is not complete: the phenomenon of neutrino oscillations, the evidence for dark matter and the matter-antimatter asymmetry cannot be explained within the framework of the SM. The SM is also affected by some theoretical issues even within the Higgs sector i.e., the instability of the Higgs vacuum and Higgs mass under quantum corrections. To extend the theory further, which can incorporate all observed phenomena, one of the most advantageous directions would be to discover new degrees of freedom at the collider experiments. However, in the absence of a direct evidence of beyond standard model (BSM) particle, we are standing in an era where new physics (NP) can show up as a tiny deviation from the predictions of the SM. In such a situation, the rare decay modes of mesons can play a very crucial role. As the SM amplitudes themselves are loop suppressed, these rare processes are very sensitive to the presence of heavy particles (if any) contributing to the modes at the tree level or via loop process and can provide indirect evidence of NP.

In this thesis we have studied the rare decay $B \to K^* \ell^+ \ell^-$. The rich angular analysis of this mode enables to obtain plethora of observables in various experiments like LHCb, Belle, *BABAR* and thus glorifies the mode as an important place to look for possible evidence of

NP. The theoretical estimates thus need to be extremely reliable in order to make a conclusive claim on the existence or non-existence of NP. In contrast of the works available in literature, where the comparison between the measurements of various observables like branching fraction, helicity fraction, asymmetry etc, with their theoretical prediction depends predominantly on the hadronic parameters, we adopt an approach having minimal dependency on these hadronic estimates. Relying on symmetry arguments like Lorentz symmetry, gauge symmetry and heavy quark symmetry we either parametrize or eliminate the hadronic parameters from our analysis. This leads to constrain and/or provide evidence of the BSM interactions in a complete model independent and reliable way.

Several hints of lepton non universality, observed in B meson decays, have intrigued the community as unlike the case for fully hadronic and semileptonic decay modes that suffer from large strong interaction corrections, the theoretical uncertainties in these observables cancel out in the SM. We address such deviations in terms of effective operators with minimal parameters. The thesis is organized as following chapters.

The rare mode $B \to K^* \ell^+ \ell^-$

The decay $B \to K^* \ell^+ \ell^-$ provides plethora of observables which are obtained by studying the full angular distribution [1]. In this section we briefly discuss the theoretical framework derived to take into account almost all possible contributions within the SM. We start with the observables to be the F_L, $F_\perp$, A_4, A_5, $A_{\rm FB}$, A_7, A_8, A_9 and $d\Gamma/dq^2 \equiv \Gamma_f$. The observables $F_\perp$, A_4, A_5, $A_{\rm FB}$, A_7, A_8 and A_9 are related to the CP averaged observables S_3, S_4, S_5, $A_{\rm FB}^{\rm LHCb}$, S_7, S_8 and S_9 measured by LHCb [2] as

$$F_\perp = \frac{1 - F_L + 2S_3}{2},\ A_4 = -\frac{2}{\pi} S_4,\ A_5 = \frac{3}{4} S_5,\ A_{\rm FB} = -A_{\rm FB}^{\rm LHCb},$$
$$A_7 = \frac{3}{4} S_7,\ A_8 = -\frac{2}{\pi} S_8,\ A_9 = \frac{3}{2\pi} S_9. \qquad (0.0.1)$$

In the massless lepton limit the decay is described in terms of six transversity amplitudes which can be written as,

$$\mathcal{A}_\lambda^{L,R} = C_{L,R}^\lambda \mathcal{F}_\lambda - \widetilde{\mathcal{G}}_\lambda = (\widetilde{C}_9^\lambda \mp C_{10})\mathcal{F}_\lambda - \widetilde{\mathcal{G}}_\lambda. \tag{0.0.2}$$

This form of the amplitude is the most general parametric form of the SM amplitude for $B \to K^* \ell^+ \ell^-$ decay that comprehensively takes into account all contributions up to $\mathcal{O}(G_F)$ within it. The form includes all short-distance and long-distance effects, factorizable and non-factorizable contributions and resonance contributions. In Eq. (0.0.2), C_9 and C_{10} are Wilson coefficients with $\widetilde{C}_9^\lambda$ being the redefined "effective" Wilson coefficient defined such that

$$\widetilde{C}_9^\lambda = C_9 + \Delta C_9^{(\text{fac})}(q^2) + \Delta C_9^{\lambda,(\text{non-fac})}(q^2) \tag{0.0.3}$$

where $\Delta C_9^{(\text{fac})}(q^2)$, $\Delta C_9^{\lambda,(\text{non-fac})}(q^2)$ correspond to factorizable and soft gluon non-factorizable contributions [3,4]. Strong interaction effects coming from electromagnetic corrections to hadronic operators do not affect C_{10}. $\mathcal{F}_\lambda$ and $\widetilde{\mathcal{G}}_\lambda$ are q^2 dependent form factors for $B \to K^*$ transition.

Model independent relation among observables

In order to disentangle the NP effect, one needs clean tests of the SM. Starting with the gauge structure of the SM, in this section we derive a relation among observables, which provides a consistency check for the data, having minimal dependency on hadronic uncertainties. We introduce two variables r_λ and ε_λ which contain real and imaginary contributions of the amplitude (Eq. (0.0.2)) respectively [5],

$$r_\lambda \equiv \frac{\text{Re}(\widetilde{\mathcal{G}}_\lambda)}{\mathcal{F}_\lambda} - \text{Re}(\widetilde{C}_9^\lambda) \quad \text{and} \quad \varepsilon_\lambda \equiv \text{Im}(\widetilde{C}_9^\lambda)\mathcal{F}_\lambda - \text{Im}(\widetilde{\mathcal{G}}_\lambda). \tag{0.0.4}$$

This leads to a simplification in the algebra of a set of nine equations with nine observables expressed in terms of ten parameters (three for each r_λ, $\mathcal{F}_\lambda$ and ε_λ and one for C_{10}) and interestingly allows us to eliminate almost all of them giving a non-trivial relation among the observables shown in Eq. (0.0.5). The relation is valid for the entire q^2 region and is derived by restricting ourselves to rely only on one hadronic input. The dependency on this hadronic parameter P_1 enters through the iterative solutions of ε_λ's [5] which are proportional to the observables A_7, A_8 and A_9.

$$A_4 = \frac{2\sqrt{2}\,\varepsilon_\parallel \varepsilon_0}{\pi \Gamma_f} + \frac{8 A_5 A_{\rm FB}}{9\pi\left(F_\perp - \frac{2\varepsilon_\perp^2}{\Gamma_f}\right)} + \sqrt{2}\,\frac{\sqrt{\left(F_L - \frac{2\varepsilon_0^2}{\Gamma_f}\right)\left(F_\perp - \frac{2\varepsilon_\perp^2}{\Gamma_f}\right) - \frac{8}{9}A_5^2}\;\sqrt{\left(F_\parallel - \frac{2\varepsilon_\parallel^2}{\Gamma_f}\right)\left(F_\perp - \frac{2\varepsilon_\perp^2}{\Gamma_f}\right) - \frac{4}{9}A_{\rm FB}^2}}{\pi\left(F_\perp - \frac{2\varepsilon_\perp^2}{\Gamma_f}\right)}. \quad (0.0.5)$$

The form-factor ratio P_1 is unaltered by higher order QCD corrections (in α_s) [4] and can be evaluated in terms of meson masses given by,

$$\mathsf{P}_1 = \frac{\mathcal{F}_\perp}{\mathcal{F}_\parallel} = -\frac{\sqrt{\lambda(m_B^2, m_{K^*}^2, q^2)}}{(m_B^2 + m_{K^*}^2 - q^2)} \qquad \text{in leading } 1/m_B \text{ expansion.}$$

Thus it can be considered as a reliable theoretical input in the relation (0.0.5) which takes into account almost all possible effects within the SM such as factorizable and non-factorizable contributions, resonance effects etc and hence provides a smoking gun signal to NP.

Incorporation of lepton mass effect is shown in Ref. [5], however in the absence of the measurements of angular observables A_{10} and A_{11}, dependency of the relation among observables on hadronic estimates increases in this limit.

Hadronic parameter extraction and right-handed currents

The theoretical estimates of the semileptonic mode $B \to K^*\ell^+\ell^-$ need to be extremely reliable in order to make a conclusive claim on the existence or non-existence of NP. In this section we show how some of the parameters can be extracted directly from LHCb measurements allowing us to verify our theoretical understanding. The amplitude given in Eq. (0.0.2) is used to express the observables $F_\perp$, F_L, $A_{\rm FB}$, A_5 and A_4 as [6]

$$F_\perp = u_\perp^2 + 2\zeta,\ F_L\mathsf{P}_2^2 = u_0^2 + 2\zeta,\ A_{\rm FB}^2 = \frac{9\zeta}{2\mathsf{P}_1^2}(u_\parallel \pm u_\perp)^2,$$
$$A_5^2 = \frac{9\zeta}{4\mathsf{P}_2^2}(u_0 \pm u_\perp)^2,\ A_4 = \frac{\sqrt{2}}{\pi\mathsf{P}_1\mathsf{P}_2}(2\zeta \pm u_0 u_\parallel). \tag{0.0.6}$$

$$\text{where, } \mathsf{P}_1 = \frac{\mathcal{F}_\perp}{\mathcal{F}_\parallel},\quad \mathsf{P}_2 = \frac{\mathcal{F}_\perp}{\mathcal{F}_0},\quad \zeta = \frac{\mathcal{F}_\perp^2 C_{10}^2}{\Gamma_f},\quad u_\lambda^2 = \frac{2}{\Gamma_f}\frac{\mathcal{F}_\perp^2}{\mathcal{F}_\lambda^2}\Big(\mathrm{Re}(\widetilde{\mathcal{G}}_\lambda) - \mathrm{Re}(\widetilde{C}_9^\lambda)\mathcal{F}_\lambda\Big)^2. \tag{0.0.7}$$

We find the solutions for five independent hadronic parameters P_1, P_2, ζ, u_0 and $u_\perp$ from the above mentioned five set of equations of observables using 3fb^{-1} of LHCb data [2]. The allowed region for the solution in P_1–P_2 plane for $q^2 \in [6, 8]\,\text{GeV}^2$ is shown in the left panel of Fig. 1. Similar regions for all eight bins in q^2 and also in different planes of variables are extensively studied in Ref. [6]. It should be noted that the contribution arising from charmonium resonances can be parametrized in Wilson coefficient C_9 [7] and as by definition the parameters P_1, P_2 are independent of $\widetilde{C}_9^\lambda$, imply their solutions are also independent of resonance contributions. Hence any discrepancy observed in P_1–P_2 plane can not be accounted by resonance effects. With the obtained solutions for P_1, P_2, ζ and using measured branching fraction Γ_f, the form factors $\mathcal{F}_\lambda$ can be extracted which are related to the well known form factors V, A_1 and A_{12} [8]. The extracted values are given in right panel of Fig. 1 and discrepancies can be seen in several q^2 bins in comparison

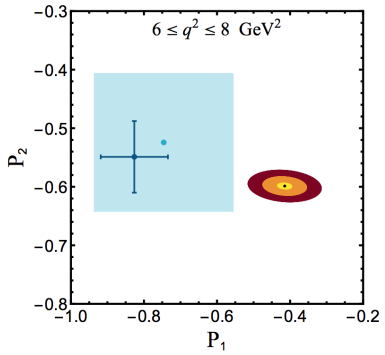

q^2 [GeV^2]	$V(q^2)$	$A_1(q^2)$	$A_{12}(q^2)$
[0.1, 0.98]	0.677 ± 0.092	0.570 ± 0.077	0.246 ± 0.034
	(3.05σ)	(3.40σ)	(0.88σ)
[1.1, 2.5]	0.625 ± 0.071	0.409 ± 0.046	0.326 ± 0.047
	(2.78σ)	(2.00σ)	(0.69σ)
[6.0, 8.0]	0.485 ± 0.045	0.598 ± 0.073	0.252 ± 0.025
	(1.27σ)	(3.18σ)	(1.78σ)
[11.0, 12.5]	0.166 ± 0.018	0.560 ± 0.065	0.450 ± 0.054
	(5.64σ)	(1.76σ)	(1.81σ)
[15.0, 17.0]	0.828 ± 0.120	0.649 ± 0.098	0.496 ± 0.074
	(2.79σ)	(1.38σ)	(1.51σ)

Figure 1. (left panel) The solutions obtained using LHCb data in P_1–P_2 plane where the yellow, orange and red regions denote 1σ, 3σ, and 5σ confidence level regions for $q^2 \in [6, 8]\,\text{GeV}^2$, respectively. The blue error bar is the prediction from LCSR calculations [8]. The light blue bands denote exact solutions for the SM observables including charmonium resonances from Ref. [7] parametrization. (right panel) The mean and $\pm 1\sigma$ errors (upper line) for the LHCb data extracted values of form factors V, A_1, A_{12} and the deviation in confidence level (lower line) with their theoretical estimates are highlighted for some q^2 bins where the discrepancies are significant.

with the estimate of light-cone-sum rule (LCSR) [8] and lattice results [9].

Another interesting result leads us to determine the nature of the possible signal of NP observed above. At low recoil energy of K^* meson, only three independent form factors describe the entire $B \to K^* \ell^+ \ell^-$ decay and there exist a relation among the form factors at leading order in $1/m_B$ expansion in a modified heavy quark effective theory framework given by [10, 11],

$$\frac{\widetilde{\mathcal{G}}_\parallel}{\mathcal{F}_\parallel} = \frac{\widetilde{\mathcal{G}}_\perp}{\mathcal{F}_\perp} = \frac{\widetilde{\mathcal{G}}_0}{\mathcal{F}_0} = -\kappa \frac{2 m_b m_B C_7}{q^2}, \tag{0.0.8}$$

where $\kappa \approx 1$. Therefore from Eq. (0.0.7), one finds $u_0 = u_\parallel = u_\perp$ must hold as long as non-factorizable charm loop contributions are negligible. We find that this relation does not hold for either of the bins $q^2 \in [15, 17]\,\text{GeV}^2$ or $q^2 \in [17, 19]\,\text{GeV}^2$ as listed in Table 5.2. The variable $u_\parallel$ is not independent due to the constraint that helicity fractions add up to one.

The mentioned relation is exact at a special point in the q^2 i.e., the kinematic endpoint q^2_{max}. The heavy quark symmetry breaking corrections are negligible and the non-factorizable

q^2 [GeV^2]	u_0	$u_\perp$
[15, 17]	0.000 ± 0.016	0.367 ± 0.025
[17, 19]	0.166 ± 0.014	0.260 ± 0.048
[15, 19]	0.120 ± 0.007	0.244 ± 0.026

Table 1. The values of u_0 and $u_\perp$ obtained from fit to 3 fb^{-1} of LHCb data [2].

contributions are polarization independent at $q^2_{\rm max}$. Interestingly, we find that an alternation in the relation is possible in presence of right-handed (RH) current operators O'_9 and O'_{10} [12]. With respective couplings C'_9 and C'_{10}, the amplitudes modify as

$$\begin{aligned}\mathcal{A}_\perp^{L,R} &= ((\widetilde{C}_9^\perp + C'_9) \mp (C_{10} + C'_{10}))\mathcal{F}_\perp - \widetilde{\mathcal{G}}_\perp,\\ \mathcal{A}_{\parallel,0}^{L,R} &= ((\widetilde{C}_9^{\parallel,0} - C'_9) \mp (C_{10} - C'_{10}))\mathcal{F}_{\parallel,0} - \widetilde{\mathcal{G}}_{\parallel,0}\,.\end{aligned} \tag{0.0.9}$$

Due to difference in contributions for different helicities, in the presence of RH currents one expects $u_0 = u_\parallel \neq u_\perp$ at $q^2 = q^2_{\rm max}$ without any approximation. To test the relation among u_λ's in light of LHCb data, we expand the observables F_L, $F_\perp$, $A_{\rm FB}$ and A_5 around $q^2_{\rm max}$ assuming a polynomial form. The details are given in Ref. [12] and is beyond the scope of this thesis. The zeroth order coefficients of the observable expansions are assumed from the constraints arising from Lorentz invariance and decay kinematics derived in Ref. [13], whereas all the higher order coefficients are extracted by fitting the polynomials with 14 bin LHCb data. The limiting analytic expressions for $u_\lambda/\sqrt{2\zeta}$ at $q^2 = q^2_{\rm max}$, which have explicit dependence on the RH couplings C'_9 and C'_{10}, are evaluated completely from data. This enables us to predict the allowed region in $C'_{10}/C_{10} - C'_9/C_{10}$ plane as shown in Fig. 2. The SM prediction (the origin) remains on a 3σ significance level contour providing evidence of RH currents.

Lepton flavor non-universality

The intriguing discrepancies between the SM expectations and the data for the neutral-current observables R_K [14] and R_{K^*} [15], as well as the charged-current observables $R(D)$

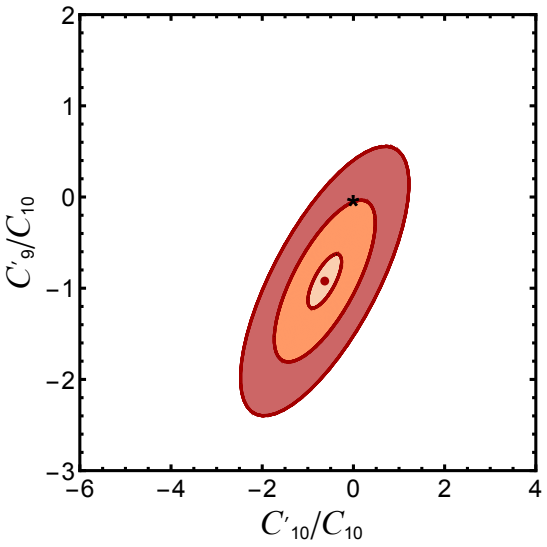

Figure 2. In $C'_{10}/C_{10} - C'_9/C_{10}$ plane, the yellow, orange and red regions correspond to 1σ, 3σ and 5σ significance level, respectively. The only one SM input r/C_{10} is varied as a nuisance parameter. The SM predictions is indicated by the stars. Strong evidence of RH current is pronounced from the plot.

and $R(D^*)$ [16] have drawn great attentions. In this chapter we show that an simultaneous explanation can be achieved in an effective theory with only two unknown parameters. We propose a model involving two four-fermi operators in terms of the second and third generation (weak-eigenstate) fields [17]

$$\mathcal{H}^{\rm NP} = A_1\,(\bar{Q}_{2L}\gamma_\mu L_{3L})\,(\bar{L}_{3L}\gamma^\mu Q_{3L}) + A_2\,(\bar{Q}_{2L}\gamma_\mu Q_{3L})\,(\bar{\tau}_R\gamma^\mu \tau_R), \tag{0.0.10}$$

where we demand $A_2 = A_1$. This operator contributes to $R(D^{(*)})$ however the contribution to $R_{K^{(*)}}$ can be generated by the simplest of field rotations for the left-handed leptons from the unprimed (flavor) to the primed (mass) basis, namely

$$\tau = \cos\theta\,\tau' + \sin\theta\,\mu'\,, \qquad \nu_\tau = \cos\theta\,\nu'_\tau + \sin\theta\,\nu'_\mu\,. \tag{0.0.11}$$

A chi-square fit to observables $R(D)$, $R(D^*)$, R_K, $R^{\rm low}_{K^*}$, $R^{\rm cntr}_{K^*}$, $d{\rm BR}(B_s \to \phi\mu\mu)/dm^2_{\mu\mu}$ (in the bin $m^2_{\mu\mu} \in [1:6]\,{\rm GeV}^2$) with best fit points $A_1(=A_2) = -2.92\,{\rm TeV}^{-2}$, $\sin\theta = \pm 0.022$ provides a reasonable explanation to all observables except for $R^{\rm low}_{K^*}$, while being consistent with all data. We illustrate, in Fig. 3, that allowing a 20% breaking of the relation as given by $A_2 = 4A_1/5$, the fit can be improved remarkably. The origin of this split between the A_i can be attributed as the difference to the quantum numbers of the leptonic fields un-

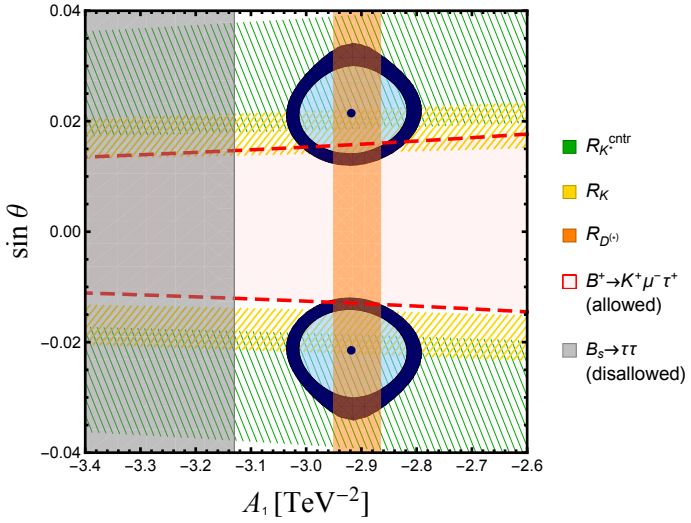

Figure 3. The fit for $A_2 = 4A_1/5$, with the bands around the best-fit points corresponding to 95% and 99% C.L. Also shown are the 1σ bands from $R_{K^{(*)}}$ and $R(D)$, and the 95% upper limits from $B_s \to \tau\tau$ and $B^+ \to K^+\mu^-\tau^+$.

der an as yet unidentified gauge symmetry, with the attendant anomaly cancellation being effected by either invoking heavier fermionic fields or through other means.

Conclusions and outlook

In this thesis we have studied rare semileptonic decays of B meson where the effect of physics beyond the SM can be predominant. In particular, we focus on the flavor changing neutral current decay $B \to K^*\ell^+\ell^-$ where using the four-body angular analysis, plethora of observables are measured in experiments. We have developed a formalism to incorporate almost all possible effects within the SM. The approach adopted in our work differs from the other approaches in literature in terms of minimal dependency on hadronic uncertainties.

Discrepancies are found in form-factor values of $B \to K^*$ transition extracted form data, compared to their theoretical estimates. Our study includes complex contributions of the amplitudes and systematics have also been added for bin-bias. We have argued that presence of $c\bar{c}$ resonances can not affect two specific hadronic parameters, where deviations have been seen, by construction. The interesting behavior of variables u_λ at low recoil energy of the K^* meson provides important consequences to identify the possible presence

of NP interactions. In a later study it leads to provide strong evidence of RH currents derived at endpoint limit. The conclusions are drawn using heavy quark symmetry which are reliable at this kinematic endpoint.

We also address the minimal modification to the SM in terms of an effective theory that can explain the anomalies seen in charged as well as neutral current decays of B mesons. Taking all the data into account, we find that with just two new parameters, the χ^2/d.o.f. can be reduced from 7 (in the SM) to below 3 while being consistent with all other data. In addition, this class of models predicts some interesting signatures both in the context of B decays as well as high-energy collisions.

There are several directions that one can make progress in the context of rare B decays. It will be interesting to implement the similar approach in other semileptonic decay processes as well, where the hints of BSM interactions seen in this work and/or other kinds of NP interactions can also be investigated. In view of enormous amount of collecting data, if the discussed discrepancies observed in experiments are established, our studies will help the reconstruction of high-scale physics, underlying the aforementioned anomalies, as ultraviolet completions of the identified four-fermion operators.

1 Prologue

The standard model (SM) of particle physics is completed with the discovery of Higgs boson, the last remaining particle. However, there exist some clear indications that the framework of the SM is not complete: the phenomenon of neutrino oscillations, the evidence for dark matter and the matter-antimatter asymmetry cannot be explained. The SM is also affected by some theoretical issues even within the Higgs sector i.e., the instability of the Higgs vacuum and Higgs mass under quantum corrections. To extend the theory further and incorporate all observed phenomena, one of the most advantageous way would be to discover new particles at the collider experiments. However, in the absence of a direct evidence of beyond standard model (BSM) particle, during the last 10 years of search, we are standing in an era where new physics (NP) can show up as a tiny deviation from the prediction of the SM. In such a situation, the rare decay modes of hadrons can play a very crucial role. As the SM amplitudes themselves are loop suppressed, these rare processes are very sensitive to the presence of new heavy particles (if any) contributing to the modes at the tree level or via loop process and can provide indirect evidence of NP.

History also endorses the importance of loop suppressed rare decays. It is known now, that, in the SM there are six quarks, which are grouped into three families or flavors. All six quarks have been identified with experimental observations. However, much before the discovery of the 2nd up-type quark i.e, c quark, its existence was hinted from the experimental observation of tiny ratio $\mathrm{Br}(K_L \to \mu^+\mu^-)/\mathrm{Br}(K^+ \to \mu^+\bar{\nu_\mu}) \sim 10^{-9}$. The suppression arises in these flavor changing neutral current (FCNC) processes due to the

fact that the contributions of the c quark and the u quark almost cancel each other and is known as Glashow, Iliopolus, Maiani (GIM) mechanism.

Currently very intensive research work is concentrated on studies of the rare decays of hadrons from both theoretical and experimental sides. At LHC, the LHCb collaboration is aimed at analyzing various decays of b- and c- hadrons. The powerful B factory Belle and it's future extension Belle-2 are dedicated to study the properties and behavior of the B and D mesons within small uncertainties.

The decays of hadrons are studied in an effective theory approach at an energy scale of the mass of the b quark. The effect of all the heavy degrees of freedoms are encoded in the Wilson coefficients which depend on the cut off scale of the theory. In the works available in literature, the comparison between the measurements of various observables like branching fraction, helicity fraction, asymmetry etc, with their theoretical prediction depends predominantly on the hadronic parameters. Thus using results from the mentioned experiments, in order to confirm/falsify the presence of BSM physics the accurate knowledge of hadronic inputs are crucial.

In this thesis, we study some specific rare decay modes of B mesons which are sensitive to NP effects. The thesis is divided into two parts where the first part is devoted to extensively investigate the semileptonic decay mode $B \to K^* \ell^+ \ell^-$. In the last part we combine several other decays to explain the anomalies observed in both neutral current and charged current transitions of B meson hinting towards lepton non-universality.

With a very brief introduction to the topic flavor physics in chapter 2, we discuss the current and upcoming upgrades of the experiments. We start in chapter 3 aiming to present an example of a formalism with minimal dependency on hadronic parameters for the decay $B \to K^* \ell^+ \ell^-$. The decay $B \to K^* \ell^+ \ell^-$ provides plethora of observables which are obtained by studying the full angular distribution [1]. These CP averaged observables are the well known helicity fractions: F_L, $F_\perp$, the asymmetries, constructed out of the real part of the amplitude: A_4, A_5, $A_{\rm FB}$, the asymmetries dealing with the imaginary part of

the amplitude A_7, A_8, A_9 and the differential decay rate $d\Gamma/dq^2$ where q^2 is the dilepton invariant mass square.

We demonstrate how the nonfactorizable contributions, arising from soft gluon emission of the charm loop, can be parametrically included in the amplitude for this mode. In the effective theory at an energy scale of the b quark mass, the c quarks are dynamical degrees of freedom and the effect of nonfactorizable contributions can be cast in terms of non local operators. Using the methods developed in Ref. [3], we parametrize the effect of nonfactorizable contributions based on Lorentz symmetry and gauge symmetry. As a consequence, this allows us to write the most general parametric form of the SM amplitude for $B \to K^* \ell^+ \ell^-$ decay that comprehensively takes into account all contributions up to $O(G_F)$ within it. The form includes all short-distance and long-distance effects, factorizable and non-factorizable contributions and resonance contributions.

In chapter 4, using the general form of the amplitude we derive a relation among all nine CP averaged observables in a complete model independent way. It involves only one hadronic parameter and relates all the observables. The derivation is based on the SM gauge structure and incorporates finite lepton and quark masses, complex amplitudes enabling resonance contributions to be included, electromagnetic correction to hadronic operators at all orders and all factorizable and nonfactorizable contributions to the decay. The breakdown of the relation with the measurements of observables by LHCb will provide a smoking gun signal of NP. It is interesting to note that the relation remains valid except in the presence of NP operators that result in modified angular distribution. Hence we do not expect to see the discrepancy in presence of right-handed (RH) currents or extra vector current contributing to the decay.

We study the behavior of LHCb data for this particular mode $B \to K^* \ell^+ \ell^-$ in chapter 5 in a different way than the one discussed above. Since the theoretical estimates of the mode need to be extremely reliable in order to make a conclusive claim on the existence or non-existence of NP, we show how some of the hadronic parameters can be extracted

directly from LHCb measurements allowing us to verify our theoretical understanding. Using the general form of the amplitude we express five observables $F_\perp$, F_L, $A_{\rm FB}$, A_5, A_4 in terms of five independent hadronic parameters P_1, P_2, ζ, u_0, $u_\perp$ and find the solutions for the parameters for 3fb^{-1} of LHCb data [2]. With the obtained solutions for P_1, P_2, ζ and using measured branching fraction, the well known form factors V, A_1 and A_{12} [8] are extracted which show discrepancies in certain q^2 region while compared to the estimates available from light-cone sum-rule (LCSR) calculations and lattice results.

Another interesting observation at the very high q^2 region yields important consequences to identify the possible evidence of a NP scenario. It is shown in Refs. [10, 11] that at low recoil energy of K^* meson, only three independent form factors describe the entire $B \to K^*\ell^+\ell^-$ decay and there exist a relation among the form factors at leading order in $1/m_B$ expansion in a modified heavy quark effective theory (HQET) framework. We find as a consequence of this relation, the parameters u_λ's should be equal namely $u_0 = u_\parallel = u_\perp$. However, the extracted values of u_λ from the data fail to obey the constraint. We further observe that the relation among u_λ's is exact at a special point in the q^2 i.e., the kinematic endpoint $q^2_{\rm max}$. The heavy quark symmetry breaking corrections are negligible and the non-factorizable contributions are polarization independent at $q^2_{\rm max}$. An alternation in the relation is only possible in presence of RH current operators. Due to difference in contributions for different helicities, in the presence of RH currents one expects $u_0 = u_\parallel \neq u_\perp$ at $q^2 = q^2_{\rm max}$ without any approximation. To test the relation among u_λ's in light of LHCb data, we expand the observables F_L, $F_\perp$, $A_{\rm FB}$ and A_5 around $q^2_{\rm max}$ assuming a polynomial form. The details of the derivation is beyond the scope of this thesis. The limiting analytic expressions for $u_\lambda/\sqrt{2\zeta}$ at $q^2 = q^2_{\rm max}$, which are evaluated completely from data enable us to predict the allowed region in the RH coupling plane. We find the SM prediction remains on a 3σ significance level contour providing a strong evidence of RH currents.

In chapter 6 we investigate the intriguing discrepancies between the SM expectations and

the data for the neutral-current observables R_K [14] and R_{K^*} [15], as well as the charged-current observables $R(D)$ and $R(D^*)$ [16] which have drawn a lot of attention. These observables are constructed out of the ratios given as for the neutral current sector

$$R_{K^{(*)}} \equiv \frac{\mathrm{BR}(B \to K^{(*)}\mu^+\mu^-)}{\mathrm{BR}(B \to K^{(*)}e^+e^-)},$$

and an analogous ratio for the charged-current sector

$$R(D^{(*)}) \equiv \frac{\mathrm{BR}(B \to D^{(*)}\tau\nu)}{\mathrm{BR}(B \to D^{(*)}\ell\nu)},$$

with $\ell = e$ or μ, and thus the hadronic uncertainties cancel out to a large extent.

Several measurements of $R(D)$ and $R(D^*)$ by the *BABAR* [18], Belle [19,20], and LHCb [21] collaborations indicated an upward deviation from the SM expectations. Combining the individual results, the discrepancies are at $\sim 2.3\sigma$ and $\sim 3.4\sigma$ respectively. On inclusion of the correlation between the data, the combined significance is at $\sim 4.1\sigma$ level from the SM predictions [16]. The data on R_K and R_{K^*}, on the other hand, lie systematically below the SM expectations corresponding to 2.6σ, $\sim 2\sigma$ shortfalls from the SM expectations.

In an effective theory approach we provide a possible and simultaneous explanation to all the four anomalies $R_{K^{(*)}}$, $R(D^{(*)})$ in terms of minimal set of NP operators. We present a simple phenomenological model with just two parameters which explains all the anomalies while being consistent with all other data. We also identify complementary measurements at currently operating experiments that will not only serve to confirm/falsify our explanation, but hint to a deeper understanding of the underlying dynamics.

In chapter 7 we summarize the main results of the thesis and also discuss about some future research directions. Appendices include some computational details and results to make the thesis self-contained.

2 A brief introduction to flavor physics

The term 'flavor' is used in particle physics to represent several copies of same quantity say, fields which are assigned same quantum numbers under certain gauge representations. In this chapter we give a very brief introduction to the topic flavor physics, especially the quark flavor sector. For detailed and involved reviews Refs. [22–26] can be useful.

Not only is the Universe stranger than we think, it is stranger than we can think - Werner Heisenberg

2.1 Flavor in the standard model

The most successful model describing almost all the phenomena in nature is the standard model of particle physics. The three main ingredients in constructing the Lagrangian for the SM are following.

• The gauge group: $\mathcal{G}_{\rm SM} = SU(3)_c \times SU(2)_L \times U(1)_Y$

• The representations of the fields under this $\mathcal{G}_{\rm SM}$ gauge group:

Matter	Flavor	$\mathcal{G}_{\rm SM}$
$Q_\alpha \equiv \begin{pmatrix} u_{L\alpha} \\ d_{L\alpha} \end{pmatrix}$	$\begin{pmatrix} u_L \\ d_L \end{pmatrix}, \begin{pmatrix} c_L \\ s_L \end{pmatrix}, \begin{pmatrix} t_L \\ b_L \end{pmatrix},$	$(\mathbf{3}, \mathbf{2}, 1/6)$
$u_{R\alpha}$	$u_R,\ c_R,\ t_R$	$(\mathbf{3}, \mathbf{1}, 2/3)$
$d_{R\alpha}$	$d_R,\ s_R,\ b_R$	$(\mathbf{3}, \mathbf{1}, -1/3)$
$L_\alpha \equiv \begin{pmatrix} \nu_{L\alpha} \\ \ell_{L\alpha} \end{pmatrix}$	$\begin{pmatrix} \nu_{eL} \\ e_L \end{pmatrix}, \begin{pmatrix} \nu_{\mu L} \\ \mu_L \end{pmatrix}, \begin{pmatrix} \nu_{\tau L} \\ \tau_L \end{pmatrix},$	$(\mathbf{1}, \mathbf{2}, -1/2)$
$e_{R\alpha}$	$e_R,\ \mu_R,\ \tau_R$	$(\mathbf{1}, \mathbf{1}, -1)$
$\Phi \equiv \begin{pmatrix} \phi^+ \\ \phi^0 \end{pmatrix}$	–	$(\mathbf{1}, \mathbf{2}, 1/2)$

Gauge fields	Force
G^a_μ	Strong
$W^\pm_\mu,\ Z^0_\mu$	Weak
A_μ	Electromagnetic

Table 2.1. The SM particle content, symmetry representations and forces.

The fermion fields Q_α and L_α are left-handed quark and lepton doublets whereas the $u_{R\alpha}$ ($d_{R\alpha}$) and $e_{R\alpha}$ are right-handed up-type (down-type) quark and lepton doublets, respectively. The only scalar doublet Φ, in the theory, is the SM Higgs doublet. The mediators for strong, weak and electromagnic interactions are the G^a_μ, $W^\pm_\mu$, Z^0_μ and A_μ gauge bosons, respectively.

• The pattern of spontaneous symmetry breaking: The EW symmetry is spontaneously broken to the electromagnetic one i.e., $SU(2)_L \times U(1)_Y \Longrightarrow U(1)_Q$ through the non zero

vacuum expectation value (vev) of the Higgs field.

The most general renormalizable Lagrangian for the SM can be written as

$$\mathcal{L}_{\rm SM} = \mathcal{L}_{\rm kin} + \mathcal{L}_{\rm Higgs} + \mathcal{L}_{\rm Yukawa}. \tag{2.1.1}$$

The kinetic part $\mathcal{L}_{\rm kin}$ includes self interaction of Non-abelian gauge fields and also the gauge interaction of matter through the covariant derivative expressed in terms of the physical gauge bosons

$$\mathcal{D}_\mu = \partial_\mu - ig_s G^a_\mu \frac{\lambda_a}{2} - ig\left(W^+_\mu T_+ + W^-_\mu T_-\right) - ieA_\mu\, q - \frac{ig}{c_W} Z^0_\mu \left(T_3 - s^2_W\, q\right). \tag{2.1.2}$$

Here $T_\pm$ are the combinations of $SU(2)_L$ generators in doublet representation and T_3 being the diagonal one. The electric charge q is a linear combination of weak hypercharge Y and T_3 given by $q = Y + T_3$.

The Higgs part $\mathcal{L}_{\rm Higgs}$, responsible for the EW symmetry breaking, is given by

$$\mathcal{L}_{\rm Higgs} = \mu^2|\Phi|^2 - \lambda|\Phi|^4. \tag{2.1.3}$$

The Yukawa part of the Lagrangian $\mathcal{L}_{\rm Yukawa}$ contains

$$\mathcal{L}_{\rm Yukawa} = y^e_{ij}\, \bar{L}^i \Phi\, e^j_R + y^d_{ij}\, \bar{Q}^i\, \Phi\, d^j_R + y^u_{ij}\, \bar{Q}^i\, \widetilde{\Phi}\, u^j_R + \text{ h.c} \tag{2.1.4}$$

where $\widetilde{\Phi} = \epsilon_{ab}\Phi^*$ the conjugate Higgs field.

In the absence of the Yukawa interactions i.e., $y^{e,d,u}_{ij} = 0$, The SM Lagrangian has a larger global symmetry. The Lagrangian remains invariant under the unitary rotation of the fields

$$Q \to U_Q\, Q\,, \quad u_R \to U_u\, u_R, \quad d_R \to U_d\, d_R, \quad L \to U_L\, L, \quad e_R \to U_e\, e_R. \tag{2.1.5}$$

where $U_j^\dagger U_j = U_j U_j^\dagger = 1, \quad j \in \{Q, u, d, L, e\}$. Since there are $N_f = 3$ copies of each field representation, these are $N_f \times N_f$ matrices. Thus for total 3 representations of quark fields and 2 for the lepton fields the total symmetry group $\mathcal{G}_{\text{global}}$ is $U(3)^5$ which is known as *flavor symmetry*.

$$\mathcal{G}_{\text{global}} = U(3)^5 = SU(3)^3_{\text{quark}} \times SU(3)^2_{\text{lepton}} \times U(1)^5 \tag{2.1.6}$$

Quantum effects break the each $U(1)$ symmetry however some specific combinations like $U(1)_{\text{B-L}}$ is non-anomalous.

The Yukawa interactions explicitly break the flavor symmetry and is the origin of non-trivial flavor structure of the SM. The gauge interaction are divided into two parts the charged current (CC) and neutral current (NC) interactions as follows.

$$\mathcal{L}_{CC} = \frac{g}{\sqrt{2}} \left(\overline{u}_{L\alpha} \gamma^\mu d_{L\alpha} W_\mu^+ + \overline{e}_{L\alpha} \gamma^\mu \nu_{L\alpha} W_\mu^- \right) + \text{h.c.}\,, \tag{2.1.7}$$

$$\mathcal{L}_{NC} = e q_f \overline{f} \gamma^\mu f A_\mu + \frac{g}{c_W} \overline{f} \gamma^\mu \left(g_V^f - g_A^f \gamma_5 \right) f Z_\mu \tag{2.1.8}$$

where g_V^f and g_A^f are the vector and axial vector coupling of Z boson to fermions, respectively which are given by $g_V^f = \frac{1}{2} T_3^f - s_W^2 q_f, \quad g_A^f = \frac{1}{2} T_3^f$.

2.2 The effective weak Hamiltonian

The effective theory approach is an important tool to study a theory where various different energy scales are present. The formalism includes only the relevant degrees of freedom at the scale where the theory is probed and all the heavy degrees of freedoms are being integrated out. This leads to simplification in the analysis and easily allows to extract out the relevant results. A schematic time line for treating various models, including the SM by assuming presence of some physics beyond the SM, as effective theories is shown in Fig. 2.1.

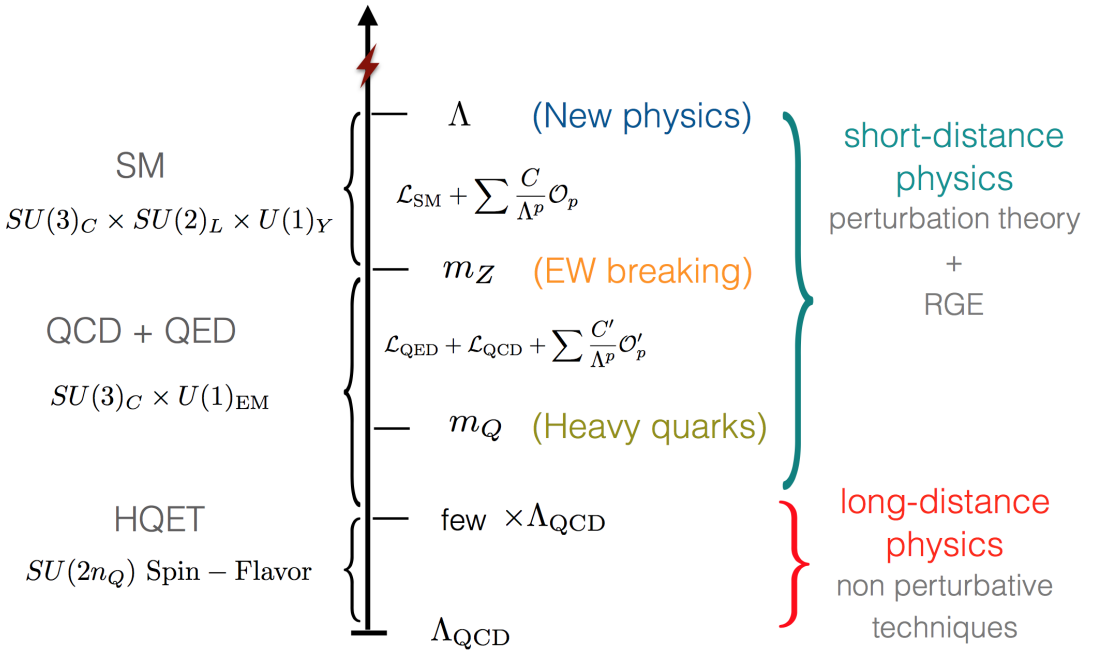

Figure 2.1. A schematic time-line for effective theories.

To study the weak decays of hadrons the role of strong interaction has to be carefully considered. It is done with the use of the powerful tool known as operator product expansion (OPE). As the typical binding energy of a hadron is $\mathcal{O}(1\,\text{GeV})$ which is much below the EW scale, the OPE formalism deals with an expansion in $1/m_W^2$ powers of the W boson propagator. The integration of heavy degrees of freedom generates local operators. Thus a general effective Hamiltonian can be written in a form

$$\mathcal{H}_{\text{eff}} = \frac{G_F}{\sqrt{2}} \sum_i \lambda_i^{\text{CKM}} C_i(\mu)\, O_i(\mu) \tag{2.2.1}$$

where λ_i^{CKM} contains Cabibbo-Kobayashi-Maskawa (CKM) factors, $C_i(\mu)$ are the Wilson coefficients and O_i are local operators governing the process under consideration.

The amplitudes for a decay of a B meson to final state F can be computed by

$$A(B \to F) = \langle F \,|\, \mathcal{H}_{\text{eff}} \,|\, B \rangle = \frac{G_F}{\sqrt{2}} \sum_i \lambda_i^{\text{CKM}} C_i(\mu) \langle F \,|\, O_i(\mu) \,|\, B \rangle \tag{2.2.2}$$

where the hadronic matrix element estimates $\langle F \,|\, O_i(\mu) \,|\, B \rangle$ require non perturbative tech-

niques.

It can be seen from Eq. (2.2.2) that OPE essentially divided the amplitude of $B \to F$ transition in to two parts; short-distance and long distance contributions separated by the energy scale μ known as factorization scale. The short distance effects are included in the Wilson coefficients which can be calculated perturbatively. These coefficients include the contributions from integrating out the heavy particles such as top quarks, gauge bosons W and Z, and any new heavy particle present in SM extensions. All effects of QCD interactions above the factorization scale are contained in these coefficients and are independent of external states. Thus the Wilson coefficients are process independent in the sense that it do not depend on the hadron under consideration and only the corresponding quark level transition is relevant. On the other hand, the matrix element includes all contributions below the OPE factorization scale and thus needs non perturbative techniques. The evaluation of long distance contributions are done using various methods like LCSR, Lattice QCD, HQET etc. The LCSR calculations are done in the large recoil energy limit of the final state meson where as the Lattice QCD and HQET results involve assumptions which are valid at the low recoil energy.

2.3 B physics and the excitements

In current days, very intensive research works are motivated to study the rare decays of hadrons from both theoretical and experimental sides . Within LHC, apart from the CMS and ATLAS collaborations, the full LHCb group is devoted to analyze various different decays of hadrons. The LHCb detector is designed to study CP violation in B-hadron decays at the LHC. LHCb covers a polar angular aperture between approximately 10 and 300 mrad (250 mrad) in the bending (non-bending) plane and exploits the sharply peaked forward-backward $b\bar{b}$ production cross section. Up to 2018, LHCb will have accumulated $\sim$ 8 fb^{-1} of integrated luminosity and special care will be taken for improved precision

and extra sensitivity to the rarest decay modes. The detector will also be upgraded to run at a luminosity of up to 2×10^{33} cm^{-2} s^{-1}, a factor of 5 increase. A combination of these improvements will allow around an order of magnitude increase in precision compared to the current standing.

The powerful B factory Belle experiment is dedicated to study the properties and behavior of the B and D mesons within small uncertainties. Both the KEKB accelerator and the Belle detector are undergoing a major upgrade with the aim to take data at a peak luminosity of $\sim$ 1036 cm^{-2} s^{-1}, approximately 40 times higher than its predecessor. The expectation is that Belle-II will accumulate 50 ab^{-1} in $\sim$ 5 years giving approximately 50 times the current Belle data. Due to the clean e^+e^- environment, Belle-II has several significant advantages compared to LHCb, such as very efficient trigger and tagging system, excellent reconstruction of neutral particles: γ , π^0, K_L and neutrinos via missing energy.

Apart from the improvement in measurements of various CKM elements, LHCb and Belle have measured several rare decay processes up to great accuracy. Among such modes, $B_{(s)} \to \mu^+\mu^-$ extremely rare helicity suppressed decay, has been observed at more than $\sim 5\sigma$ significance. The experimental measurements of branching fractions of these modes lie close to their SM prediction and thus constrain many BSM scenarios like Minimal Super Symmetric Model (MSSM), Two-Higgs-Doublet Model (2HDM) etc.

In context of rare B decay modes, there exists several long lasting as well as recently measured discrepancies such as, the deviation between the inclusive and exclusive measurements of the CKM elements V_{ub} and V_{cb} where the exclusive measurements from different channels, for both the elements, lie below the corresponding inclusive data [16]. A discrepancy is observed in the angular observable P'_5 in $B \to K^*\ell\ell$ mode both in 1 fb^{-1} and 3 fb^{-1} LHCb [2] data. The well known R_K [14], $R(D^{(*)})$ [16] anomalies measured in various experiments in last few years and the recently the interest is boosted with the measurements of R_{K^*} [15] anomaly. These deviations have drawn lot of attentions from both theory as well as experimental sides. In the theoretical studies, more intense and

improved techniques are being developed to estimate the hadronic parameters present in the concerning decay modes. Whereas experiments are dedicated to improve the statistics of the observed discrepancies and also to look for such effects in other decay channels as well. In view of various new measurements, improved systematics of current results and also the future updates of these experiments, it is very exciting time to study decay modes of hadrons.

3 The rare mode $B \to K^* \ell^+ \ell^-$

In this chapter we study the rare semileptonic decay $B \to K^* \ell^+ \ell^-$. In the SM the amplitude for this mode is penguin and box diagram mediated (as shown in Fig. 3.1) and thus is loop suppressed. With the subsequent decay of $K^* \to K\pi$, the full 4-body angular analysis enables to measure several observables at experiments. Therefore this mode is considered an important place to understand the effect of SM physics as well as confirm/constrain the new phenomena beyond the SM.

The content of this chapter is based on the work done with Rahul Sinha and Diganta Das [5].

If we knew what it was we were doing, it would not be called research, would it? - Albert Einstein

3.1 Introduction

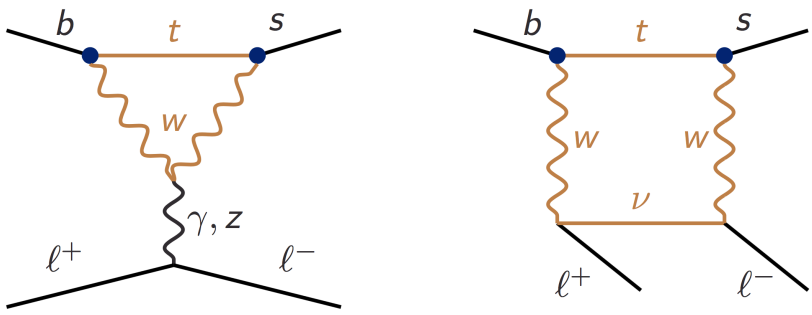

Figure 3.1. The penguin and box diagrams for $b \to s\ell^+\ell^-$ transition.

It is a historical fact that several discoveries in particle physics were preceded by indirect evidence through quantum loop contributions. It is for this reason that significant attention is devoted in studying loop processes. The muon magnetic moment is one of the best examples of such a process where precision calculations have been done in order to search for NP by comparing the theoretical expectation with experimental observation. It is a testimony to such searches for NP beyond the SM that both theoretical estimates and experimental observation have reached a precision where the hadronic effects even for the lepton magnetic moment dominate the discrepancy between theory and observation. Indirect searches for NP often involve precision measurement of a single quantity that is compared to a theoretical estimate that also needs to be very accurately calculated. Unfortunately, hadronic estimates involve calculation of long distance QCD effects which cannot easily be done accurately, limiting the scope of such searches. There exist, however, certain decay modes which involve the measurement of several observables that can be related to each other with minimal assumptions and completely calculable QCD contributions within the SM . A well known example [1,27] of such a process is the semileptonic penguin decay $B \to K^* \ell^+ \ell^-$, where ℓ is either the electron or the muon.

FCNC transitions are known to be sensitive to NP contributions. However, hadronic flavor changing neutral current receive short and long-distance QCD contributions that are not

easy to estimate reliably. It is evident from the data collected by the Belle, *BABAR* at the B-factories, CLEO, CDF, Tevatron, CMS and LHCb that NP does not show up as a large and unambiguous effect. This has bought into focus the need for approaches that are theoretically cleaner i.e., where the hadronic uncertainties are much smaller than the effects of NP that are being probed. Hence, to effectively search for NP it is crucial to separate the effect of NP from hadronic uncertainties that can contribute to the decay. The decay mode $B \to K^* \ell^+ \ell^-$ is regarded [27] as significant in this attempt. The full angular analysis of the final state gives rise to a multitude of observables [1, 28] which can be measured as function of the dilepton invariant mass.

In this chapter we review the theoretical framework required to describe $B \to K^* \ell^+ \ell^-$ and derive the most general parametric form of the amplitude describing the decay in Sec. 3.2. The amplitude written is notionally exact in the SM. In Sec. 3.3 we construct all the observables in terms of the amplitude derived in Sec. 3.2. Here we retain the lepton mass as well as the strange quark mass that appears in the short-distance Hamiltonian describing this decay.

3.2 Theoretical Framework

In this section we will discuss the most general form of the amplitude that can describe the exclusive decay mode $B \to K^* \ell^+ \ell^-$ in the SM. The description of the decay $B \to K^* \ell^+ \ell^-$ requires as the first step the separation of short-distance effects which involve perturbative QCD and weak interaction from the long-distance QCD contributions in an effective Hamiltonian. As is well explained in literature, exclusive decay modes are a challenge to describe theoretically. This difficulty arises not only in the need to know hadronic form factors accurately but also from the existence of "nonfactorizable " contributions that do not correspond to form factors. These contributions originate from electromagnetic corrections to the matrix element of purely hadronic operators in the effective Hamiltonian.

It has been demonstrated [4] that these non- factorizable corrections can be computed allowing exclusive decay such as $B \to K^*\gamma$ and $B \to K^*\ell^+\ell^-$ to be treated systematically much as their inclusive decay counterparts. It is based on this theoretical understanding that we will write the most general from of the amplitude for $B \to K^*\ell^+\ell^-$ in the SM. Our approach will be to examine the various factorizable and nonfactorizable contributions to the process and write the most general parametric form of the amplitude without making any attempt to evaluate it.

The decays $B \to K^*\ell^+\ell^-$ occurs at the quark level via a $b \to s\ell^+\ell^-$ FCNC transition. The short-distance effective Hamiltonian for the inclusive process $b \to s\ell^+\ell^-$ is given in the SM by [29–31],

$$\mathcal{H}_{\text{eff}} = -4\frac{G_F}{\sqrt{2}}\Big[V_{tb}V_{ts}^*\Big(C_1O_1^c + C_2O_2^c + \sum_{i=3}^{10} C_iO_i\Big) + V_{ub}V_{us}^*\Big(C_1(O_1^c - O_1^u) + C_2(O_2^c - O_2^u)\Big)\Big]. \tag{3.2.1}$$

The local operators O_i are as given in Ref. [30], however, for completeness we present the relevant operators that are dominant:

$$\begin{aligned} O_7 &= \frac{e}{g^2}[\bar{s}\sigma_{\mu\nu}(m_bP_R + m_sP_L)b]F^{\mu\nu}, \\ O_9 &= \frac{e^2}{g^2}(\bar{s}\gamma_\mu P_L b)\,\bar{\ell}\gamma^\mu\ell, \\ O_{10} &= \frac{e^2}{g^2}(\bar{s}\gamma_\mu P_L b)\,\bar{\ell}\gamma^\mu\gamma_5\ell, \end{aligned}$$

where $g\,(e)$ is the strong (electromagnetic)coupling constant, $P_{L,R} = (1 \mp \gamma_5)/2$ are the left and right chiral projection operators and $m_b\,(m_s)$ are the running $b\,(s)$ quark mass in the $\overline{\text{MS}}$ scheme. The Wilson coefficients C_i encode all the short-distance effects and are calculated in perturbation theory at a matching scale $\mu = M_W$ up to desired order in the strong coupling constant α_s before being evolved down to the scale $\mu = m_b \approx 4.8\text{GeV}$. All

NP contributions to $B \to K^* \ell^+ \ell^-$ contribute exclusively to C_i; this includes new Wilson coefficients corresponding to new operators that arise from NP.

Significant effort (see Refs. [32, 33] for reviews) has gone into evaluating the Wilson coefficients up to next-to-next-to-leading-logarithmic (NNLL) order. As has been stressed earlier [33] it is important to remember that "the construction of the effective Hamiltonian by means of operator product expansion and renormalization group methods can be done fully in the perturbative framework. The fact that the decaying hadron are bound states of quarks is irrelevant for this construction." This implies that the C_i are decay mode independent. The dependence on the mode enters only through the matrix element of local bilinear quark operators O_i, i.e. $\langle f|O_i|B\rangle$, which encodes the long-distance contributions. Since the decay amplitude cannot depend on the scale μ, $\langle f|O_i|B\rangle$ must depend on the scale μ as well. The cancellation of μ dependence generally involves several terms in the operator product expansion. Since the calculation of the hadronic matrix element involves long-distance contributions, non-perturbative methods are required. Much progress has been made in these calculations using HQET as a tool. However, the dominant theoretical error in the amplitude arises due to the lack of reliable calculations of the hadron matrix element.

The simple picture of the decay presented above is unfortunately not accurate enough; there exist several corrections making a reliable estimate of the decay amplitude a challenge. The difficulty goes beyond accurately estimating the form factors involved in the hadron matrix element. There exist [4] additional nonfactorizable and long-distance contributions which arise from electromagnetic corrections to the matrix elements of purely hadronic operators in the Hamiltonian that cannot be absorbed into hadronic form factors. These contributions are generated by current-current operators $O_{1,2}$ and penguin operators $O_{3-6,8}$, combined with electromagnetic interaction of quarks to produce $\ell^+\ell^-$. The complication in dealing with these corrections is that the average distances between the photon emission and the weak interaction points are not necessarily short resulting in essentially

non local contributions to the decay amplitude which cannot be reduced to local form factors. A further challenge is that each such contribution has to identified and estimated one by one. The intermediate charm quark (and in principle the up quark) loops can couple to lepton pairs via a virtual photon and even though these effects are subdominant numerically in certain kinematical regions, they cannot be completely neglected. The other quarks contribute negligibly (except for resonant contribution which we will discuss later) to $O_{1,2}$ and penguin operators $O_{3-6,8}$ for $B \to K^* \ell^+ \ell^-$ as they are either CKM suppressed or have small accompanying Wilson coefficient. A remarkable effort [34–36] has gone into understanding the details of the hadronic contributions in B decays and in particular to $B \to K^* \ell^+ \ell^-$. It is fortunate that the remarkable progress made so far, enables us to write a completely accurate parametric form of the amplitude for this mode in the SM.

LHCb has observed a broad peaking structure [37, 38] in the dimuon spectrum of $B \to K \ell^+ \ell^-$. It would be of interest to see if this observation of broad resonances has implication on $B \to K^* \ell^+ \ell^-$ mode, since long-distance effects would have to be included systematically. The decay mode $B \to K^* \ell^+ \ell^-$ carries more information [1, 28] on the dynamics as compared to the counterpart pseudoscalar mode $B \to K \ell^+ \ell^-$, since the K^* polarization can also be measured. In order to study the dependence of the amplitude on the helicity of the K^* we further consider the decay $K^* \to K\pi$ or the decay process $B \to K^* \ell^+ \ell^- \to (K\pi)_{K^*} \ell^+ \ell^-$. This further step itself does not complicate matters. The decay amplitude in terms of hadronic matrix elements must therefore include direct contributions proportional to C_7, C_9 and C_{10} multiplied by $B \to K^*$ form factors and contributions from non local hadronic matrix elements $\mathcal{H}_i$ such that [3],

$$
\begin{aligned}
A(B(p) \to K^*(k) \ell^+ \ell^-) = \frac{G_F \alpha}{\sqrt{2}\pi} V_{tb} V_{ts}^* \Bigg[\Bigg\{ & \widehat{C}_9 \langle K^* | \bar{s} \gamma^\mu P_L b | \bar{B} \rangle \\
& - \frac{2\widehat{C}_7}{q^2} \langle K^* | \bar{s} i \sigma^{\mu\nu} q_\nu (m_b P_R + m_s P_L) b | \bar{B} \rangle - \frac{16\pi^2}{q^2} \sum_{i=\{1-6,8\}} \widehat{C}_i \mathcal{H}_i^\mu \Bigg\} \bar{\ell} \gamma_\mu \ell \\
& + \widehat{C}_{10} \langle K^* | \bar{s} \gamma^\mu P_L b | \bar{B} \rangle \, \bar{\ell} \gamma_\mu \gamma_5 \ell \Bigg],
\end{aligned}
\tag{3.2.2}
$$

where, $p = q + k$ with q being the dilepton invariant momentum and the non local hadron matrix element $\mathcal{H}_i^\mu$ is given by

$$\mathcal{H}_i^\mu = \langle K^*(k)|i \int d^4x\, e^{iq\cdot x} T\{j_{em}^\mu(x), \mathcal{O}_i(0)\}|\bar{B}(p)\rangle.$$

In Eq. (3.2.2), we have introduced *new notional theoretical parameters* $\widehat{C}_7$, $\widehat{C}_9$ *and* $\widehat{C}_{10}$ *to indicate the true values of Wilson coefficients, which are by definition not dependent on the order of the perturbative calculation in* α_s $(= g^2/(4\pi))$ *to which they are evaluated*. Our definition is explicit and should not be confused with those defined earlier in literature. The amplitude expressed in Eq. (3.2.2) is *notionally complete and free from any approximations*. In this thesis we do not attempt to estimate the hadronic matrix element involved in Eq. (3.2.2), instead we use Lorentz invariance to write out the most general form of the hadron matrix elements $\langle K^*|\bar{s}\gamma^\mu P_L b|\bar{B}(p)\rangle$ and $\langle K^*|\bar{s}i\sigma^{\mu\nu}q_\nu P_{R,L} b|\bar{B}(p)\rangle$ which may be defined as

$$\begin{aligned}\langle K^*(\epsilon^*,k))|\bar{s}\gamma^\mu P_L b|B(p)\rangle = \epsilon_\nu^*\Big(&\mathcal{X}_0\, q^\mu q^\nu + \mathcal{X}_1\left(g^{\mu\nu} - \frac{q^\mu q^\nu}{q^2}\right)\\ &+\mathcal{X}_2\left(k^\mu - \frac{k.q}{q^2}q^\mu\right)q^\nu + i\mathcal{X}_3\,\epsilon^{\mu\nu\rho\sigma}\,k_\rho q_\sigma\Big), \qquad (3.2.3)\\ \langle K^*(\epsilon^*,k))|i\bar{s}\sigma^{\mu\nu}q_\nu P_{R,L} b|B(p)\rangle = \epsilon_\nu^*\Big(&\pm\mathcal{Y}_1\left(g^{\mu\nu} - \frac{q^\mu q^\nu}{q^2}\right)\\ &\pm\mathcal{Y}_2\left(k^\mu - \frac{k.q}{q^2}q^\mu\right)q^\nu + i\mathcal{Y}_3\,\epsilon^{\mu\nu\rho\sigma}\,k_\rho q_\sigma\Big). \qquad (3.2.4)\end{aligned}$$

We have written Eq. (3.2.3) such that the vector part of the current in $\langle K^*(\epsilon^*,k))|\bar{s}\gamma^\mu P_L b|B(p)\rangle$ is conserved and only the $\mathcal{X}_0$ term in the divergence of the axial part survives. Equation (3.2.4) is also written so as to ensure that $\langle K^*|i\bar{s}\sigma^{\mu\nu}q_\nu P_{R,L} b|B\rangle q_\mu = 0$. The relations between $\mathcal{X}_{0,1,2,3}$ and $\mathcal{Y}_{1,2,3}$ and the form factors conventionally defined for on-shell K^* are discussed in appendix A.1. It should be noted that form factors $\mathcal{X}_{0,1,2,3}$ and $\mathcal{Y}_{1,2,3}$ are functions of q^2 and k^2, but we suppress the explicit dependence for simplicity of notation. The subsequent decay of the K^*, i.e., $K^*(k) \to K(k_1)\pi(k_2)$ can be easily taken into account [1, 30] resulting in the hadronic matrix element $\langle [K(k_1)\pi(k_2)]_{K^*}|\bar{s}\gamma^\mu P_L b|B(p)\rangle$ being

written as

$$\langle [K(k_1)\pi(k_2)]_{K^*}|\bar{s}\gamma^\mu P_L b|B(p)\rangle = D_{K^*}(k^2) W_\nu \left(\mathcal{X}_0\, q^\mu q^\nu + \mathcal{X}_1 \left(g^{\mu\nu} - \frac{q^\mu q^\nu}{q^2} \right) + \mathcal{X}_2 \left(k^\mu - \frac{k.q}{q^2} q^\mu \right) q^\nu + i\mathcal{X}_3\, \epsilon^{\mu\nu\rho\sigma}\, k_\rho q_\sigma \right), \tag{3.2.5}$$

$$\langle [K(k_1)\pi(k_2)]_{K^*}|i\bar{s}\sigma^{\mu\nu} q_\nu P_{R,L} b|B(p)\rangle = D_{K^*}(k^2) W_\nu \left(\pm\, \mathcal{Y}_1 \left(g^{\mu\nu} - \frac{q^\mu q^\nu}{q^2} \right) \pm \mathcal{Y}_2 \left(k^\mu - \frac{k.q}{q^2} q^\mu \right) q^\nu + i\mathcal{Y}_3\, \epsilon^{\mu\nu\rho\sigma}\, k_\rho q_\sigma \right), \tag{3.2.6}$$

where, the subscript K^* in $[K(k_1)\pi(k_2)]_{K^*}$ indicates that the final sate is produced by the decay of a K^*, $D_{K^*}(k^2)$ is the K^* propagator, so that

$$|D_{K^*}(k^2)|^2 = \frac{g^2_{K^*K\pi}}{(k^2 - m^2_{K^*})^2 + (m_{K^*}\Gamma_{K^*})^2}, \tag{3.2.7}$$

with $g_{K^*K\pi}$ being the $K^*K\pi$ coupling and the other parameters introduced are

$$W_\nu = K_\nu - \xi k_\nu,\ K = k_1 - k_2,\ k = k_1 + k_2,\ \xi = \frac{k_1^2 - k_2^2}{k^2}.$$

The most general expression for the hadronic matrix element $\mathcal{H}_i^\mu$ can also be written using Lorentz invariance. Since this hadronic matrix element arises from non local contributions at the quark level, it involves introducing "new" form factors $\mathcal{Z}_1^i$, $\mathcal{Z}_2^i$ and $\mathcal{Z}_3^i$ corresponding to nonfactorizable contribution from each $\mathcal{H}_i^\mu$ in analogy with those introduced in Eq. (3.2.3) as follows:

$$\begin{aligned} \mathcal{H}_i^\mu &= \langle K^*(\epsilon^*, k)|i \int d^4x\, e^{iq\cdot x} T\{j^\mu_{em}(x), \mathcal{O}_i(0)\}|\bar{B}(p)\rangle \\ &= \epsilon^*_\nu \Big(\mathcal{Z}_1^i\, (g^{\mu\nu} - \frac{q^\mu q^\nu}{q^2}) + \mathcal{Z}_2^i\, (k^\mu - \frac{k.q}{q^2} q^\mu) q^\nu + i\mathcal{Z}_3^i\, \epsilon^{\mu\nu\rho\sigma}\, k_\rho q_\sigma \Big). \end{aligned} \tag{3.2.8}$$

Our definition follows Ref. [4] of "nonfactorizable " and includes those corrections that are not contained in the definition of form factors introduced in Eqs. (3.2.3) and (3.2.4).

Here the most general form of $\mathcal{H}_i^\mu$ is written to ensure the conservation of EM current i.e, $q_\mu \mathcal{H}_i^\mu = 0$.

The non local effects represented by $\mathcal{H}_i^\mu$ can be taken into account by absorbing the contributions into redefined $\widehat{C}_9$ and modifying the contribution from the electromagnetic dipole operator O_7. The electromagnetic corrections to operators $O_{1-6,8}$ can also contribute to $B \to K^*\gamma$ at $q^2 = 0$. Since, only the Wilson coefficient $\widehat{C}_7$ contributes to $B \to K^*\gamma$, the charm loops at $q^2 = 0$ must contribute to $\widehat{C}_7$ in order for the Wilson coefficient to be process independent. It is easily seen that the effect of this is to modify the $\widehat{C}_7 \langle K\pi|\bar{s}i\sigma^{\mu\nu}q_\nu(m_b P_R + m_s P_L)b|\bar{B}\rangle$ terms such that the form factors and Wilson coefficients mix in an essentially inseparable fashion. This holds true even for the leading logarithmic contributions [4, 39]. Both factorizable and nonfactorizable contributions arising from electromagnetic corrections to hadronic operators up to all orders can in principle be included in this approach. The remaining contributions can easily be absorbed into a redefined "effective" Wilson coefficient $\widehat{C}_9$ defined such that

$$\widehat{C}_9 \to \widetilde{C}_9^{(j)} = \widehat{C}_9 + \Delta C_9^{(\text{fac})}(q^2) + \Delta C_9^{(j),(\text{non-fac})}(q^2) \tag{3.2.9}$$

where, $j = 1, 2, 3$ and $\Delta C_9^{(\text{fac})}(q^2)$, $\Delta C_9^{(\text{non-fac})}(q^2)$ correspond to factorizable and soft gluon nonfactorizable contributions. Note that the nonfactorizable contributions necessitates the introduction of new form factors $\mathcal{Z}_j$ and the explicit dependence on $\mathcal{Z}_j/\mathcal{X}_j$ is absorbed in defining

$$\Delta C_9^{(\text{fac})} + \Delta C_9^{(j),(\text{non-fac})} = -\frac{16\pi^2}{q^2} \sum_{i=\{1-6,8\}} \widehat{C}_i \frac{\mathcal{Z}_j^i}{\mathcal{X}_j}, \tag{3.2.10}$$

resulting in the j dependence of the term as indicated. We also mention that there is no nonfactorizable correction term in Eq. (3.2.8) analogous to $\mathcal{X}_0$ (in Eq. (3.2.3)) due EM current conservation as discussed above.

The corresponding corrections to $\widehat{C}_7$ are taken into by the replacement,

$$\frac{2(m_b+m_s)}{q^2}\widehat{C}_7\,\mathcal{Y}_j \to \widetilde{\mathcal{Y}}_j = \frac{2(m_b+m_s)}{q^2}\widehat{C}_7\,\mathcal{Y}_j + \cdots, \tag{3.2.11}$$

where the dots indicate other factorizable and nonfactorizable contributions and the factor $2(m_b+m_s)/q^2$ has been absorbed in the form factors $\widetilde{\mathcal{Y}}_j$. Note that the $\widetilde{\mathcal{Y}}_j$'s are in general complex because of the nonfactorizable contributions to the Wilson coefficient $\widehat{C}_7$, but on-shell quarks and resonances do not contribute to them. It should be noted that $\widetilde{C}_9^{(j)}$ includes contributions from both factorizable and nonfactorizable effects, whereas $\widehat{C}_{10}$ is unaffected by strong interaction effects coming from electromagnetic corrections to hadronic operators. The use of a 'widetilde' versus 'widehat' throughout the chapter is also meant as a notation to indicate this fact. It should be noted that $\widehat{C}_{10}$ is real in the SM, whereas, $\widetilde{C}_9^{(j)}$ and $\widetilde{\mathcal{Y}}_j$ are in general complex within the SM. The amplitude in Eq. (3.2.2) can therefore be written as

$$\begin{aligned}
A(B(p)z \to [K(k_1)\pi(k_2)]_{K^*}\ell^+\ell^-) = \frac{G_F\alpha}{\sqrt{2}\pi}V_{tb}V_{ts}^* D_{K^*}(k^2)\Big[\Big\{ & C_L W.q\mathcal{X}_0\, q^\mu \\
& + C_L^{(1)}\mathcal{X}_1\left(K^\mu - \frac{W.q}{q^2}q^\mu - \xi k^\mu\right) + C_L^{(2)}W.q\mathcal{X}_2\left(k^\mu - \frac{k.q}{q^2}q^\mu\right) + iC_L^{(3)}\mathcal{X}_3\,\epsilon^{\mu\nu\rho\sigma}K_\nu k_\rho q_\sigma \\
& - \left(\zeta\,\widetilde{\mathcal{Y}}_1\left(K^\mu - \frac{W.q}{q^2}q^\mu - \xi k^\mu\right) + \zeta W.q\,\widetilde{\mathcal{Y}}_2\left(k^\mu - \frac{k.q}{q^2}q^\mu\right) + i\,\widetilde{\mathcal{Y}}_3\,\epsilon^{\mu\nu\rho\sigma}K_\nu k_\rho q_\sigma\right)\Big\}\bar{\ell}\gamma_\mu P_L\ell \\
& + L \to R\Big],
\end{aligned} \tag{3.2.12}$$

where, $C_{L,R} = \widehat{C}_9 \mp \widehat{C}_{10}$, $C_{L,R}^{(j)} = \widetilde{C}_9^{(j)} \mp \widehat{C}_{10}$ and $\zeta = (m_b - m_s)/(m_b + m_s)$. It may be noted that no assumptions are made in obtaining Eq. (3.2.12) from Eq. (3.2.2). The form factors defined are not limited by power corrections in HQET [40]. We emphasize that Eq. (3.2.12) continues to be notionally exact. In our approach we will relate observables, hence, we do not need to evaluate the Wilson coefficients and form factors. Only in doing so approximations need to be made. In appendix A.1 comparative relation between the

amplitude in Eq. (3.2.12) and the leading order expression excluding nonfactorizable contributions used widely in literature are presented. These approximations are unnecessary for the discussions in this chapter and are presented only as clarification of our notation and as ready reference for readers wanting to examine Eq. (3.2.12) in limiting conditions.

3.3 Angular Distribution and observables.

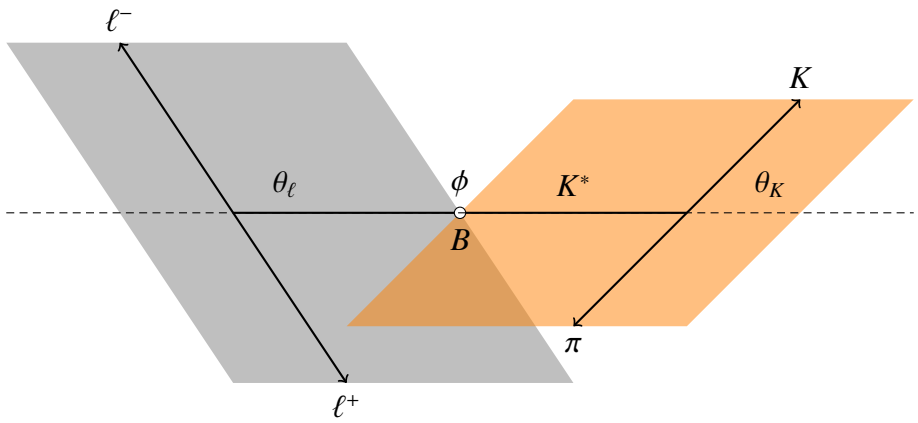

Figure 3.2. Kinematic variables in B rest frame.

The decay $\bar{B}(p) \to K^*(k)\ell^+(q_1)\ell^-(q_2)$,with $K^*(k) \to K(k_1)\pi(k_2)$ on the mass shell, is completely describe by four independent kinematic variables. These kinematic variables are the lepton-pair invariant mass squared $q^2 = (q_1 + q_2)^2$, and the three angles ϕ, θ_ℓ and θ_K as defined in Fig. 3.2. The angle ϕ is the angle between the decay planes formed by $\ell^+\ell^-$ and $K\pi$. The angles θ_ℓ and θ_K are defined as follows: assuming that the K^* has a momentum along the positive z direction in B rest frame, θ_K is the angle between the K and the $+z$ axis and θ_ℓ is the angle of the ℓ^- with the $+z$ axis. The differential decay distribution of $B \to K^*\ell^+\ell^-$ is written as

$$\begin{aligned}\frac{d^4\Gamma(B \to K^*\ell^+\ell^-)}{dq^2\, d\cos\theta_\ell\, d\cos\theta_K\, d\phi} = I(q^2,\theta_\ell,\theta_K,\phi) = \frac{9}{32\pi}\Big[&I_1^s \sin^2\theta_K + I_1^c \cos^2\theta_K + (I_2^s \sin^2\theta_K \\ &+ I_2^c \cos^2\theta_K)\cos 2\theta_\ell + I_3 \sin^2\theta_K \sin^2\theta_\ell \cos 2\phi + I_4 \sin 2\theta_K \sin 2\theta_\ell \cos\phi \\ &+ + I_5 \sin 2\theta_K \sin\theta_\ell \cos\phi + I_6^s \sin^2\theta_K \cos\theta_\ell + I_7 \sin 2\theta_K \sin\theta_\ell \sin\phi\end{aligned}$$

$$+ I_8 \sin 2\theta_K \sin 2\theta_\ell \sin\phi + I_9 \sin^2\theta_K \sin^2\theta_\ell \sin 2\phi\Big]. \tag{3.3.1}$$

The angular coefficients I's, which can be measured from the study of the angular distribution, are q^2 dependent. But for convenience we will suppress the explicit q^2 dependence.

The I's are conveniently expressed in terms of "seven" amplitudes. These comprise the six transversity amplitudes that survive in the massless lepton limit and an amplitude $\mathcal{A}_t$ that contributes only if the mass m of the lepton is finite. The six transversity amplitudes $\mathcal{A}^{L,R}_{\perp,\parallel,0}$, where $\perp$, $\parallel$ and 0 represent the polarizations of the on-shell K^* and L, R denote the chirality of the lepton current. The explicit expression for I's in terms of the transversity amplitudes $\mathcal{A}^{L,R}_{\perp,\parallel,0}$ and $\mathcal{A}_t$ are

$$I_1^s = \frac{(2+\beta^2)}{4}\Big[|\mathcal{A}^L_\perp|^2 + |\mathcal{A}^L_\parallel|^2 + (L\to R)\Big] + \frac{4m^2}{q^2}\mathrm{Re}(\mathcal{A}^L_\perp \mathcal{A}^{R\,*}_\perp + \mathcal{A}^L_\parallel \mathcal{A}^{R^*}_\parallel), \tag{3.3.2a}$$

$$I_1^c = |\mathcal{A}^L_0|^2 + |\mathcal{A}^R_0|^2 + \frac{4m^2}{q^2}[\,|\mathcal{A}_t|^2 + 2\mathrm{Re}(\mathcal{A}^L_0 \mathcal{A}^{R^*}_0)], \tag{3.3.2b}$$

$$I_2^s = \frac{\beta^2}{4}\Big[|\mathcal{A}^L_\perp|^2 + |\mathcal{A}^L_\parallel|^2 + (L\to R)\Big], \tag{3.3.2c}$$

$$I_2^c = -\beta^2\Big[|\mathcal{A}^L_0|^2 + (L\to R)\Big], \tag{3.3.2d}$$

$$I_3 = \frac{\beta^2}{2}\Big[|\mathcal{A}^L_\perp|^2 - |\mathcal{A}^L_\parallel|^2 + (L\to R)\Big], \tag{3.3.2e}$$

$$I_4 = \frac{\beta^2}{\sqrt{2}}\Big[\mathrm{Re}(\mathcal{A}^L_0 \mathcal{A}^{L^*}_\parallel) + (L\to R)\Big], \tag{3.3.2f}$$

$$I_5 = \sqrt{2}\beta\Big[\mathrm{Re}(\mathcal{A}^L_0 \mathcal{A}^{L\,*}_\perp) - (L\to R)\Big], \tag{3.3.2g}$$

$$I_6^s = 2\beta\Big[\mathrm{Re}(\mathcal{A}^L_\parallel \mathcal{A}^{L\,*}_\perp) - (L\to R)\Big], \tag{3.3.2h}$$

$$I_7 = \sqrt{2}\beta\Big[\mathrm{Im}(\mathcal{A}^L_0 \mathcal{A}^{L^*}_\parallel) - (L\to R)\Big], \tag{3.3.2i}$$

$$I_8 = \frac{1}{\sqrt{2}}\beta^2\Big[\mathrm{Im}(\mathcal{A}^L_0 \mathcal{A}^{L\,*}_\perp) + (L\to R)\Big], \tag{3.3.2j}$$

$$I_9 = \beta^2\Big[\mathrm{Im}(\mathcal{A}^{L^*}_\parallel \mathcal{A}^L_\perp) + (L\to R)\Big], \tag{3.3.2k}$$

where

$$\beta = \sqrt{1 - \frac{4\,m^2}{q^2}}.$$

We have dropped the explicit q^2 dependence of the transversity amplitudes $\mathcal{A}^{L,R}_{\perp,\parallel,0}$ and $\mathcal{A}_t$ for notational simplicity.

The seven amplitudes can be written in terms of the form factors $\mathcal{X}_{0,1,2,3}$ and $\mathcal{Y}_{1,2,3}$ as follows:

$$\mathcal{A}^{L,R}_{\perp} = N\sqrt{2}\lambda^{1/2}(m_B^2, m_{K^*}^2, q^2)\Big[(\widetilde{C}_9^{(3)} \mp \widehat{C}_{10})\mathcal{X}_3 - \widetilde{\mathcal{Y}}_3\Big], \tag{3.3.3a}$$

$$\mathcal{A}^{L,R}_{\parallel} = 2\sqrt{2}N\Big[(\widetilde{C}_9^{(1)} \mp \widehat{C}_{10})\mathcal{X}_1 - \zeta\,\widetilde{\mathcal{Y}}_1\Big], \tag{3.3.3b}$$

$$\mathcal{A}^{L,R}_{0} = \frac{N}{2m_{K^*}\sqrt{q^2}}\Big[(\widetilde{C}_9^{(2)}\kappa \mp \widehat{C}_{10})\{4k.q\mathcal{X}_1 + \lambda(m_B^2, m_{K^*}^2, q^2)\mathcal{X}_2\} - \zeta\{4k.q\widetilde{\mathcal{Y}}_1 + \lambda(m_B^2, m_{K^*}^2, q^2)\widetilde{\mathcal{Y}}_2\}\Big], \tag{3.3.3c}$$

$$\mathcal{A}_t = -\frac{N}{m_K^*}\sqrt{q^2}\lambda^{1/2}(m_B^2, m_{K^*}^2, q^2)\widehat{C}_{10}\,\mathcal{X}_0, \tag{3.3.3d}$$

where,

$$\kappa = 1 + \frac{\widetilde{C}_9^{(1)} - \widetilde{C}_9^{(2)}}{\widetilde{C}_9^{(2)}}\frac{4k.q\mathcal{X}_1}{4k.q\mathcal{X}_1 + \lambda(m_B^2, m_{K^*}^2, q^2)\mathcal{X}_2},$$

$\lambda(a,b,c) \equiv a^2 + b^2 + c^2 - 2(ab + bc + ac)$ and N is the normalization constant. In the narrow width approximation for the K^*, $|D_{K^*}(k^2)|^2$ simplifies to

$$|D_{K^*}(k^2)|^2 = \frac{48\pi^2 m_{K^*}^4}{\lambda^{3/2}(m_{K^*}^2, m_K^2, m_\pi^2)}\delta(k^2 - m_{K^*}^2). \tag{3.3.4}$$

This results in simplifying N to,

$$N = V_{tb}V_{ts}^*\left[\frac{G_F^2\alpha^2}{3\cdot 2^{10}\pi^5 m_B^3}q^2\sqrt{\lambda(m_B^2, m_{K^*}^2, q^2)}\beta\right]^{1/2}.$$

We note that in principle the effect of finite K^* resonance width can easily be taken into account, however, we make no attempt to do so as the value of the normalization constant is not going to be used anywhere in our calculation.

The six transversity amplitudes described by Eqs. (3.3.3a) – (3.3.3c) which survive in the

massless lepton case, can be rewritten in a short-form notation by introducing new form factors $\mathcal{F}_\lambda$ and $\widetilde{\mathcal{G}}_\lambda$ as follows,

$$\mathcal{A}_\lambda^{L,R} = C_{L,R}^\lambda \mathcal{F}_\lambda - \widetilde{\mathcal{G}}_\lambda = (\widetilde{C}_9^\lambda \mp \widehat{C}_{10})\mathcal{F}_\lambda - \widetilde{\mathcal{G}}_\lambda. \tag{3.3.5}$$

The expressions of $\mathcal{F}_\lambda$ and $\widetilde{\mathcal{G}}_\lambda$ can be obtained by comparing Eq. (3.3.5) with Eqs. (3.3.3a) – (3.3.3c) and are given in appendix-A.1. $\mathcal{F}_\lambda$ and $\widetilde{\mathcal{G}}_\lambda$ are q^2 dependent form factors, suitably defined to include both factorizable and nonfactorizable corrections to all orders [27]. The form-factor dependence of $\widetilde{C}_9^{(j)}$ indicated by 'j' in Eqs. (3.3.3a) – (3.3.3c) is now translated to an effective helicity 'λ' dependence of Wilson coefficient $\widetilde{C}_9^\lambda$ as

$$\widetilde{C}_9^\perp \equiv \widetilde{C}_9^{(3)}, \quad \widetilde{C}_9^\parallel \equiv \widetilde{C}_9^{(1)}, \quad \widetilde{C}_9^0 \equiv \widetilde{C}_9^{(2)}\kappa. \tag{3.3.6}$$

It is easily seen that $\mathcal{F}_\lambda$ and $\widetilde{\mathcal{G}}_\lambda$ are proportional to $\mathcal{X}_j$ and $\widetilde{\mathcal{Y}}_j$ respectively. Thus $\mathcal{F}_\lambda$'s are completely real and $\widetilde{\mathcal{G}}_\lambda$'s are complex in SM. All imaginary contributions to the amplitude arise from the complex $\widetilde{C}_9^\lambda$ and $\widetilde{\mathcal{G}}_\lambda$. An interesting observation is that $\mathcal{A}_\lambda^{L,R}$ remains unchanged if the nonfactorizable contributions between $\widetilde{\mathcal{G}}_\lambda$ and $\widetilde{C}_9^\lambda$ are rearranged. This observation differs from the conclusion obtained in Ref. [27] because $\widetilde{C}_9^\lambda$ are now helicity dependent and implies that $\widetilde{\mathcal{G}}_\lambda$ and $\widetilde{C}_9^\lambda$ cannot be individually extracted.

Using very general arguments it is easy to see that the form of the amplitude described in Eq. (3.3.5) is the most general possible and the full decay amplitude can be completely described by them for the massless case. The amplitude must be described by the helicity of the K^* and can be divided into two parts one that depends on the chirality of the lepton and another that does not. It is easily noted that the term described by $\mathcal{F}_\lambda$ is chirality dependent whereas the contribution corresponding to the effective photon vertex $\widetilde{\mathcal{G}}_\lambda$ is not. The form factors $\mathcal{F}_\lambda$ and $\widetilde{\mathcal{G}}_\lambda$ depend only on the helicity and the chirality dependence is absorbed completely into the Wilson coefficients. The coefficient of chirality dependent terms proportional to $\mathcal{F}_\lambda$ can themselves either depend on helicity or be independent of it.

Hence, the amplitudes in Eq. (3.3.5) are parametrized in terms of three terms. Throughout the rest of the thesis we will use only the form of the amplitudes in Eq. (3.3.5), which is the most general possible in the SM.

It is obvious from Eq. (3.3.1) that a complete study of the angular distribution involves eleven orthogonal terms allowing us to measure 'eleven' observables. In the limit of massless lepton there exist two relations between the coefficient I's, i.e. $I_1^c = -I_2^c$ and $I_1^s = 3I_2^s$. This reduces the number of independent observables to 'nine'. In a previous work [27] the mode $B \to K^* \ell^+ \ell^-$ was studied in the limit of massless lepton and under the assumption of vanishing CP violation and absence of resonance contributions in the q^2 domains considered. Under these approximations $I_{7,8,9} = 0$ and the number of useful observables reduce to only 'six'. In this chapter we carefully examine each of these assumptions and in particular take into account resonance contributions and the effect of massless lepton. As emphasized in Sec. 3.2 we have taken into account charm loop effects. The charm loop effect and other resonance contributions can make the amplitude complex. In the discussions that ensue we will assume that the amplitude is complex and ensure that all SM contributions, both factorizable and nonfactorizable , are taken into account completely when writing the most general parametrized amplitude.

Within SM, CP violation is expected to be extremely tiny and essentially unobservable [1, 28] at the current level of experimental accuracy. In Ref. [1] the CP violating asymmetry was evaluated to be $\sim 3 \times 10^{-4}$. This would imply that one need at the very least 10^7 reconstructed events in this decay channel to observe the asymmetry at 1σ. Given this we have justifiably ignored CP violation in this channel and any observation of CP violation at the current level of experimental sensitivity would constitute an unambiguous signal of NP. In view of this, we ignore CP violation hence forth. It may be noted that CP violation can be easily included in our approach. However, we ignore it because it is not central to our discussion and we do not wish to complicate our notation accounting for unobservable effects within the SM. Under the assumption of vanishing CP violation the

conjugate mode $\bar{B} \to \bar{K}^* \ell^+ \ell^-$ has an identical decay distribution except that $I_{5,6,8,9}$ switch signs to become $-I_{5,6,8,9}$ in the differential decay distribution [1, 28].

Integration over $\cos\theta_K$, $\cos\theta_\ell$ and ϕ results in the differential decay rate with respect to the invariant lepton mass:

$$\frac{d\Gamma}{dq^2} = \sum_{\lambda=0,\|,\perp} (|\mathcal{A}_\lambda^L|^2 + |\mathcal{A}_\lambda^R|^2). \tag{3.3.7}$$

We define the relevant observables to be the three helicity fractions defined as

$$F_L = \frac{|\mathcal{A}_0^L|^2 + |\mathcal{A}_0^R|^2}{\Gamma_f}, \tag{3.3.8a}$$

$$F_\| = \frac{|\mathcal{A}_\|^L|^2 + |\mathcal{A}_\|^R|^2}{\Gamma_f}, \tag{3.3.8b}$$

$$F_\perp = \frac{|\mathcal{A}_\perp^L|^2 + |\mathcal{A}_\perp^R|^2}{\Gamma_f}, \tag{3.3.8c}$$

where $\Gamma_f \equiv \sum_\lambda (|\mathcal{A}_\lambda^L|^2 + |\mathcal{A}_\lambda^R|^2)$ and $F_L + F_\| + F_\perp = 1$. The other observables are the six asymmetries defined below. The well-known forward-backward asymmetry $A_{\rm FB}$ is defined conventionally as,

$$A_{\rm FB} = \frac{\left[\int_0^1 - \int_{-1}^0\right] d\cos\theta_\ell \frac{d^2(\Gamma - \bar{\Gamma})}{dq^2 d\cos\theta_\ell}}{\int_{-1}^1 d\cos\theta_\ell \frac{d^2(\Gamma + \bar{\Gamma})}{dq^2 d\cos\theta_\ell}}, \tag{3.3.9}$$

and isolates the contribution from the I_6 term in Eq. (3.3.1). Contributions from I_4 and I_5 in Eq. (3.3.1) are extracted by the two angular asymmetries,

$$A_4 = \frac{\left[\int_{-\pi/2}^{\pi/2} - \int_{\pi/2}^{3\pi/2}\right] d\phi \left[\int_0^1 - \int_{-1}^0\right] d\cos\theta_K \left[\int_0^1 - \int_{-1}^0\right] d\cos\theta_\ell \frac{d^4(\Gamma + \bar{\Gamma})}{dq^2 d\cos\theta_\ell d\cos\theta_K d\phi}}{\int_0^{2\pi} d\phi \int_{-1}^1 d\cos\theta_K \int_{-1}^1 d\cos\theta_\ell \frac{d^4(\Gamma + \bar{\Gamma})}{dq^2 d\cos\theta_\ell d\cos\theta_K d\phi}}, \tag{3.3.10}$$

$$A_5 = \frac{\Big[\int_{-\pi/2}^{\pi/2} - \int_{\pi/2}^{3\pi/2}\Big]d\phi\Big[\int_0^1 - \int_{-1}^0\Big]d\cos\theta_K \int_{-1}^1 d\cos\theta_\ell \, \dfrac{d^4(\Gamma - \bar{\Gamma})}{dq^2 d\cos\theta_\ell d\cos\theta_K d\phi}}{\displaystyle\int_0^{2\pi} d\phi \int_{-1}^1 d\cos\theta_K \int_{-1}^1 d\cos\theta_\ell \, \frac{d^4(\Gamma + \bar{\Gamma})}{dq^2 d\cos\theta_\ell d\cos\theta_K d\phi}} \,. \tag{3.3.11}$$

The three new observables not considered in Ref. [27] are A_7, A_8 and A_9. These are nonzero if the amplitude is complex. They may be described in analogy as,

$$A_7 = \frac{\Big[\int_0^{\pi} - \int_{\pi}^{2\pi}\Big]d\phi\Big[\int_0^1 - \int_{-1}^0\Big]d\cos\theta_K \int_{-1}^1 d\cos\theta_\ell \, \dfrac{d^4(\Gamma + \bar{\Gamma})}{dq^2 d\cos\theta_\ell d\cos\theta_K d\phi}}{\displaystyle\int_0^{2\pi} d\phi \int_{-1}^1 d\cos\theta_K \int_{-1}^1 d\cos\theta_\ell \, \frac{d^4(\Gamma + \bar{\Gamma})}{dq^2 d\cos\theta_\ell d\cos\theta_K d\phi}} \,, \tag{3.3.12}$$

$$A_8 = \frac{\Big[\int_0^{\pi} - \int_{\pi}^{2\pi}\Big]d\phi\Big[\int_0^1 - \int_{-1}^0\Big]d\cos\theta_K\Big[\int_0^1 - \int_{-1}^0\Big]d\cos\theta_\ell \dfrac{d^4(\Gamma - \bar{\Gamma})}{dq^2 d\cos\theta_\ell d\cos\theta_K d\phi}}{\displaystyle\int_0^{2\pi} d\phi \int_{-1}^1 d\cos\theta_K \int_{-1}^1 d\cos\theta_\ell \, \frac{d^4(\Gamma + \bar{\Gamma})}{dq^2 d\cos\theta_\ell d\cos\theta_K d\phi}} \,, \tag{3.3.13}$$

$$A_9 = \frac{\Big[\int_0^{\pi/2} - \int_{\pi/2}^{\pi} + \int_0^{\pi} - \int_{3\pi/2}^{2\pi}\Big]d\phi\Big[\int_{-1}^1 d\cos\theta_K\Big]\Big[\int_{-1}^1 d\cos\theta_\ell\Big] \dfrac{d^4(\Gamma - \bar{\Gamma})}{dq^2 d\cos\theta_\ell d\cos\theta_K d\phi}}{\displaystyle\int_0^{2\pi} d\phi \int_{-1}^1 d\cos\theta_K \int_{-1}^1 d\cos\theta_\ell \, \frac{d^4(\Gamma + \bar{\Gamma})}{dq^2 d\cos\theta_\ell d\cos\theta_K d\phi}} \,. \tag{3.3.14}$$

The well-known forward-backward asymmetry $A_{\rm FB}$ and the five other angular asymmetries, A_4, A_5, A_7, A_8 and A_9 can be written directly in terms of the transversity amplitudes as follows:

$$A_{FB} = \frac{3}{2}\frac{\mathrm{Re}(\mathcal{A}_\parallel^L \mathcal{A}_\perp^{L^*} - \mathcal{A}_\parallel^R \mathcal{A}_\perp^{R^*})}{\Gamma_f}, \tag{3.3.15}$$

$$A_4 = \frac{\sqrt{2}}{\pi}\frac{\mathrm{Re}(\mathcal{A}_0^L \mathcal{A}_\parallel^{L^*} + \mathcal{A}_0^R \mathcal{A}_\parallel^{R^*})}{\Gamma_f}, \tag{3.3.16}$$

$$A_5 = \frac{3}{2\sqrt{2}}\frac{\mathrm{Re}(\mathcal{A}_0^L \mathcal{A}_\perp^{L^*} - \mathcal{A}_0^R \mathcal{A}_\perp^{R^*})}{\Gamma_f}, \tag{3.3.17}$$

$$A_7 = \frac{3}{2\sqrt{2}} \frac{\mathrm{Im}(\mathcal{A}_0^L \mathcal{A}_\parallel^{L^*} - \mathcal{A}_0^R \mathcal{A}_\parallel^{R^*})}{\Gamma_f}, \tag{3.3.18}$$

$$A_8 = \frac{\sqrt{2}}{\pi} \frac{\mathrm{Im}(\mathcal{A}_0^L \mathcal{A}_\perp^{L^*} + \mathcal{A}_0^R \mathcal{A}_\perp^{R^*})}{\Gamma_f}, \tag{3.3.19}$$

$$A_9 = \frac{3}{2\pi} \frac{\mathrm{Im}(\mathcal{A}_\parallel^{L^*} \mathcal{A}_\perp^L + \mathcal{A}_\parallel^{R^*} \mathcal{A}_\perp^R)}{\Gamma_f}. \tag{3.3.20}$$

The observables A_4, A_5, A_{FB}, A_7, A_8 and A_9 are related to the CP averaged observables S_4, S_5, $A_{\mathrm{FB}}^{\mathrm{LHCb}}$, S_7, S_8 and S_9 measured by LHCb [41] as follows respectively,

$$\begin{aligned} A_4 &= -\frac{2}{\pi} S_4, \quad A_5 = \frac{3}{4} S_5, \quad A_{\mathrm{FB}} = -A_{\mathrm{FB}}^{\mathrm{LHCb}}, \\ A_7 &= \frac{3}{4} S_7, \quad A_8 = -\frac{2}{\pi} S_8, \quad A_9 = \frac{3}{2\pi} S_9. \end{aligned} \tag{3.3.21}$$

We emphasize that our observables $A_{4,5,7,8,9}$ are CP conserving asymmetries and in particular A_9 and should not be confused with the CP violating asymmetry measured by LHCb [41] also denoted by A_9. In our notation we would refer to the CP violating asymmetries as $A_{4,5,6,7,8,9}^{CP}$. The observables F_L and A_{FB} have been measured by different experiments BABAR, Belle, CDF and LHCb [37, 41–46]. By doing a angular analysis in the angle ϕ, LHCb has measured the observable S_3 [41]. S_3 is related to the transversity helicity fraction $F_\perp$ through the relation

$$S_3 = -\frac{1 - F_L - 2F_\perp}{2}. \tag{3.3.22}$$

3.4 Summary

In this chapter we have derived the most general parametric form of the amplitude of the decay mode $B \to K^* \ell^+ \ell^-$. Using Lorentz and gauge symmetry we parametrize the effect of hadronic uncertainties especially the non-factorizable contributions which arise due to the non local interactions. The parametric form incorporates complex amplitudes

enabling resonance contributions to be included, electromagnetic correction to hadronic operators at all orders and all factorizable and nonfactorizable contributions to the decay. The formalism derived in this chapter is an important step to pursue the detailed study on the decay $B \to K^* \ell^+ \ell^-$ which will be discussed in the subsequent chapters. The observables F_L, $F_\perp$, A_4, A_5, $A_{\rm FB}$, A_7, A_8 and A_9 defined in this chapter are not independent and we explore the relation between them in the next chapter.

4 Model independent relation among observables

In this chapter we continue to analyze the rare decay mode $B \to K^* \ell^+ \ell^-$. We extend the theoretical framework derived in the last chapter resulting in a test for the SM gauge structure. A relation among observables is derived in a complete model independent way and is sensitive to new operators which may arise from BSM interactions.

This chapter is based on Ref. [5].

The method of guessing the equation seems to be a pretty effective way of guessing new laws. - Richard P. Feynman

4.1 Introduction

In Ref. [27] an interesting relation between the various observables that can be measured in the mode $B \to K^* \ell^+ \ell^-$ was derived. The derivation was based on a few assumptions that are reasonable. These included ignoring the mass of the lepton ℓ and the s-quark that appears in the short-distance Hamiltonian describing the decay. The decay amplitude was assumed to be real, thereby ignoring the extremely tiny CP violation, the small imaginary contribution to the amplitude that arises from the Wilson coefficient C_9 which is complex in general and the dilepton resonances which were presumed to be removed from the experimental analysis. These assumptions reduced the number of nonzero observables to only six. In this chapter, we carefully *redo the analysis without making any kind of approximation, however, innocuous*. Our approach once again is to derive the most general parametric form of the decay amplitude, which results in a relation between the several related observables.

In this chapter we generalize the derivation in Ref. [27] to incorporate a complex decay amplitude, eliminating the need to ignore imaginary contributions arising from C_9 and ensuring that the new relation is valid even when resonance contributions are not excluded from the (experimental) analysis. This implies that the new relation derived in this chapter involves all the nine CP conserving observables that can be measured using this mode. The derivation of the new relation does not depend on theoretical values of the Wilson coefficients and does not require making any assumptions on the form factors; in particular we do not limit the form-factor to any power of $\Lambda_{\rm QCD}/m_b$ expansion in HQET [47,48]. In fact, the derivation of the new relation itself does not require HQET. The new derivation parametrically incorporates all short-distance and long-distance effects including resonance contributions, as well as, factorizable and nonfactorizable contributions. We also include complete electromagnetic (EM) corrections to hadronic operators up to all orders. Finally, we retain the lepton mass and the s-quark mass. We envisage that the derivation

to be exact in all respects and the new relation obtained here to be one of the cleanest tests of the SM in B decays.

The LHCb Collaboration has measured [41] all the possible CP conserving observables through an angular analysis. These independent measurements consist of the differential decay rate with respect to the dilepton invariant mass, two independent helicity fractions and six angular asymmetries. Three of the asymmetries are zero unless there exist imaginary contributions to the decay amplitudes. If these asymmetries are measured to be zero in the future, the relation between the observables would be free from any hadronic parameter as derived in Ref. [27]. While these asymmetries are currently measured to be small and consistent with zero, there could, however, exist contributions from wide resonances which might still be permitted within statistical errors. Including these asymmetries in the analysis to account for complex amplitudes results in a modification of the relation purely between observables. The modifying terms now involve a single hadronic parameter in addition to being proportional to the three asymmetries. Hence, SM can be tested or equivalently NP contributions can be probed reliably with the knowledge of just one hadronic parameter. It is interesting that all effort to estimate long and short-distance QCD contributions now need to be focused only on accurately estimating this single parameter. Since the asymmetries involved in modifying terms (which arise from complex amplitudes) are already constrained to be small, the results are not very sensitive to the single hadronic parameter. We find that the inclusion of imaginary contributions to the amplitude must always reduce the parameter space. This would enhance any discrepancy that may be observed even when the imaginary part of the amplitudes are ignored. We use the 1 fb^{-1} LHCb data to show how our relation can be used to test the SM and find NP that might contribute to this decay.

A new relation between observables is derived in Sec. 4.2 under the assumption of massless lepton, but retaining all other effects and contribution. In Sec. 4.3 we generalize the new relation derived in Sec. 4.2 to include the mass of the lepton that had been ignored

earlier. We rederive two simple limits of the relation between observables that hold at zero crossings of other asymmetries such as the forward-backward asymmetry. The values of all the observables at kinematic endpoints of the dilepton invariant mass are easily understood in Sec. 4.4. A numerical analysis is presented in Sec. 4.5 that tests the validity of the relation derived assuming SM. We discuss the constraints already imposed by the $1\,\text{fb}^{-1}$ LHCb data [41], but refrain from drawing even the obvious conclusions given that results for $3\,\text{fb}^{-1}$ data will soon be presented. In Sec. 4.6 we summarize the significant results obtained in this chapter.

4.2 The massless lepton limit.

In this section we generalize the approach developed in Refs. [27] to include all contributions from the SM that were ignored as their effects are sub-dominant, except that we still restrict our discussion to the limit where the lepton is massless. The corrections arising from massive leptons will be taken into account later in Sec 4.3. In particular we will consider the possibility that the amplitudes $\mathcal{A}_\lambda^{L,R}$ are in general complex. As already mentioned the imaginary contribution can be totally attributed to the complex $\widetilde{C}_9^\lambda$ and $\widetilde{\mathcal{G}}_\lambda$. This would include loop contributions that are both factorizable and nonfactorizable and all resonance contributions. We also take into account that the nonfactorizable contributions can introduce an 'effective helicity (λ) dependence' in the Wilson coefficient $\widetilde{C}_9^\lambda$.

In Ref. [27] a new variable r_λ was introduced that led to significant simplification. We once again introduce the same "real variable" r_λ defined as,

$$r_\lambda = \frac{\text{Re}(\widetilde{\mathcal{G}}_\lambda)}{\mathcal{F}_\lambda} - \text{Re}(\widetilde{C}_9^\lambda). \tag{4.2.1}$$

Since, we now consider $\widetilde{C}_9^\lambda$ and $\widetilde{\mathcal{G}}_\lambda$ to be complex in general, we have modified r_λ to include only the real contributions i.e, $\text{Re}(\widetilde{C}_9^\lambda)$ and $\text{Re}(\widetilde{\mathcal{G}}_\lambda)$. The amplitude $\mathcal{A}_\lambda^{L,R}$ in Eq. (3.3.5)

can thus be written as,

$$\begin{aligned}\mathcal{A}_\lambda^{L,R} &= (\widetilde{C}_9^\lambda \mp \widehat{C}_{10})\mathcal{F}_\lambda - \widetilde{\mathcal{G}}_\lambda \\ &= (\mp\widehat{C}_{10} - r_\lambda)\mathcal{F}_\lambda + i\varepsilon_\lambda, \end{aligned} \tag{4.2.2}$$

where $\varepsilon_\lambda \equiv \mathrm{Im}(\widetilde{C}_9^\lambda)\mathcal{F}_\lambda - \mathrm{Im}(\widetilde{\mathcal{G}}_\lambda)$. The use of ε_λ is not necessarily meant to imply that the imaginary parts are negligibly small. We make no such assumption. It is, however, to be expected that the imaginary contributions are subdominant. The presence of the ε_λ term introduces three extra variables in comparison to the discussion in Ref. [27]. However, we now have three extra observables A_7, A_8 and A_9. Hence, dealing with complex amplitude introduces only a technical difficulty of solving for additional variables. We begin by expressing the observables F_L, $F_\parallel$, $F_\perp$, A_4, A_5, A_{FB}, A_7, A_8 and A_9 in terms of $\widehat{C}_{10}$, r_λ, $\mathcal{F}_\lambda$ and ε_λ as follows:

$$F_L\Gamma_f = 2\mathcal{F}_0^2(r_0^2 + \widehat{C}_{10}^2) + 2\varepsilon_0^2, \tag{4.2.3}$$

$$F_\parallel\Gamma_f = 2\mathcal{F}_\parallel^2(r_\parallel^2 + \widehat{C}_{10}^2) + 2\varepsilon_\parallel^2, \tag{4.2.4}$$

$$F_\perp\Gamma_f = 2\mathcal{F}_\perp^2(r_\perp^2 + \widehat{C}_{10}^2) + 2\varepsilon_\perp^2, \tag{4.2.5}$$

$$\sqrt{2}\pi A_4\Gamma_f = 4\mathcal{F}_0\mathcal{F}_\parallel(r_0 r_\parallel + \widehat{C}_{10}^2) + 4\varepsilon_0\varepsilon_\parallel, \tag{4.2.6}$$

$$\sqrt{2}A_5\Gamma_f = 3\mathcal{F}_0\mathcal{F}_\perp\widehat{C}_{10}(r_0 + r_\perp), \tag{4.2.7}$$

$$A_{\mathrm{FB}}\Gamma_f = 3\mathcal{F}_\parallel\mathcal{F}_\perp\widehat{C}_{10}(r_\parallel + r_\perp), \tag{4.2.8}$$

$$\sqrt{2}A_7\Gamma_f = 3\widehat{C}_{10}(\mathcal{F}_0\varepsilon_\parallel - \mathcal{F}_\parallel\varepsilon_0), \tag{4.2.9}$$

$$\pi A_8\Gamma_f = 2\sqrt{2}(\mathcal{F}_0 r_0\varepsilon_\perp - \mathcal{F}_\perp r_\perp\varepsilon_0), \tag{4.2.10}$$

$$\pi A_9\Gamma_f = 3(\mathcal{F}_\perp r_\perp\varepsilon_\parallel - \mathcal{F}_\parallel r_\parallel\varepsilon_\perp). \tag{4.2.11}$$

One immediately concludes that

$$2\frac{\varepsilon_0^2}{\Gamma_f} \leq F_L, \tag{4.2.12}$$

$$2\frac{\varepsilon_{\parallel}^2}{\Gamma_f} \leq F_{\parallel}, \tag{4.2.13}$$

$$2\frac{\varepsilon_{\perp}^2}{\Gamma_f} \leq F_{\perp}. \tag{4.2.14}$$

Equations (4.2.3)–(4.2.8) can be easily transformed to the form in Ref. [27] by the redefinition of the observables F_L, $F_{\parallel}$, $F_{\perp}$ and A_4 as

$$F'_{\lambda} = F_{\lambda} - \frac{2\varepsilon_{\lambda}^2}{\Gamma_f}, \tag{4.2.15}$$

$$A'_4 = A_4 - \frac{2\sqrt{2}\varepsilon_0\varepsilon_{\parallel}}{\pi\Gamma_f}. \tag{4.2.16}$$

It should be noted that $F'_L + F'_{\parallel} + F'_{\perp} \leq 1$. Since only the ratios of the form factors $\mathcal{F}_{\lambda}$ play a role in the relations we wish to derive we define ratios of form factors P_1, P_2 and P_3:

$$\mathsf{P}_1 = \frac{\mathcal{F}_{\perp}}{\mathcal{F}_{\parallel}}, \tag{4.2.17}$$

$$\mathsf{P}_2 = \frac{\mathcal{F}_{\perp}}{\mathcal{F}_0}, \tag{4.2.18}$$

$$\mathsf{P}_3 = \frac{\mathcal{F}_{\perp}}{\mathcal{F}_0 + \mathcal{F}_{\parallel}} \equiv \frac{\mathsf{P}_1\mathsf{P}_2}{\mathsf{P}_1 + \mathsf{P}_2}. \tag{4.2.19}$$

Following these redefinitions Eqs. (4.2.3)–(4.2.8) can be recast into three sets of equations just as done in Ref. [27]. The three sets of equation are:

◇ **Set-I**

$$F'_{\parallel}\Gamma_f = 2\frac{\mathcal{F}_{\perp}^2}{\mathsf{P}_1^2}(r_{\parallel}^2 + \widehat{C}_{10}^2) \tag{4.2.20}$$

$$F'_{\perp}\Gamma_f = 2\mathcal{F}_{\perp}^2(r_{\perp}^2 + \widehat{C}_{10}^2) \tag{4.2.21}$$

$$A_{\rm FB}\Gamma_f = 3\frac{\mathcal{F}_{\perp}^2}{\mathsf{P}_1}\widehat{C}_{10}(r_{\parallel} + r_{\perp}) \tag{4.2.22}$$

◇ **Set-II**

$$F'_L\Gamma_f = 2\frac{\mathcal{F}_\perp^2}{\mathsf{P}_2^2}(r_0^2 + \widehat{C}_{10}^2) \tag{4.2.23}$$

$$F'_\perp\Gamma_f = 2\mathcal{F}_\perp^2(r_\perp^2 + \widehat{C}_{10}^2) \tag{4.2.24}$$

$$\sqrt{2}A_5\Gamma_f = 3\frac{\mathcal{F}_\perp^2}{\mathsf{P}_2}\widehat{C}_{10}(r_0 + r_\perp) \tag{4.2.25}$$

◇ **Set-III**

$$(F'_L + F'_\parallel + \sqrt{2}\pi A'_4)\Gamma_f = 2\frac{\mathcal{F}_\perp^2}{\mathsf{P}_3^2}(r_\wedge^2 + \widehat{C}_{10}^2) \tag{4.2.26}$$

$$F'_\perp\Gamma_f = 2\mathcal{F}_\perp^2(r_\perp^2 + \widehat{C}_{10}^2) \tag{4.2.27}$$

$$(A_{\rm FB} + \sqrt{2}A_5)\Gamma_f = 3\frac{\mathcal{F}_\perp^2}{\mathsf{P}_3}\widehat{C}_{10}(r_\wedge + r_\perp) \tag{4.2.28}$$

In the above we have defined $r_\wedge$ as

$$r_\wedge = \frac{r_\parallel \mathsf{P}_2 + r_0\mathsf{P}_1}{\mathsf{P}_2 + \mathsf{P}_1}, \tag{4.2.29}$$

Of the nine equations defined in the three sets only six of them are independent. These are the three equations Eqs. (4.2.20)–(4.2.22) in Set-I, two equations (4.2.23) and (4.2.25) from Set-II and Eq. (4.2.26) of Set-III. It is easy to see that Set-II and Set-III can be obtained from Set-I by the following replacements:

- **Set-II from Set-I**

  $F'_\parallel \to F'_L$, $A_{\rm FB} \to \sqrt{2}A_5$, $r_\parallel \to r_0$ and $\mathsf{P}_1 \to \mathsf{P}_2$ (or $\mathcal{F}_\parallel \to \mathcal{F}_0$).

- **Set-III from Set-I**

  $F'_\parallel \to F'_L + F'_\parallel + \sqrt{2}\pi A'_4$, $A_{\rm FB} \to A_{\rm FB} + \sqrt{2}A_5$, $r_\parallel \to r_\wedge$ and $\mathsf{P}_1 \to \mathsf{P}_3$ (or $\mathcal{F}_\parallel \to \mathcal{F}_\parallel + \mathcal{F}_0$).

It is obvious that we only need to solve Set-I to obtain $r_\parallel$ and $r_\perp$ in terms of P_1, $F'_\parallel$, $F'_\perp$ and $A_{\rm FB}$. The solutions to Set-II and Set-III can be obtained by simple replacements.

The solution of Set-I gives (from appendix. A.2)

$$r_{\parallel} = \pm\frac{\sqrt{\Gamma_f}}{\sqrt{2}\mathcal{F}_\perp}\frac{(\mathsf{P}_1^2 F'_{\parallel} + \frac{1}{2}\mathsf{P}_1 Z'_1)}{\sqrt{\mathsf{P}_1^2 F'_{\parallel} + F'_\perp + \mathsf{P}_1 Z'_1}}, \tag{4.2.30}$$

$$r_{\perp} = \pm\frac{\sqrt{\Gamma_f}}{\sqrt{2}\mathcal{F}_\perp}\frac{(F'_{\perp} + \frac{1}{2}\mathsf{P}_1 Z'_1)}{\sqrt{\mathsf{P}_1^2 F'_{\parallel} + F'_\perp + \mathsf{P}_1 Z'_1}}, \tag{4.2.31}$$

where Z'_1 is defined as,

$$Z'_1 = \sqrt{4F'_{\parallel}F'_{\perp} - \frac{16}{9}A_{\rm FB}^2}. \tag{4.2.32}$$

The solution to Set-II is now easily seen to be

$$r_0 = \pm\frac{\sqrt{\Gamma_f}}{\sqrt{2}\mathcal{F}_\perp}\frac{(\mathsf{P}_2^2 F'_{L} + \frac{1}{2}\mathsf{P}_2 Z'_2)}{\sqrt{\mathsf{P}_2^2 F'_{L} + F'_\perp + \mathsf{P}_2 Z'_2}}, \tag{4.2.33}$$

$$r_{\perp} = \pm\frac{\sqrt{\Gamma_f}}{\sqrt{2}\mathcal{F}_\perp}\frac{(F'_{\perp} + \frac{1}{2}\mathsf{P}_2 Z'_2)}{\sqrt{\mathsf{P}_2^2 F'_{L} + F'_\perp + \mathsf{P}_2 Z'_2}}, \tag{4.2.34}$$

with Z'_2 defined as,

$$Z'_2 = \sqrt{4F'_L F'_{\perp} - \frac{32}{9}A_5^2}. \tag{4.2.35}$$

On comparing the solutions for $r_\perp$ in Eqs. (4.2.31) and (4.2.34) obtained from Set-I and Set-II respectively, we obtain a relation for P_2 in terms of P_1 and observables to be

$$\mathsf{P}_2 = \frac{2\mathsf{P}_1 A_{\rm FB} F'_\perp}{s\sqrt{2}A_5(2F'_\perp + Z'_1\mathsf{P}_1) - Z'_2\mathsf{P}_1 A_{\rm FB}}, \tag{4.2.36}$$

with $s \in \{-1, +1\}$. To remove the ambiguities in the P_2 solution let us divide Eq. (4.2.25) by Eq. (4.2.22) and using Eqs. (4.2.30) – (4.2.34) we get

$$\begin{aligned}\frac{\sqrt{2}A_5}{A_{\rm FB}} &= \frac{\mathsf{P}_1}{\mathsf{P}_2}\frac{\sqrt{\mathsf{P}_2^2 F'_L + F'_\perp + \mathsf{P}_2 Z'_2}}{\sqrt{\mathsf{P}_1^2 F'_{\parallel} + F'_\perp + \mathsf{P}_1 Z'_1}} \\ &= \frac{\mathsf{P}_1}{\mathsf{P}_2}\frac{(2F'_\perp + \mathsf{P}_2 Z'_2)}{(2F'_\perp + \mathsf{P}_1 Z'_1)}.\end{aligned} \tag{4.2.37}$$

Substituting it in Eq. (4.2.36) we have

$$s(2F'_\perp + \mathsf{P}_2 Z'_2) - Z'_2 \mathsf{P}_2 = 2F'_\perp,$$

which is valid for the whole q^2 region only for $s = 1$.

Finally we write the $r_\perp$ solution obtained from Set-III:

$$r_\perp = \pm \frac{\sqrt{\Gamma_f}}{\sqrt{2}\mathcal{F}_\perp} \frac{(F'_\perp + \frac{1}{2}\mathsf{P}_3 Z'_3)}{\sqrt{\mathsf{P}_3^2(F'_\parallel + F'_L + \sqrt{2}\pi A'_4) + F'_\perp + \mathsf{P}_3 Z'_3}}, \tag{4.2.38}$$

where Z'_3 is defined as,

$$Z'_3 = \sqrt{4(F'_L + F'_\parallel + \sqrt{2}\pi A'_4)F'_\perp - \frac{16}{9}(A_{\rm FB} + \sqrt{2}A_5)^2}. \tag{4.2.39}$$

Analogous comparison of solutions for $r_\perp$ in Eqs. (4.2.31) and (4.2.38) obtained from Set-I and Set-III respectively, results in a relation for P_3 in terms of P_1:

$$\mathsf{P}_3 = \frac{2\mathsf{P}_1 A_{\rm FB} F'_\perp}{(A_{\rm FB} + \sqrt{2}A_5)(2F'_\perp + Z'_1 \mathsf{P}_1) - Z'_3 \mathsf{P}_1 A_{\rm FB}}. \tag{4.2.40}$$

The ambiguity in the P_3 solution is also taken to be positive for the same reason as the P_2 solution. The form-factor ratio P_3 is not however independent of P_1 and P_2 and is related by Eq. (4.2.19). Substituting Eqs. (4.2.36) and (4.2.40) in Eq. (4.2.19) we obtain the relation between the observables as:

$$Z'_3 = Z'_1 + Z'_2. \tag{4.2.41}$$

The relations derived so far involve the primed observables that depend on $\varepsilon_\perp$, $\varepsilon_\parallel$ and ε_0.

However, the ε_λ's can be solved using A_7, A_8 and A_9 from Eqs. (4.2.9)–(4.2.11) to give

$$\varepsilon_\perp = \frac{\sqrt{2}\pi\Gamma_f}{(r_0 - r_\parallel)\mathcal{F}_\perp}\left[\frac{A_9\mathsf{P}_1}{3\sqrt{2}} + \frac{A_8\mathsf{P}_2}{4} - \frac{A_7\mathsf{P}_1\mathsf{P}_2 r_\perp}{3\pi\widehat{C}_{10}}\right], \tag{4.2.42}$$

$$\varepsilon_\parallel = \frac{\sqrt{2}\pi\Gamma_f}{(r_0 - r_\parallel)\mathcal{F}_\perp}\left[\frac{A_9 r_0}{3\sqrt{2}r_\perp} + \frac{A_8\mathsf{P}_2 r_\parallel}{4\mathsf{P}_1 r_\perp} - \frac{A_7\mathsf{P}_2 r_\parallel}{3\pi\widehat{C}_{10}}\right], \tag{4.2.43}$$

$$\varepsilon_0 = \frac{\sqrt{2}\pi\Gamma_f}{(r_0 - r_\parallel)\mathcal{F}_\perp}\left[\frac{A_9\mathsf{P}_1 r_0}{3\sqrt{2}\mathsf{P}_2 r_\perp} + \frac{A_8 r_\parallel}{4r_\perp} - \frac{A_7\mathsf{P}_1 r_0}{3\pi\widehat{C}_{10}}\right]. \tag{4.2.44}$$

A point to be noted that the $(\varepsilon_\lambda/\Gamma_f^{1/2})$'s are free from the form factor $\mathcal{F}_\perp$ and Γ_f as can easily be seen from the expressions for $r_\parallel$, $r_\perp$ and r_0 (Eqs. (4.2.30), (4.2.31) and (4.2.33)), as well as $\widehat{C}_{10}$ derived in Eq. (A.2.12). Indeed, since P_2 can be expressed in terms P_1 and observables using Eq. (4.2.36), it is easy to see that *each of the ε_λ's are completely expressed in terms of observables and the form-factor ratio* P_1. However, these solutions are essentially iterative, since the r_λ's and $\widehat{C}_{10}$ are derived in terms of the primed observables that depend on ε_λ. If the $(\varepsilon_\lambda/\Gamma_f^{1/2})$ are small as should be expected, accurate solutions for them can be found with a few iterations.

Solving for A_4 from Eq. (4.2.41) the relation among the observables is,

$$\begin{aligned} A_4 = {} & \frac{2\sqrt{2}\varepsilon_\parallel\varepsilon_0}{\pi\Gamma_f} + \frac{8A_5A_{\rm FB}}{9\pi\left(F_\perp - \dfrac{2\varepsilon_\perp^2}{\Gamma_f}\right)} \\ & + \sqrt{2}\,\frac{\sqrt{\left(F_L - \dfrac{2\varepsilon_0^2}{\Gamma_f}\right)\left(F_\perp - \dfrac{2\varepsilon_\perp^2}{\Gamma_f}\right) - \dfrac{8}{9}A_5^2}\;\sqrt{\left(F_\parallel - \dfrac{2\varepsilon_\parallel^2}{\Gamma_f}\right)\left(F_\perp - \dfrac{2\varepsilon_\perp^2}{\Gamma_f}\right) - \dfrac{4}{9}A_{\rm FB}^2}}{\pi\left(F_\perp - \dfrac{2\varepsilon_\perp^2}{\Gamma_f}\right)}. \end{aligned} \tag{4.2.45}$$

This relation for A_4 in terms of other observables F_L, $F_\perp$, A_5, $A_{\rm FB}$, A_7, A_8 and A_9 is a generalization of the relation derived in Ref. [27]. A point to be noted is that while we have solved for the observable A_4, we could have used Eq. (4.2.41) to derive an expression for any of the other observable. However, only the solution for A_4 is unique and hence the

one we consider. The validity of this relation is a test of the consistency of the values of all measured observables. Unlike the expression obtained in Ref. [27], we now have a relation between observables that depends on only one hadronic parameter, the ratio of form factors P_1. It is interesting to note that P_1 does not receive nonfactorizable contributions and is uncorrected by charm loop effects. Since, P_1 is independent of the universal wave functions [4, 49] in HQET, it can be reliably calculated as an expansion in both the strong coupling constant α_s and $\Lambda_{\rm QCD}/m_b$. The dependence of A_4 on P_1 is rather weak, since the observables A_7, A_8 and A_9 are observed to be small and are currently consistent with zero as expected [41]. If A_7, A_8 and A_9 are all observed to be zero, it is easy to see from Eqs. (4.2.42)–(4.2.44) that $\varepsilon_\perp = \varepsilon_\parallel = \varepsilon_0 = 0$ reducing the relation in Eq. (4.2.45) to

$$A_4 = \frac{8A_5A_{\rm FB}}{9\pi F_\perp} + \sqrt{2}\,\frac{\sqrt{F_LF_\perp - \frac{8}{9}A_5^2}\,\sqrt{F_\parallel F_\perp - \frac{4}{9}A_{\rm FB}^2}}{\pi F_\perp} \tag{4.2.46}$$

which was derived in Ref. [27]. Interestingly, in the limit of vanishing imaginary contributions, A_4 can be expressed purely in terms of observables and is free from any form factor or their ratio. In appendix. A.1 it is shown that both P_1 and P_2 are always negative. An interesting observation that $A_{\rm FB}$ and A_5 always have same signs can be then made from the relation in Eq. (4.2.37). Hence, we can arrive to a conclusion that, from Eq. (4.2.45) the observable A_4 is always positive unless the term proportional to $\varepsilon_\parallel\varepsilon_0$ is negative and it dominates over the rest of the terms in the expression.

A_4 is an observable and hence must always be real. This places constraints on the arguments of the radicals, which are directly related to the fact that Z_1', Z_2' and Z_3' are all real. The constraint that Z_1' is real in turn implies that

$$F_\parallel F_\perp - \frac{4}{9}A_{\rm FB}^2 \geq F_\parallel F_\perp\Big(\frac{2\varepsilon_\parallel^2}{\Gamma_f F_\parallel} + \frac{2\varepsilon_\perp^2}{\Gamma_f F_\perp} - \frac{4\varepsilon_\parallel^2\varepsilon_\perp^2}{\Gamma_f^2 F_\parallel F_\perp}\Big). \tag{4.2.47}$$

In Eqs. (4.2.12)– (4.2.14), we showed that $0 \leq \dfrac{2\varepsilon_\lambda^2}{\Gamma_f F_\lambda} \leq 1$, implying that the rhs of

Eq. (4.2.47) must itself be greater than zero. This imposes the following constraint:

$$F_{\parallel}F_{\perp} - \frac{4}{9}A_{\rm FB}^2 \geq 0. \tag{4.2.48}$$

A similar constraint arising from Z_2' and Z_3' also being real implies that

$$F_L F_{\perp} - \frac{8}{9}A_5^2 \geq 0, \tag{4.2.49}$$

$$(F_L + F_{\parallel} + \sqrt{2}\pi A_4)F_{\perp} - \frac{4}{9}(A_{\rm FB} + \sqrt{2}A_5)^2 \geq 0. \tag{4.2.50}$$

The equality in the above three relations holds only when a minimum of two of the ε_λ's are zero. For example, $\varepsilon_{\parallel}$ and $\varepsilon_{\perp}$ are zero for the equality to hold in Eq. (4.2.48), whereas ε_0 and $\varepsilon_{\perp}$ are zero for Eq. (4.2.49). The three inequalities in Eqs. (4.2.48)–(4.2.50) impose constraints on the parameter space of observables. It is obvious that nonzero ε_λ's will in general restrict the parameter space of observables even further. We emphasize that this conclusion is valid without any exception. We will come back to this point in Sec. 4.5 when we discuss the tests of the relation for A_4 in Eq. (4.2.45).

4.3 Generalization to include lepton masses.

In this section we extend the model independent approach developed in the previous section (Sec. 4.2) to include the lepton mass m. One of the consequences of retaining the lepton mass is the need to include an additional amplitude in order to describe the full decay rate, since the term proportional to q_μ in the amplitude cannot be dropped for the massive lepton case (for a review [30]). In addition to the six amplitude $\mathcal{A}_\lambda^{L,R}$ where $\lambda \in \{0, \parallel, \perp\}$ the decay amplitude also depends on $\mathcal{A}_t$, resulting in a total of seven amplitudes. These amplitudes are given in Eqs. (3.3.3a) – (3.3.3d). In addition, since the massive leptons are no longer chirality eigenstates, terms involving admixtures of helicities that are proportional to m^2/q^2 (see Eqs. (3.3.2a) and (3.3.2b)) contribute to the

differential decay rate.

These additional contributions complicate the extraction of the helicity amplitudes. The observables F_L, $F_\parallel$, $F_\perp$, A_4, A_5 and $A_{\rm FB}$ given in Sec. 4.2 are modified because of the presence of the new transversity amplitude $\mathcal{A}_t$ and helicity admixture terms in the decay distribution. This in turn results in modifying the relations in Eqs. (4.2.45) and (4.2.46). The effect of the mass of the lepton is always included in the measured observables and it is not possible to measure any observable without the mass effects. In order to distinguish the "hypothetical observables without the mass effects" considered in Sec. 4.2 from these true observables, we define them with a superscript "o" and relate to the massless limit observables as:

$$\Gamma_f^{\rm o} = \beta^2\Gamma_f + 3\mathbb{T}_1, \tag{4.3.1a}$$

$$F_L^{\rm o} = \frac{1}{\Gamma_f^{\rm o}}(\beta^2\Gamma_f F_L + \mathbb{T}_1), \tag{4.3.1b}$$

$$F_\parallel^{\rm o} = \frac{1}{\Gamma_f^{\rm o}}(\beta^2\Gamma_f F_\parallel + \mathbb{T}_1), \tag{4.3.1c}$$

$$F_\perp^{\rm o} = \frac{1}{\Gamma_f^{\rm o}}(\beta^2\Gamma_f F_\perp + \mathbb{T}_1), \tag{4.3.1d}$$

$$A_4^{\rm o} = \frac{\Gamma_f}{\Gamma_f^{\rm o}}\beta^2 A_4, \tag{4.3.1e}$$

$$A_5^{\rm o} = \frac{\Gamma_f}{\Gamma_f^{\rm o}}\beta A_5, \tag{4.3.1f}$$

$$A_{\rm FB}^{\rm o} = \frac{\Gamma_f}{\Gamma_f^{\rm o}}\beta A_{\rm FB}, \tag{4.3.1g}$$

$$A_7^{\rm o} = \frac{\Gamma_f}{\Gamma_f^{\rm o}}\beta A_7, \tag{4.3.1h}$$

$$A_8^{\rm o} = \frac{\Gamma_f}{\Gamma_f^{\rm o}}\beta^2 A_8, \tag{4.3.1i}$$

$$A_9^{\rm o} = \frac{\Gamma_f}{\Gamma_f^{\rm o}}\beta^2 A_9. \tag{4.3.1j}$$

In the above we have defined

$$\mathbb{T}_1 = (1 + E_1)\,\frac{m^2}{q^2}\Gamma_f \;\text{ where}$$
$$E_1 = \frac{|\mathcal{A}_t|^2}{\Gamma_f} + \frac{2}{\Gamma_f}\mathrm{Re}[\mathcal{A}_\parallel^L \mathcal{A}_\parallel^{R^*} + \mathcal{A}_\perp^L \mathcal{A}_\perp^{R^*} + \mathcal{A}_0^L \mathcal{A}_0^{R^*}].$$

Using

$$2\,\mathrm{Re}[\mathcal{A}_\lambda^L \mathcal{A}_\lambda^{R^*}] = |\mathcal{A}_\lambda^L + \mathcal{A}_\lambda^R|^2 - \Gamma_f F_\lambda$$

and the Cauchy-Schwarz inequality, we find

$$\mathbb{T}_1 = (|\mathcal{A}_t|^2 + \sum_{\lambda=\{\parallel,\perp,0\}} |\mathcal{A}_\lambda^L + \mathcal{A}_\lambda^R|^2)\frac{m^2}{q^2} \tag{4.3.2}$$
$$\leq (|\mathcal{A}_t|^2 + 2\Gamma_f)\frac{m^2}{q^2} \tag{4.3.3}$$

which is always positive and bounded. This bound is important since $\mathbb{T}_1$ has not been measured so far. $\mathbb{T}_1$ can also be expressed in terms of angular coefficients as,

$$\frac{\mathbb{T}_1}{\Gamma_f^o} = \frac{1}{3} - \frac{4I_2^s - I_2^c}{3\Gamma_f^o}$$
$$= \frac{1}{3} - \frac{16}{9}A_{10} + \frac{64}{27}A_{11} \tag{4.3.4}$$

and measured in terms of two new observables A_{10} and A_{11}, defined in terms of angular asymmetries as follows:

$$A_{10} = \frac{\displaystyle\int_0^{2\pi} d\phi \int_0^1 d\cos\theta_K \Big[\int_{-1}^{-1/2} - \int_{-1/2}^{1/2} + \int_{1/2}^{1}\Big] d\cos\theta_\ell \, \frac{d^4(\Gamma + \bar{\Gamma})}{dq^2 d\cos\theta_\ell d\cos\theta_K d\phi}}{\displaystyle\int_0^{2\pi} d\phi \int_{-1}^1 d\cos\theta_K \int_{-1}^1 d\cos\theta_\ell \, \frac{d^4(\Gamma + \bar{\Gamma})}{dq^2 d\cos\theta_\ell d\cos\theta_K d\phi}}, \tag{4.3.5}$$

$$A_{11} = \frac{\int_0^{2\pi} d\phi \Big[\int_{-1}^{-1/2} - \int_{-1/2}^{1/2} + \int_{1/2}^{1}\Big] d\cos\theta_K \Big[\int_{-1}^{-1/2} - \int_{-1/2}^{1/2} + \int_{1/2}^{1}\Big] d\cos\theta_\ell \, \frac{d^4(\Gamma+\bar{\Gamma})}{dq^2 d\cos\theta_\ell d\cos\theta_K d\phi}}{\int_0^{2\pi} d\phi \int_{-1}^{1} d\cos\theta_K \int_{-1}^{1} d\cos\theta_\ell \, \frac{d^4(\Gamma+\bar{\Gamma})}{dq^2 d\cos\theta_\ell d\cos\theta_K d\phi}}. \tag{4.3.6}$$

If the two asymmetries A_{10} and A_{11} are measured experimentally then we can get the estimate of the correction term arising due to lepton masses. However, from Eq. (4.3.2) it can be seen that $\mathbb{T}_1$ is proportional to lepton mass (square) m^2/q^2 which is very small and difficult to measure except at small q^2. In the limit of zero lepton mass $\mathbb{T}_1$ vanishes which gives a constraint on these two observables by,

$$A_{10} - \frac{4}{3}A_{11} = \frac{3}{16}. \tag{4.3.7}$$

A deviation from this relation would indicate the effect of the nonzero lepton mass and provide an estimate of the size the mass corrections. The observables are re-expressed in terms of the variables r_λ (defined in Eq. (4.2.1)) as follows:

$$F_L^o \Gamma_f^o = 2\beta^2 \frac{\mathcal{F}_\perp^2}{\mathsf{P}_2^2}(r_0^2 + \widehat{C}_{10}^2) + 2\beta^2\varepsilon_0^2 + \mathbb{T}_1, \tag{4.3.8}$$

$$F_\parallel^o \Gamma_f^o = 2\beta^2 \frac{\mathcal{F}_\perp^2}{\mathsf{P}_1^2}(r_\parallel^2 + \widehat{C}_{10}^2) + 2\beta^2\varepsilon_\parallel^2 + \mathbb{T}_1, \tag{4.3.9}$$

$$F_\perp^o \Gamma_f^o = 2\beta^2 \mathcal{F}_\perp^2(r_\perp^2 + \widehat{C}_{10}^2) + 2\beta^2\varepsilon_\perp^2 + \mathbb{T}_1, \tag{4.3.10}$$

$$\sqrt{2}\pi A_4^o \Gamma_f^o = 4\beta^2 \frac{\mathcal{F}_\perp^2}{\mathsf{P}_1\mathsf{P}_2}(r_0 r_\parallel + \widehat{C}_{10}^2) + 4\beta^2\varepsilon_0\varepsilon_\parallel, \tag{4.3.11}$$

$$\sqrt{2}A_5^o \Gamma_f^o = 3\beta \frac{\mathcal{F}_\perp^2}{\mathsf{P}_2}\widehat{C}_{10}(r_0 + r_\perp), \tag{4.3.12}$$

$$A_{\rm FB}^o \Gamma_f^o = 3\beta \frac{\mathcal{F}_\perp^2}{\mathsf{P}_1}\widehat{C}_{10}(r_\parallel + r_\perp), \tag{4.3.13}$$

$$\sqrt{2}A_7^o \Gamma_f^o = 3\beta\widehat{C}_{10}(\mathcal{F}_0\varepsilon_\parallel - \mathcal{F}_\parallel\varepsilon_0), \tag{4.3.14}$$

$$\pi A_8^o \Gamma_f^o = 2\sqrt{2}\beta^2(\mathcal{F}_0 r_0 \varepsilon_\perp - \mathcal{F}_\perp r_\perp \varepsilon_0), \tag{4.3.15}$$

$$\pi A_9^o \Gamma_f^o = 3\beta^2(\mathcal{F}_\perp r_\perp \varepsilon_\parallel - \mathcal{F}_\parallel r_\parallel \varepsilon_\perp). \tag{4.3.16}$$

In analogy with the previous solutions of P_2 and P_3 in Eqs. (4.2.36) and (4.2.40) using the three sets (Set-I, II, III) we can solve for P_2 and P_3 once again in terms of P_1 and "true observables" as,

$$\mathsf{P}_2 = \frac{2\mathsf{P}_1 A_{\rm FB}^{\rm o}(F_\perp^{\rm o} - \frac{\mathcal{T}_\perp}{\Gamma_f^{\rm o}})}{\sqrt{2}A_5^{\rm o}\Big(2(F_\perp^{\rm o} - \frac{\mathcal{T}_\perp}{\Gamma_f^{\rm o}}) + Z_1^{\rm o}\mathsf{P}_1\Big) - Z_2^{\rm o}\mathsf{P}_1 A_{\rm FB}^{\rm o}}, \tag{4.3.17}$$

$$\mathsf{P}_3 = \frac{2\mathsf{P}_1 A_{\rm FB}^{\rm o}(F_\perp^{\rm o} - \frac{\mathcal{T}_\perp}{\Gamma_f^{\rm o}})}{(A_{\rm FB}^{\rm o} + \sqrt{2}A_5^{\rm o})\Big(2(F_\perp^{\rm o} - \frac{\mathcal{T}_\perp}{\Gamma_f^{\rm o}}) + Z_1^{\rm o}\mathsf{P}_1\Big) - Z_3^{\rm o}\mathsf{P}_1 A_{\rm FB}^{\rm o}}, \tag{4.3.18}$$

where positive sign ambiguity is chosen for P_2 and P_3 solutions because of the same reason discussed in the massless case. The definitions of $Z_1^{\rm o}$, $Z_2^{\rm o}$ and $Z_3^{\rm o}$ are given by

$$Z_1^{\rm o} = \sqrt{4(F_\parallel^{\rm o} - \frac{\mathcal{T}_\parallel}{\Gamma_f^{\rm o}})(F_\perp^{\rm o} - \frac{\mathcal{T}_\perp}{\Gamma_f^{\rm o}}) - \frac{16}{9}\beta^2 A_{\rm FB}^{\rm o2}}, \tag{4.3.19}$$

$$Z_2^{\rm o} = \sqrt{4(F_L^{\rm o} - \frac{\mathcal{T}_0}{\Gamma_f^{\rm o}})(F_\perp^{\rm o} - \frac{\mathcal{T}_\perp}{\Gamma_f^{\rm o}}) - \frac{32}{9}\beta^2 A_5^{\rm o2}}, \tag{4.3.20}$$

$$Z_3^{\rm o} = \sqrt{4\Big((F_L^{\rm o} - \frac{\mathcal{T}_0}{\Gamma_f^{\rm o}}) + (F_\parallel^{\rm o} - \frac{\mathcal{T}_\parallel}{\Gamma_f^{\rm o}}) + \sqrt{2}\pi A_4^{\rm o} - \frac{4\beta^2\varepsilon_0\varepsilon_\parallel}{\Gamma_f^{\rm o}}\Big)(F_\perp^{\rm o} - \frac{\mathcal{T}_\perp}{\Gamma_f^{\rm o}}) - \frac{16}{9}\beta^2(A_{\rm FB}^{\rm o} + \sqrt{2}A_5^{\rm o})^2}. \tag{4.3.21}$$

To simplify notation we have defined

$$\mathcal{T}_\lambda = \mathbb{T}_1 + 2\beta^2\varepsilon_\lambda^2\,; \qquad \lambda \in \{0, \perp, \|\} \tag{4.3.22}$$

Substituting Eqs. (4.3.17) and (4.3.18) in Eq.(4.2.19) we can get the condition valid over whole q^2 range as:

$$Z_3^{\rm o} = Z_1^{\rm o} + Z_2^{\rm o}. \tag{4.3.23}$$

The ε_λ's can be solved as was done in the previous section using Eqs. (4.3.14)–(4.3.16) to give

$$\varepsilon_\perp = \frac{\sqrt{2}\pi\Gamma_f^o}{\beta^2(r_0-r_\parallel)\mathcal{F}_\perp}\left[\frac{A_9^o \mathsf{P}_1}{3\sqrt{2}} + \frac{A_8^o \mathsf{P}_2}{4} - \frac{A_7^o \beta \mathsf{P}_1 \mathsf{P}_2 r_\perp}{3\pi \widehat{C}_{10}}\right], \tag{4.3.24}$$

$$\varepsilon_\parallel = \frac{\sqrt{2}\pi\Gamma_f^o}{\beta^2(r_0-r_\parallel)\mathcal{F}_\perp}\left[\frac{A_9^o r_0}{3\sqrt{2} r_\perp} + \frac{A_8^o \mathsf{P}_2 r_\parallel}{4\mathsf{P}_1 r_\perp} - \frac{A_7^o \beta \mathsf{P}_2 r_\parallel}{3\pi \widehat{C}_{10}}\right], \tag{4.3.25}$$

$$\varepsilon_0 = \frac{\sqrt{2}\pi\Gamma_f^o}{\beta^2(r_0-r_\parallel)\mathcal{F}_\perp}\left[\frac{A_9^o \mathsf{P}_1 r_0}{3\sqrt{2}\mathsf{P}_2 r_\perp} + \frac{A_8^o r_\parallel}{4 r_\perp} - \frac{A_7^o \beta \mathsf{P}_1 r_0}{3\pi \widehat{C}_{10}}\right]. \tag{4.3.26}$$

From Eqs. (A.2.10) – (A.2.12) it can be easily seen that the $(\varepsilon_\lambda/\Gamma_f^{o\,1/2})$'s are free from the form-factor $\mathcal{F}_\perp$ and Γ_f^o *and are completely expressed in terms of observables and the form-factor ratio* P_1. However the accurate solutions of $(\varepsilon_\lambda/\Gamma_f^{o\,1/2})$'s can be found with a few iterations as described in the previous massless case.

Solving for A_4^o from Eq. (4.3.23) the relation among the observables including lepton masses turns out

$$A_4^o = \frac{2\sqrt{2}\beta^2\varepsilon_\parallel\varepsilon_0}{\pi\Gamma_f^o} + \frac{8\beta^2 A_5^o A_{\rm FB}^o}{9\pi(F_\perp^o - \frac{\mathcal{T}_\perp}{\Gamma_f^o})} + \sqrt{2}\,\frac{\sqrt{(F_L^o - \frac{\mathcal{T}_0}{\Gamma_f^o})(F_\perp^o - \frac{\mathcal{T}_\perp}{\Gamma_f^o}) - \frac{8}{9}\beta^2 A_5^{o2}}\,\sqrt{(F_\parallel^o - \frac{\mathcal{T}_\parallel}{\Gamma_f^o})(F_\perp^o - \frac{\mathcal{T}_\perp}{\Gamma_f^o}) - \frac{4}{9}\beta^2 A_{\rm FB}^{o2}}}{\pi(F_\perp^o - \frac{\mathcal{T}_\perp}{\Gamma_f^o})}. \tag{4.3.27}$$

In analogy to the massless case, each of Z_1^o, Z_2^o and Z_3^o are also real. A real Z_1^o implies that

$$F_\parallel^o F_\perp^o - \frac{4}{9}A_{\rm FB}^{o2} \geq F_\parallel^o F_\perp^o\left(\frac{\mathcal{T}_\parallel}{\Gamma_f^o F_\parallel^o} + \frac{\mathcal{T}_\perp}{\Gamma_f^o F_\perp^o} - \frac{\mathcal{T}_\parallel \mathcal{T}_\perp}{\Gamma_f^{o2} F_\parallel^o F_\perp^o}\right) - \frac{16 m^2 A_{\rm FB}^{o2}}{9\,q^2}. \tag{4.3.28}$$

Since, $0 \leq \dfrac{\mathcal{T}_\lambda}{\Gamma_f F_\lambda^o} \leq 1$ as can be seen from Eqs. (4.3.8)–(4.3.10), we can obtain a bound on

the lhs. of Eq. (4.3.28). The bounds arising from real Z_1^o, Z_2^o and Z_3^o are

$$F_\parallel^o F_\perp^o - \frac{4}{9}A_{\rm FB}^{o2} \geq -\frac{16m^2 A_{\rm FB}^{o2}}{9\,q^2}, \tag{4.3.29a}$$

$$F_L^o F_\perp^o - \frac{8}{9}A_5^{o2} \geq -\frac{32m^2 A_5^{o2}}{9\,q^2}, \tag{4.3.29b}$$

$$(F_L^o + F_\parallel^o + \sqrt{2}\pi A_4^o)F_\perp^o - \frac{4}{9}(A_{\rm FB}^o + \sqrt{2}A_5^o)^2 \geq -\frac{16m^2(A_{\rm FB}^o + \sqrt{2}A_5^o)^2}{9\,q^2} \tag{4.3.29c}$$

respectively. Clearly the lhs. of the above inequalities can, in the worst case, be a small negative number. Comparing this with the massless case we note that while the effect of the imaginary contributions is to restrict the parameter space further the effect of mass dependent terms is to oppose this restriction. The mass term should have the maximum effect at q^2 close to $4m^2$, but as we will see in the next section (Sec. 4.4) in the limit $q^2 \to 4\,m^2$ all the asymmetries approach zero. The contribution from the mass term should hence be insignificant, indicating that in practice the allowed parameter space of observables is not noticeably altered. This conclusion is borne out to be true in numerical estimates as we will see in Sec. 4.5. We conclude, therefore, that the most conservative allowed parameter space remains unaltered even if the small lepton mass term is dropped compared to q^2 and the imaginary contributions to the amplitudes are completely ignored.

The zero crossings of angular asymmetries $A_{\rm FB}^o$, A_5^o and $A_{\rm FB}^o + \sqrt{2}A_5^o$ provide interesting limits where the relation in Eq. (4.3.27) simplifies to three independent relations with each of them providing an interesting test for NP. At the zero crossing of $A_{\rm FB}^o$, A_5^o and $A_{\rm FB}^o + \sqrt{2}A_5^o$, Eq. (4.3.27) reduces to

$$\frac{8A_5^{o2}}{9(F_L^o - \frac{\mathcal{T}_0}{\Gamma_f^o})(F_\perp^o - \frac{\mathcal{T}_\perp}{\Gamma_f^o})} + \frac{\pi^2\Big(A_4^o - \frac{2\sqrt{2}\beta^2\varepsilon_\parallel\varepsilon_0}{\pi\Gamma_f^o}\Big)^2}{2(F_L^o - \frac{\mathcal{T}_0}{\Gamma_f^o})(F_\parallel^o - \frac{\mathcal{T}_\parallel}{\Gamma_f^o})} = 1\,, \tag{4.3.30a}$$

$$\frac{4A_{\rm FB}^{\rm o2}}{9(F_\parallel^{\rm o}-\frac{\mathcal{T}_\parallel}{\Gamma_f^{\rm o}})(F_\perp^{\rm o}-\frac{\mathcal{T}_\perp}{\Gamma_f^{\rm o}})}+\frac{\pi^2\Big(A_4^{\rm o}-\frac{2\sqrt{2}\beta^2\varepsilon_\parallel\varepsilon_0}{\pi\Gamma_f^{\rm o}}\Big)^2}{2(F_L^{\rm o}-\frac{\mathcal{T}_0}{\Gamma_f^{\rm o}})(F_\parallel^{\rm o}-\frac{\mathcal{T}_\parallel}{\Gamma_f^{\rm o}})}=1\,, \tag{4.3.30b}$$

$$\frac{2(A_{\rm FB}^{\rm o2}+2A_5^{\rm o2})\Big((F_L^{\rm o}-\frac{\mathcal{T}_0}{\Gamma_f^{\rm o}})+(F_\parallel^{\rm o}-\frac{\mathcal{T}_\parallel}{\Gamma_f^{\rm o}})+\sqrt{2}\pi A_4^{\rm o}-\frac{4\beta^2\varepsilon_0\varepsilon_\parallel}{\Gamma_f^{\rm o}}\Big)}{9(F_\parallel^{\rm o}-\frac{\mathcal{T}_\parallel}{\Gamma_f^{\rm o}})(F_L^{\rm o}-\frac{\mathcal{T}_0}{\Gamma_f^{\rm o}})(F_\perp^{\rm o}-\frac{\mathcal{T}_\perp}{\Gamma_f^{\rm o}})}+\frac{\pi^2\Big(A_4^{\rm o}-\frac{2\sqrt{2}\beta^2\varepsilon_\parallel\varepsilon_0}{\pi\Gamma_f^{\rm o}}\Big)^2}{2(F_L^{\rm o}-\frac{\mathcal{T}_0}{\Gamma_f^{\rm o}})(F_\parallel^{\rm o}-\frac{\mathcal{T}_\parallel}{\Gamma_f^{\rm o}})}=1\,, \tag{4.3.30c}$$

respectively. In the limit where both the mass effect and the imaginary contributions to the Wilson coefficients $\widehat{C_7}$ and $\widehat{C_9}$ can be ignored these relations simplify to depend only on observables

$$\begin{aligned}
&\frac{8A_5^2}{9F_LF_\perp}+\frac{\pi^2A_4^2}{2F_LF_\parallel}=1 && \text{if } A_{\rm FB}=0\,,\\
&\frac{4A_{\rm FB}^2}{9F_\parallel F_\perp}+\frac{\pi^2A_4^2}{2F_LF_\parallel}=1 && \text{if } A_5=0\,,\\
&\frac{2(A_{\rm FB}^2+2A_5^2)(F_L+F_\parallel+\sqrt{2}\pi A_4)}{9F_\parallel F_LF_\perp}+\frac{\pi^2A_4^2}{2F_LF_\parallel}=1 && \text{if } A_{\rm FB}+\sqrt{2}A_5=0\,.
\end{aligned} \tag{4.3.31}$$

The zero-crossings of these observables are also interesting as the form-factor ratios P_1, P_2 and P_3 can be related to the helicity fractions at those q^2 points. Eq. (4.3.13) implies that when $A_{\rm FB}^{\rm o}=0$, $r_\parallel+r_\perp$ must be zero. Then, the expression for $r_\parallel+r_\perp$ (see Eq. (A.2.10) for the massive case in appendix A.2) gives

$$\begin{aligned}
r_\parallel+r_\perp\big|_{A_{\rm FB}^{\rm o}=0}&=\pm\frac{\sqrt{\Gamma_f^{\rm o}}}{\sqrt{2}\mathcal{F}_\perp}\Big(\sqrt{F_\perp^{\rm o}-\frac{\mathcal{T}_\perp}{\Gamma_f^{\rm o}}}+\mathsf{P}_1\sqrt{F_\parallel^{\rm o}-\frac{\mathcal{T}_\parallel}{\Gamma_f^{\rm o}}}\Big)=0\\
\Longrightarrow\mathsf{P}_1\big|_{A_{\rm FB}^{\rm o}=0}&=-\frac{\sqrt{F_\perp^{\rm o}-\frac{\mathcal{T}_\perp}{\Gamma_f^{\rm o}}}}{\sqrt{F_\parallel^{\rm o}-\frac{\mathcal{T}_\parallel}{\Gamma_f^{\rm o}}}}
\end{aligned} \tag{4.3.32}$$

P_1 can be iteratively solved from the above equation. We note that in order one has real

positive form factors by definition (Eq. (4.2.17)) P_1 is always negative. The zero crossing of $A^{\rm o}_{\rm FB}$ is observed at $q^2 = 4.9^{+1.1}_{-1.3}{\rm GeV}^2$ [41] which is in the large recoil region where it is believed that reliable calculations can be done in HQET. Hence, we can check the predictability of HQET in large recoil region, when enough data for all observables are available at this q^2 point.

Equations (4.3.17) and (4.3.18) can now be used to obtain P_2 and P_3 at the zero crossings $A^{\rm o}_5 = 0$ and $A^{\rm o}_{\rm FB} + \sqrt{2}A^{\rm o}_5 = 0$ respectively,

$$\mathsf{P}_2\big|_{A^{\rm o}_5=0} = -\frac{\sqrt{F^{\rm o}_\perp - \dfrac{\mathcal{T}_\perp}{\Gamma^{\rm o}_f}}}{\sqrt{F^{\rm o}_L - \dfrac{\mathcal{T}_0}{\Gamma^{\rm o}_f}}}, \tag{4.3.33}$$

$$\mathsf{P}_3\big|_{A^{\rm o}_{\rm FB}+\sqrt{2}A^{\rm o}_5=0} = -\frac{\sqrt{F^{\rm o}_\perp - \dfrac{\mathcal{T}_\perp}{\Gamma^{\rm o}_f}}}{\sqrt{\left((F^{\rm o}_L - \dfrac{\mathcal{T}_0}{\Gamma^{\rm o}_f}) + (F^{\rm o}_\parallel - \dfrac{\mathcal{T}_\parallel}{\Gamma^{\rm o}_f}) + \sqrt{2}\pi A^{\rm o}_4 - \dfrac{4\beta^2\varepsilon_0\varepsilon_\parallel}{\Gamma^{\rm o}_f}\right)}}. \tag{4.3.34}$$

The relation derived in Eq. (4.3.27) incorporates all the possible effects within SM. It includes a finite lepton mass, electromagnetic correction to hadronic operators at all orders and all factorizable and nonfactorizable contributions including resonances to the decay. It can be seen from the Eq. (4.3.22) the term $\mathcal{T}_\lambda/\Gamma^{\rm o}_f$ contains $\mathbb{T}_1/\Gamma^{\rm o}_f$ which is expressed in Eq. (4.3.4) in terms of the asymmetries A_{10} and A_{11} which can be measured experimentally and the other term $(\varepsilon_\lambda/\Gamma^{{\rm o}\,1/2}_f)$ depends only on the observables and one form-factor ratio P_1. Thus, the relation in Eq. (4.3.27) is complete and exact in the sense that it involves all the eleven observables and only one hadronic input which can be reliably estimated using HQET.

4.4 Observables at kinematic extreme points

In this section we will briefly discuss the limiting value of the observables at the two kinematic extremities of q^2, the dilepton invariant mass squared. The minimum q^2 value, $q^2 = q^2_{\rm min} = 4m^2$ and the endpoint $q^2 = q^2_{\rm max} = (m_B - m_{K^*})^2$. The values of the observables we obtain below can be experimentally verified and any exception must imply NP.

- **Case-I:** $q^2 = 4m^2$

It is easy to see that at $q^2_{\rm min}$ the two leptons carry equal momentum and recoil against the K^*. In the dilepton rest frame the two leptons carry zero momentum. Hence, angles θ_ℓ and ϕ cannot be defined. The angular distribution in Eq. (3.3.1) thus implies that all asymmetries i.e A_4, A_5, $A_{\rm FB}$, A_7, A_8 and A_9 must vanish in this limit. This implies that there is no preferred direction, leading to the conclusion that all helicities are equally probable.

Using the expressions of the observables derived in the previous section (Eqs. (4.3.1a) and (4.3.1b)) we can write

$$\begin{aligned} F_L^{\rm o} &= \frac{1}{\Gamma_f^{\rm o}}(\beta^2 \Gamma_f F_L + \frac{1}{3}(\Gamma_f^{\rm o} - \beta^2 \Gamma_f)) \\ &\underset{\rm fi \to 0}{=} \frac{1}{3} \end{aligned} \tag{4.4.1}$$

This limiting value holds for the other two helicity fractions as well. Hence, at the kinematic starting point we can write

$$F_\lambda^{\rm o} \underset{q^2 \to 4m^2}{=} \frac{1}{3}, \qquad \lambda \in \{L, \perp, \|\}. \tag{4.4.2}$$

We conclude that each observed helicity fraction should be $1/3$ at $q^2_{\rm min}$, which can be easily verified experimentally. The asymmetries defined in Eqs. (4.3.5) and (4.3.6) also

vanish at $q^2 = q^2_{\rm min}$ implying $(\mathbb{T}_1/\Gamma_f^{\rm o}) \to \frac{1}{3}$ (from Eq. (4.3.4)). Thus the observable $A_4^{\rm o}$ from Eq.(4.3.27) at $q^2 = q^2_{\rm min}$ is given by,

$$A_4^{\rm o} \underset{\beta\to 0}{=} \frac{\sqrt{2}}{\pi}\sqrt{F_L^{\rm o} - \frac{\mathbb{T}_1}{\Gamma_f^{\rm o}}}\sqrt{F_\parallel^{\rm o} - \frac{\mathbb{T}_1}{\Gamma_f^{\rm o}}} \underset{\substack{F_\lambda^{\rm o}\to\frac{1}{3}\\ \frac{\mathbb{T}_1}{\Gamma_f^{\rm o}}\to\frac{1}{3}}}{=} 0 \tag{4.4.3}$$

as it was expected above.

- **Case-II:** $q^2 = (m_B - m_{K^*})^2$

In this kinematic limit the K^* is at rest and the two leptons go back to back in the B meson rest frame. Therefore, we can always choose the angle ϕ to be zero. The entire decay takes place in one plane, resulting in vanishing $F_\perp$. Also, the left and right chirality of the leptons contribute equally. These together results in only the angular asymmetry A_4 being finite with all other asymmetries vanishing. The relations among the various angular coefficients at this kinematical endpoint are derived in Ref. [13] where it is explicitly shown that

$$F_L(q^2_{\rm max}) = \frac{1}{3}, \qquad A_{\rm FB}(q^2_{\rm max}) = 0. \tag{4.4.4}$$

Solving for the other observables from Eq. (3.2) of Ref. [13] we can write

$$F_\perp(q^2_{\rm max}) = 0, \qquad F_\parallel(q^2_{\rm max}) = \frac{2}{3}, \tag{4.4.5}$$

$$A_4(q^2_{\rm max}) = \frac{2}{3\pi}, \qquad A_{5,7,8,9}(q^2_{\rm max}) = 0. \tag{4.4.6}$$

These limiting values of the observables imply that $\varepsilon_\lambda \to 0$ at the extremum $q^2 = q^2_{\rm max}$ as can be seen from Eqs. (4.3.24) – (4.3.26). The lepton mass can be safely ignored at $q^2_{\rm max}$ as it would have almost no effect at this end point hence, we have dropped the 'o' index from all the observables for this discussion only. Thus, in the limit $\varepsilon_\lambda \to 0$, we find that

Eq. (4.3.27) reduces to Eq. (4.2.46). Hence, the observable A_4 at $q^2 = q^2_{\rm max}$ turns out to be

$$A_4 = \frac{8A_5A_{\rm FB}}{9\pi F_\perp} + \sqrt{2}\,\frac{\sqrt{F_LF_\perp - \frac{8}{9}A_5^2}\,\sqrt{F_\parallel F_\perp - \frac{4}{9}A_{\rm FB}^2}}{\pi F_\perp} \underset{\substack{A_{\rm FB}\to 0\\ A_5\to 0}}{=} \frac{\sqrt{2}\,\sqrt{F_LF_\parallel}}{\pi} \underset{\substack{F_L\to\frac{1}{3}\\ F_\parallel\to\frac{2}{3}}}{=} \frac{2}{3\pi}$$

which exactly matches with the limit predicted in Eq. (4.4.6).

4.5 Numerical analysis

In this section, we demonstrate the possibility of how NP could be tested using the relations derived in this chapter. The basis of our analysis is the relation, which involves all the nine observables F_L, $F_\parallel$, $F_\perp$, $A_{\rm FB}$, A_4, A_5, A_7, A_8, A_9 and a single form-factor ratio P_1 derived in Eq. (4.2.45). Since the helicity fractions are related by $F_L + F_\parallel + F_\perp = 1$, we eliminate $F_\parallel$. All the observables have been measured by LHCb Collaboration using $1\,\text{fb}^{-1}$ data. However, currently the observables A_7, A_8 and A_9 are measured to be consistent with zero. Equations (4.3.24)–(4.3.26) therefore imply that ε_λ are all consistent with zero. In Sec. 4.3 we have shown that the most conservative allowed parameter space remains unaltered even if the small lepton mass term is dropped compared to q^2 and the imaginary contributions to the amplitudes are completely ignored. Since the inclusion of ε_λ reduces the parameter space of observables, in order to check the consistency of measured observables we take a conservative approach and set all the ε_λ's to be equal to zero for the numerical analysis. Thus, the relation among the observables reduces to Eq. (4.2.46) which is in terms of six observables F_L, $F_\parallel$, $F_\perp$, $A_{\rm FB}$, A_4, A_5 and is completely free from any form-factor dependence. If A_7, A_8 and A_9 are measured to be non zero in future experiments with reduced uncertainties, ε_λ can be solved iteratively using Eqs. (4.3.24)–(4.3.26) and an exact numerical analysis can always be done. We, emphasize that a nonzero ε_λ would only restrict the allowed parameter space depicted in

Figs. 4.1, 4.2 and 4.3 further as was already pointed out in Sec. 4.3. Later in this section we will, nevertheless, solve for ε_λ in terms of A_7, A_8 and A_9 since the predicted value $A_4^{\rm pred}$ depends on the values of ε_λ.

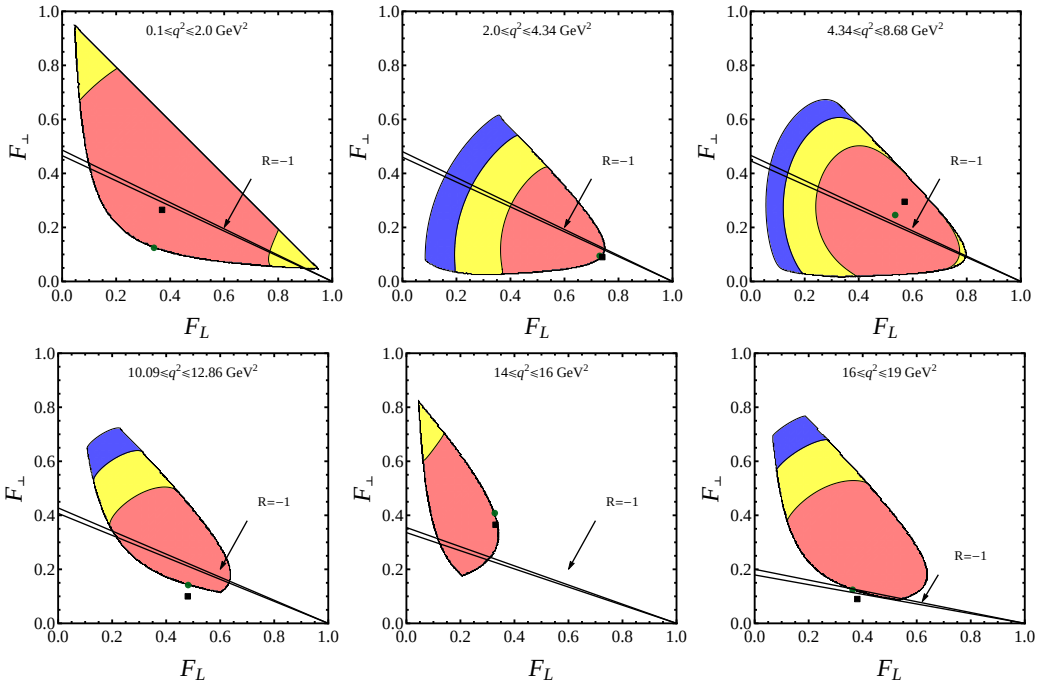

Figure 4.1. The χ^2 projection onto the plane of observables F_L and $F_\perp$. The experimental values of all the observables are taken from 1 fb^{-1} LHCb measurements Ref. [41]. The green dots corresponds to best fit value from χ^2 minimization and the black squares corresponds to the measured central value. The pink (dark), yellow (light) and blue (darkest) correspond to the 1σ, 2σ and 3σ confidence level regions respectively. If the amplitudes are real, nonfactorizable contributions vanish and the form factors were reliably evaluated at leading order in HQET then using SM estimated values of Wilson coefficients we find $F_L - F_\perp$ are constrained to lie in the narrow region between the two solid black lines. See text for details.

We use the SM relation derived in Eq. (4.2.46), for $\varepsilon_\lambda = 0$ and $4m^2/q^2 \to 0$ instead of Eq. (4.3.27), to check for consistency between measurements of all the observables. As noted above a finite value for ε_λ would provide a stronger constraint and since ε_λ's are consistent with zero, Eq. (4.2.46) provides a more conservative test. In order to perform the test we define a χ^2 function

$$\chi^2 = \frac{1}{4}\left[\left(\frac{A_4^{\rm exp} - A_4^{\rm pred}}{\Delta A_4^{\rm exp}}\right)^2 + \left(\frac{F_L^{\rm exp} - F_L}{\Delta F_L^{\rm exp}}\right)^2 + \left(\frac{F_\perp^{\rm exp} - F_\perp}{\Delta F_\perp^{\rm exp}}\right)^2 + \left(\frac{A_{\rm FB}^{\rm exp} - A_{\rm FB}}{\Delta A_{\rm FB}^{\rm exp}}\right)^2 + \left(\frac{A_5^{\rm exp} - A_5}{\Delta A_5^{\rm exp}}\right)^2\right], \tag{4.5.1}$$

where $A_4^{\rm exp}, F_L^{\rm exp}, F_\perp^{\rm exp}, A_{\rm FB}^{\rm exp}, A_5^{\rm exp}$ indicate experimental central values of the observables and $\Delta A_4^{\rm exp}, \Delta F_L^{\rm exp}, \Delta F_\perp^{\rm exp}, \Delta A_{\rm FB}^{\rm exp}, \Delta A_5^{\rm exp}$ are the experimental uncertainties. The statistical and systematic uncertainties are added in quadrature for all the numerical analysis presented. The χ^2 function in Eq. (4.5.1) is minimized in the 4-dimensional parameter space of the observables by varying each of them simultaneously within the allowed region i.e $0 \leq F_L \leq 1$, $0 \leq F_\perp \leq 1$, $-1 \leq A_{\rm FB} \leq 1$, $-1 \leq A_5 \leq 1$, while $A_4^{\rm pred}$ is taken to be the theoretically calculated value for A_4 using Eq. (4.2.46). The minimized χ^2 function is projected in different sets of planes of the observables, $(F_L, F_\perp)$, $(A_{\rm FB}, F_L)$, $(A_{\rm FB}, A_5)$ (A_5, F_L), $(A_5, F_\perp)$ and $(A_{\rm FB}, F_\perp)$ for the contour plots. In Fig. 4.1 we show the allowed domain of $F_L - F_\perp$ values for all the six q^2 bins corresponding to the q^2 values in the range $(0.1 - 2)$ GeV^2, $(2 - 4.34)$ GeV^2, $(4.34 - 8.68)$ GeV^2, $(10.09 - 12.86)$ GeV^2, $(14.0 - 16.0)$ GeV^2 and $(16.0 - 19.0)$ GeV^2. The pink, yellow and blue correspond to 1σ, 2σ and 3σ confidence level regions. The black squares correspond to the experimentally measured central value and the green points correspond to best fit values obtained by minimizing χ^2 using Eq. (4.5.1). As can be seen form Fig. 4.1 the bounds derived in this section, involving only observables, have resulted in very significantly constraining the allowed parameters range of observables.

If it were true that there are no significant nonfactorizable contributions to the decay mode, rendering $\widetilde{C}_9^\lambda$ independent of the helicity index 'λ', we can solve for $\widetilde{C}_9$ as was shown in Ref. [27]. The ratio of $\widetilde{C}_9/\widehat{C}_{10}$ so obtained could be inverted to solve for $A_{\rm FB}$ resulting in the constraint between F_L and $F_\perp$ given in Eq.(55) of Ref. [27]. The narrow constraint region between the two solid black lines depicted in $F_L - F_\perp$ plane in Fig. 4.1 is derived assuming real transversity amplitudes, form factors are calculated at leading order in $\Lambda_{\rm QCD}/m_b$ using HQET and the estimate that $\widetilde{C}_9/\widehat{C}_{10} = -1$ is used. We emphasize that except for the two solid black lines for each of the q^2 bins all other information in Fig. 4.1 is completely free from any theoretical assumption. As can be seen from Fig. 4.1 the best fit values as well as the experimentally measured central values are largely not inside the narrow constraint region within two solid black lines. This indicates that there could exist

any or all of the possibilities: imaginary contributions to the transversity amplitudes or sizable nonfactorizable contributions or higher order corrections in HQET could also be relevant.

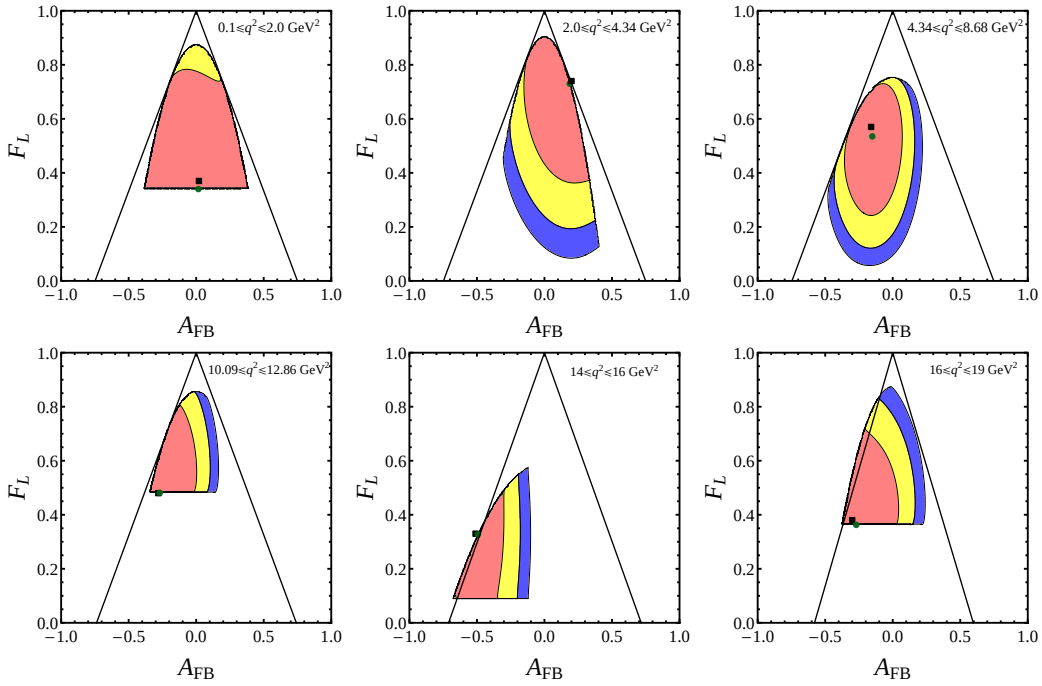

Figure 4.2. The χ^2 projection onto the plane of observables F_L and $A_{\rm FB}$. The experimental values of all the observables are taken from Ref. [41]. The color codes are the same as in Fig. 4.1. If the amplitudes are real, nonfactorizable contributions vanish and the form factors were reliably evaluated at leading order in HQET then using SM estimated values of Wilson coefficients we find $A_{\rm FB} - F_L$ are constrained to lie in the two solid black triangular region. See text for details.

The allowed range for observables $A_{\rm FB} - F_L$ is depicted in Fig. 4.2 for all the six bins. The color code and markers follow the same convention used in Fig. 4.1. The constraint of the allowed triangular region between two solid black line comes from Eq.(53) of Ref. [27]. Once again the constraint region within the solid black triangular depicted in $A_{\rm FB} - F_L$ plane is derived assuming real transversity amplitudes, form factors calculated at leading order in $\Lambda_{\rm QCD}/m_b$ using HQET and the estimate that $\widetilde{C}_9/\widehat{C}_{10} = -1$. However, note that the constraints depicted by the contour plots are completely free from any theoretical assumptions. The allowed region in the other four planes of observables i.e $A_{\rm FB} - A_5$,

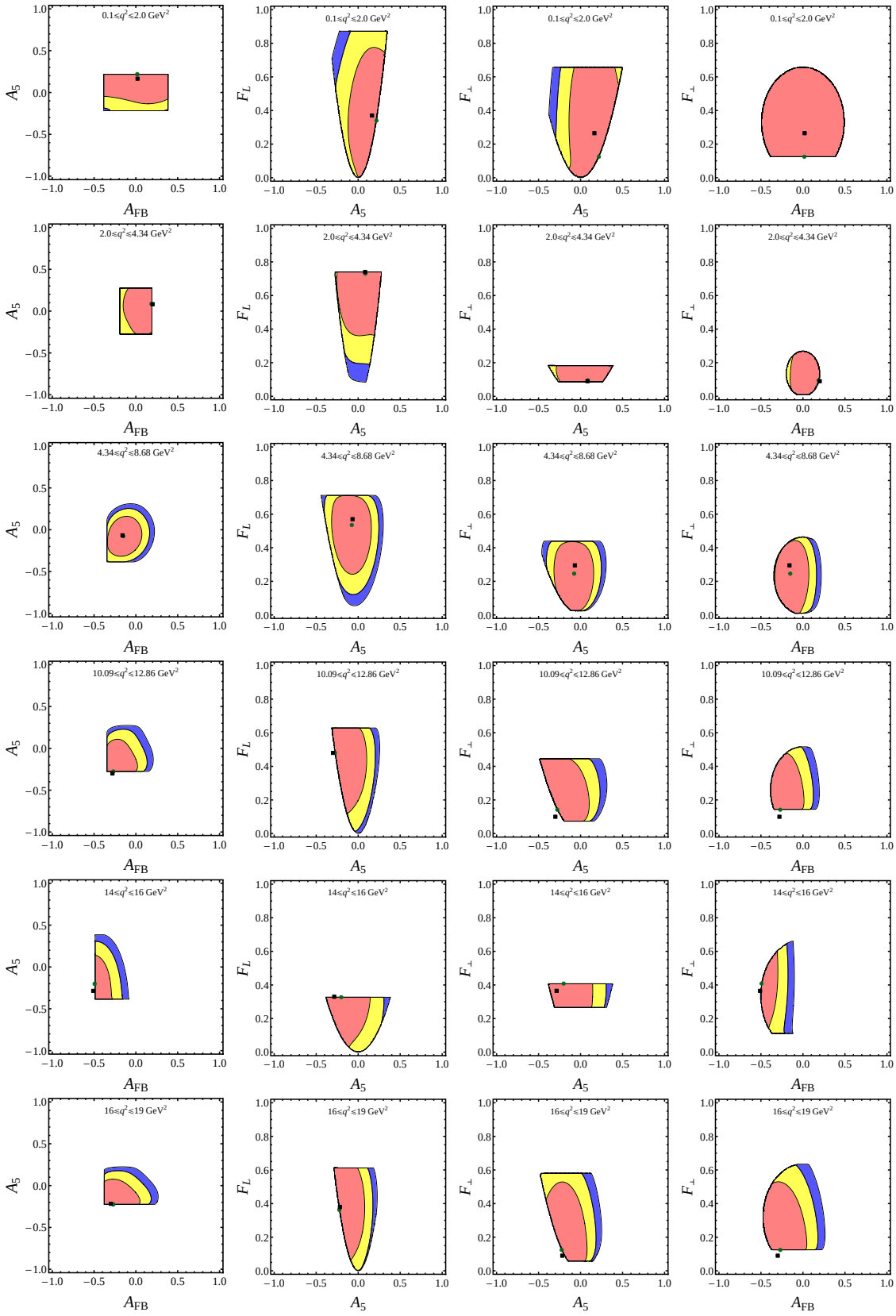

Figure 4.3. The χ^2 projection onto the sets observables $A_5 - A_{\rm FB}$, $A_5 - F_L$, $A_5 - F_\perp$ and $A_{\rm FB} - F_\perp$ for various q^2 bins going vertically from first to the sixth bin. The experimental values of all the observables are taken from Ref. [41]. The color codes are same as in Fig. 4.1.

$A_5 - F_L$, $A_5 - F_\perp$ and $A_{\rm FB} - F_\perp$ are shown in Fig. 4.3. We emphasize once again that the plots are free from any theoretical uncertainty. In most of the contour plots depicted in Figs. 4.1, 4.2 and 4.3 the best fit points (green point) lie at the edge of the boundaries except for the third bin. The experimental measured central values (black squares) are mostly overlapping with the best fit points except for fourth and sixth bin. In the fourth bin the black squares stay outside the physically allowed region. In third bin both the best fit and experimental measurement are very consistent with the allowed region and sit almost at the center of it. It is interesting to note that the best fits are always in the 1σ region perhaps validating the LHCb data set.

In Fig. 4.4 the measured Gaussian A_4 distribution is compared with the distribution of $A_4^{\rm pred}$ computed using Eq. (4.2.46). In evaluating the right-hand side of Eq. (4.2.46) we have used a Gaussian distribution of the observables F_L, $F_\perp$, A_5 and $A_{\rm FB}$ with experimental central value as the mean and errors as the standard deviation from Ref. [41]. The plots correspond to a simulated theory sample of 144, 76, 281, 169, 114 and 124 events corresponding to first through sixth q^2 bins. These may be compared with 140, 73, 271, 168, 115 and 116 events obtained for the respective bins by LHCb using 1 fb^{-1} data [41]. We have randomly chosen the number of events to be statistically consistent with the LHCb observation in each bin for this decay mode. As should be expected fewer events survive the constraint of Eq. (4.2.46) when the best fit points are at the edge of the permissible contour regions in Figs. 4.1, 4.2 and 4.3. The simulated A_4 values corresponding to the LHCb measurement for all six bins are shown in red (dark) histogram and the yellow (light) histogram corresponds to the values of $A_4^{\rm pred}$ computed using Eq. (4.2.46). For a comparison, the probability distribution function (PDF) curves corresponding to 1000 times more events are also shown for theory using brown (light) curve and data using red (dark) curve.

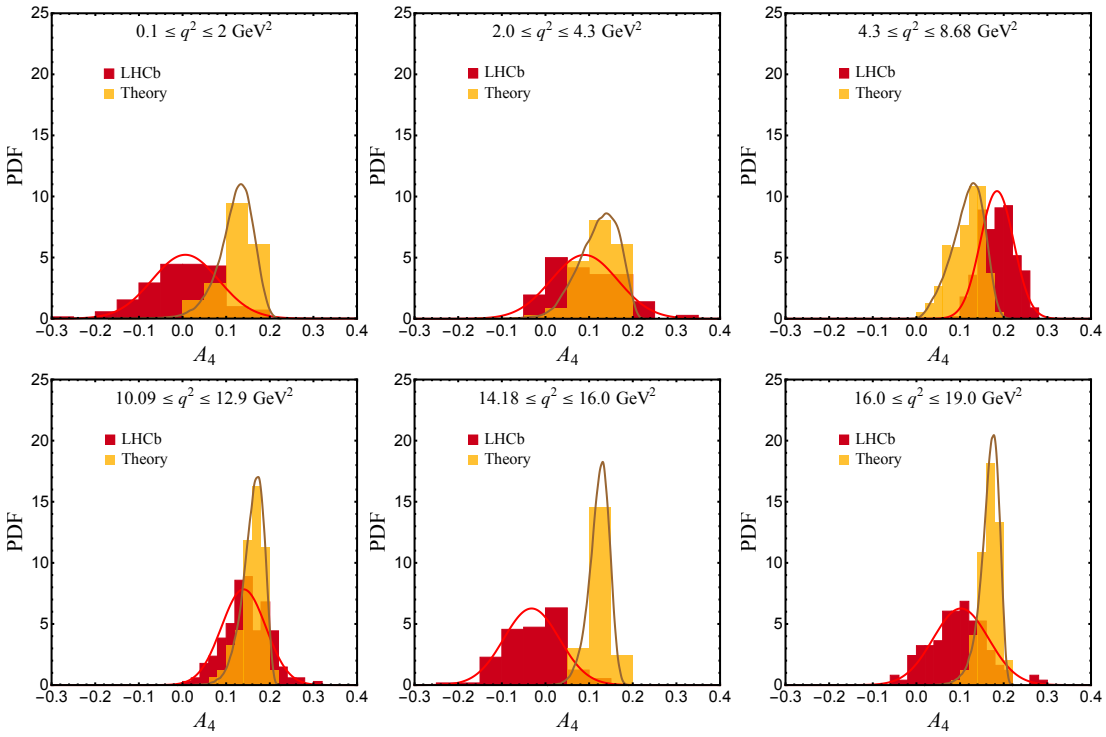

Figure 4.4. A comparison of the measured and the predicted A_4 values for the six q^2 bins assuming that A_7, A_8 and A_9 are all zero. The simulated values of A_4 assuming Gaussian error in the LHCb data are shown in red (dark), whereas the yellow (light) distributions referred to as "Theory" correspond to the values of $A_4^{\rm pred}$ computed using Eq. (4.2.46). The plots correspond to a simulated theory (LHCb 1 fb^{-1} data [41]) sample of 144 (140), 76 (73), 281 (271), 169 (168), 114 (115) and 124 (116) events corresponding to first through sixth q^2 bins as depicted in the figure. We have randomly chosen the events to be statistically consistent with the LHCb observation in each bin for this decay mode. For a comparison, the PDF curves corresponding to 1000 times more events are also shown for theory using brown (light) curve and data using red (dark) curve. We compare the two simulated distributions shown in the histograms using the Mathematica routine "DistributionFitTest" [50]. The P-values obtained by comparing the two are found to be less than 10^{-9} for each of the bins, except the second and fourth bins, where the P-values obtained are 2.54×10^{-5} and 6.47×10^{-6} respectively.

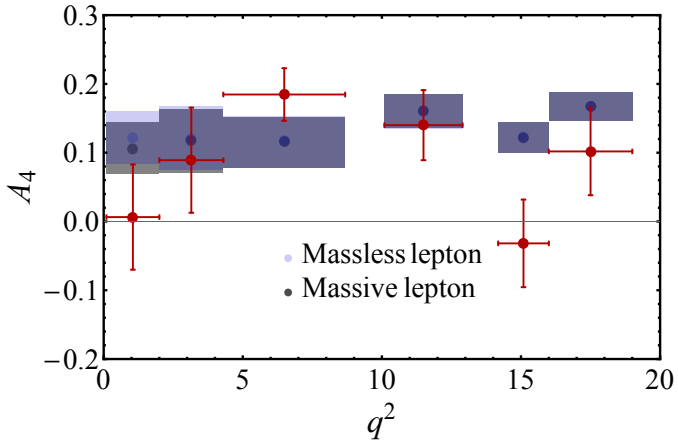

Figure 4.5. The mean values and 1σ regions for theoretically calculated A_4 distributions excluding lepton masses (Eq. (4.2.46)) and with massive leptons (Eq. (4.3.27)) are shown in purple (light) and gray (dark) bands respectively. The simulated samples consist of $50,000$ events to start with, for each bin. The observables A_7, A_8 and A_9 are assumed to be zero. The error bars in red correspond to the experimentally measured [41] central values and errors in A_4 for the respective q^2 bins.

The mean and 1σ regions for the theoretically calculated A_4^{pred} distributions are shown in Fig. 4.5. We compare the two cases where lepton masses is ignored (Eq. (4.2.46)) with the case where lepton mass is finite (Eq. (4.3.27)). The purple (light) bands correspond to the massless case and the gray (dark) bands correspond to the massive case. The error bars in red correspond to the experimentally measured [41] central values and errors in A_4 for the respective q^2 bins. The values of A_4^{pred} obtained from the Eq. (4.2.46) seem to visually agree reasonably with the experimental measurements within the error bands in all the bins except for the first and the fifth bin. A large discrepancy in fifth bin can also be seen here. There is also a slight tension in first bin, which could be partly due to the lepton mass effect. The corrections due to mass terms can be incorporated if the asymmetries A_{10} and A_{11} are measured in the future. In the absence of such measurements we have used the theoretical estimate of form factors [35, 36] to evaluate the effect of the finite mass contribution. Details are depicted in Fig. 4.5. The mass contributions only affect the first bin, the other bins are unaffected. As expected the agreement improves for the first bin if the mass contributions are added. While Fig. 4.5 indicates only a mild disagreement between the measured and predicted values of A_4, the distributions in

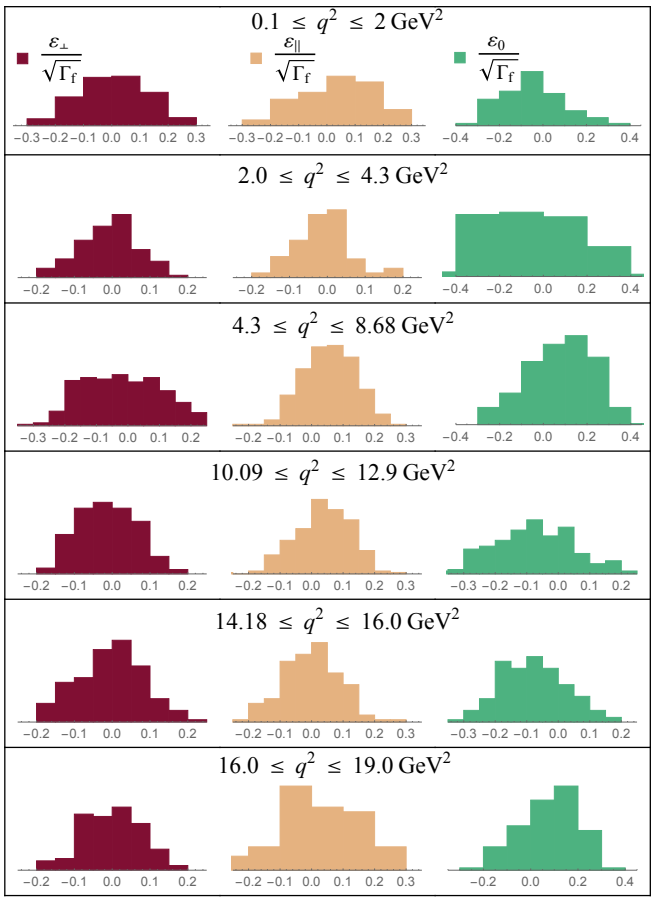

Figure 4.6. The solutions for $\varepsilon_\perp/\sqrt{I_f}$, $\varepsilon_\parallel/\sqrt{I_f}$ and $\varepsilon_0/\sqrt{I_f}$ using distributions with 140, 78, 275, 175, 113 and 113 events for first through sixth q^2 bins. The number of events are chosen to be statistically consistent with the number of events observed by LHCb [41] in each bin for this decay mode. All the ε_λ's are consistent with zero and even at extreme cases $\varepsilon_\lambda^2/I_f$ values are less than 0.2.

Fig. 4.4 carry much more information than the mean and averages. We have compared the two simulated distributions shown in the histograms using the Mathematica routine "DistributionFitTest" [50]. The P-values obtained by comparing the two are found to be less than 10^{-9} for each of the bins, except the second and fourth bins, where the P-values obtained are 2.54×10^{-5} and 6.47×10^{-6} respectively. A small P-value indicates that one should reject the hypothesis that all observables are consistent with the SM relation of Eq. (4.2.46).

In order to ascertain that the discrepancy in the A_4 enunciated using the P-values is not due to the imaginary contributions being ignored we have also preformed a simulation of all observables, including A_7 A_8 and A_9. We solved for $\varepsilon_\perp$, $\varepsilon_\parallel$ and ε_0 using Eqs. (4.3.24)

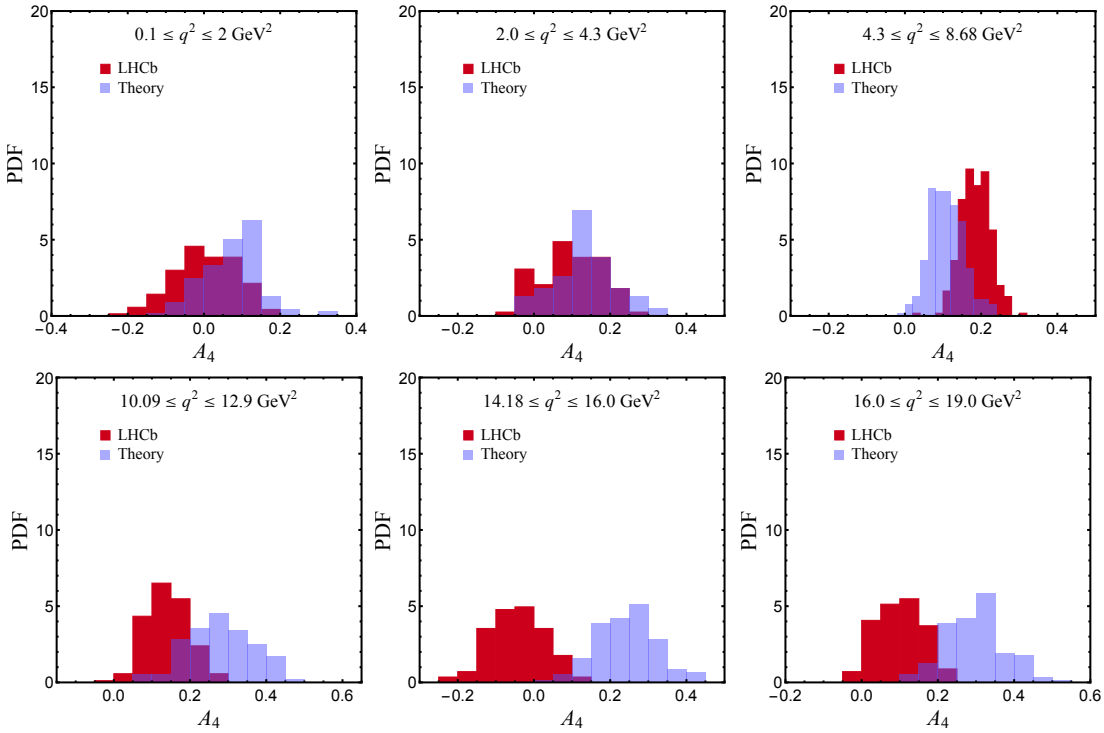

Figure 4.7. A comparison of the measured and predicted A_4 values for the six q^2 bins considering all the measured observables. The simulated values of A_4 assuming Gaussian error in the LHCb data are shown in red (dark), whereas the Blue (light) distributions referred to as "Theory" correspond to the values of $A_4^{\rm pred}$ computed using Eq. (4.3.27). The plots correspond to a simulated theory (LHCb 1 fb^{-1} data [41]) sample of 140 (140), 78 (73), 275 (271), 175 (168), 113 (115) and 113 (116) events corresponding to first through sixth q^2 bins as depicted in the figure. The number of events are chosen to be consistent statistically with the number of events observed by LHCb in each bin for this decay mode. The values of all other observables used in the two equations are randomly generated using LHCb data assuming Gaussian measurements. We find that the P-values obtained using the Mathematica routine "DistributionFitTest" [50] comparing the two distributions are always less than 10^{-9} for all bins except the second bin where the P-value is 6.78×10^{-3}.

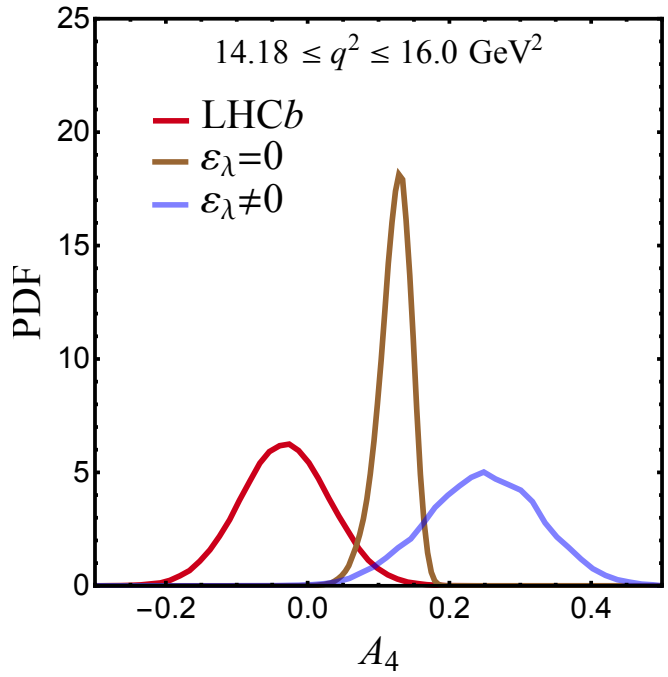

Figure 4.8. A PDF plot comparing the measured fifth bin ($14.18 \leq q^2 \leq 16.0$ GeV^2) value of A_4 with the two theoretically predicted values. One assuming $\varepsilon_\lambda = 0$ or completely real transversity amplitudes and the other with $\varepsilon_\lambda \neq 0$ or complex transversity amplitudes. The mean and errors for all the observables are assumed to be those measured by LHCb using $1\,\text{fb}^{-1}$ data set. All errors are assumed to be Gaussian. The PDFs depicted in the figure are generated using 4×10^5 random events resulting in the simulated values of A_4 for each curve. If $\varepsilon_\lambda \neq 0$ only 6708 of the points survived the constraints. The plot corresponding to LHCb A_4 measurement is shown in left most red (dark) plot, whereas the central brown (lighter) distribution corresponds to the theoretically calculated A_4 using Eq. (4.2.45) and the right most blue (light) distribution is for A_4 predicted using Eq. (4.3.27).

– (4.3.26). These values of $\varepsilon_\perp$, $\varepsilon_\parallel$ and ε_0 depend only on observables and P_1. We assume P_1 values (see Ref. [27]) to be $\mathsf{P}_1 = -0.9395, -0.9286, -0.9034, -0.8337, -0.7156$ and -0.4719 for the first through the sixth bin respectively. We only remark that if A_7, A_8 and A_9 are measured to be small the results are even more insensitive to the choice of the P_1 value. Nevertheless, we also studied the effect of varying P_1 within the range $\mathsf{P}_1 \pm 0.5$, to ascertain our claim. Details will be presented elsewhere. The ε_λ were solved iteratively and it was found that they always converged in just a few iterations. If iteration led to a value of ε_λ larger than the derived constraints permitted, a smaller allowed value was assigned and the iteration continued. In some cases an oscillatory or randomly varying pattern was observed but in these cases the starting values of the observables could not be reproduced, indicating that further constraints imposed by the chosen values of A_7, A_8 and

A_9 could not be satisfied. The solutions obtained for $\varepsilon_\lambda/\sqrt{\Gamma_f}$ are shown for each of the six bins in Fig. 4.6. It can be seen that all the ε_λ's are consistent with zero within 1σ uncertainty and even the tails of $\varepsilon_\lambda^2/\Gamma_f$ do not cross 0.2 with the current data. Having obtained the values of $\varepsilon_\lambda/\sqrt{\Gamma_f}$ we can now use the exact relation in Eq. (4.3.27) to estimate $A_4^{\rm pred}$. A comparison between the measured A_4 and the predicted value $A_4^{\rm pred}$ including contributions from A_7, A_8 and A_9 is done in Fig. 4.7. It must be emphasized that $A_4^{\rm pred}$ obtained using Eq. (4.3.27) is exact and takes into account all the contributions in SM. The asymmetries A_{10} and A_{11} (see Eqs. (4.3.5) and (4.3.6)) have not yet been measured and Fig. 4.5 indicates that the lepton mass effects are negligible for all but the first bin. We hence set $\mathbb{T}_1 = 0$ in evaluating $A_4^{\rm pred}$. This ensures that our results depend on only one theoretical parameter, the ratio of form factors P_1 and that parameter resulting in unmeasurable tiny effects do not complicate the calculations. As predicted above, an even smaller number of events are now consistent with the constraints derived in the chapter. Interestingly, $A_4^{\rm pred}$ now fits better to a Gaussian distribution as indicated by a Kolmogorov-Smirnov test [51, 52], compared to the previous case where transversity amplitudes were assumed to be real. This is indicative of the fact that the transversity amplitudes are complex. However, the values of $\varepsilon_\lambda/\sqrt{\Gamma_f}$ are not large as indicted in Fig. 4.6. We have simulated numbers of events consistent statistically with the number of events observed by LHCb in each bin. The plots as depicted in Fig. 4.7 correspond to a simulated theory (LHCb 1 fb^{-1} data [41]) sample of 140 (140), 78 (73), 275 (271), 175 (168), 113 (115) and 113 (116) events for the first through sixth q^2 bins. The values of $A_4^{\rm pred}$ predicted using Eq. (4.3.27) have a larger mean and variance as compared to values obtained using Eq. (4.2.46). The P-values still continue to be smaller than 10^{-9} for all the bins, except the second bin where the P-value is 6.78×10^{-3}, indicating that we reject the hypothesis that all observables are consistent with the exact SM relation of Eq. (4.3.27).

The PDF curves comparing the measured value of A_4 with both the theoretically predicted values assuming completely real transversity amplitudes ($\varepsilon_\lambda = 0$) and most general complex transversity amplitudes ($\varepsilon_\lambda \neq 0$) are shown in Fig. 4.8 for fifth bin ($14.18 \leq q^2 \leq$

16.0 GeV^2). We have chosen the fifth bin for this detailed study since the tension between the predicted value and experimentally observed value appears to be the largest as can be seen from Figs. 4.4, 4.5 and 4.7. The PDFs depicted in the figure are generated using 4×10^5 random events resulting in the simulated values of A_4 for each curve. If $\varepsilon_\lambda \neq 0$ only 6708 of the points survived the constraints of Eq. (4.3.27). LHCb data assuming Gaussian error is shown in leftmost red (dark) plot, whereas the central brown (lighter) distribution corresponds to the theoretically calculated A_4 using Eq. (4.2.45) and the rightmost blue (light) distribution is for A_4 predicted using Eq. (4.3.27). The values of all other observables used in the two equations are randomly generated assuming Gaussian measurements of the LHCb 1 fb^{-1} data.

In this section we have discussed the constraints already imposed by the 1 fb^{-1} LHCb data [41] on the parameter space of observables. We also compare the measured values of A_4 with those predicted using the new relations derived in this chapter. We made several observations that indicate possibly sizable nonfactorizable contributions and imaginary contribution and also possible higher order corrections in HQET to the transversity amplitudes. In addition, the P-values comparing the measured A_4 with the predicted value indicates NP. However, we refrain from drawing even the obvious conclusions given that, results for 3 fb^{-1} data will soon be presented by the LHCb Collaboration. However, we emphasize that the approach developed in this chapter could not only conclusively indicate presence of significant nonfactorizable contributions and need for higher order power corrections to form factors but also the presence of NP with larger statistics.

4.6 Summary

In this chapter we have derived a new relation involving all the CP conserving observables that can be measured in the decay $B \to K^*\ell^+\ell^-$ using an angular study of the final state for the decay. The relation provides a very clean and sensitive way to test the SM and search

for NP by probing consistency between the measured observables. The relation reduces to the one derived in Ref. [27], when certain reasonable assumptions were made. Since, the relation is intended to be used as probe in search for NP, it is imperative that no avoidable assumptions be made. We have generalized previous results with this objective in mind. The new derivation is parametrically *exact in the SM limit* and incorporates finite lepton and quark masses, complex amplitudes enabling resonance contributions to be included, electromagnetic correction to hadronic operators at all orders and all factorizable and nonfactorizable contributions to the decay.

We started by writing the most general parametric form of the transversity amplitude in the SM given in Eq. (3.3.5) that takes into account comprehensively all the contributions within SM. Unlike the derivations in Ref. [27] the general transversity amplitude is now allowed to be complex, by introducing three additional parameters ε_λ. This, however, poses no problem since there are three extra observables A_7, A_8 and A_9 given in Sec. 3.3, which are non-vanishing in the complex transversity amplitudes limit. Hence, dealing with complex amplitude introduces only a technical difficulty of solving for additional variables iteratively.

Using this general amplitude a new relation (see Eq. (4.2.46)) involving all the nine CP conserving observables is derived in Sec. 4.2, that is exact in the SM limit assuming massless leptons. The new derivation incorporates the effect of electromagnetic correction of hadronic operators to all orders and all factorizable and nonfactorizable contributions including resonance effects to the decay. In addition to the nine observables, this new relation depends only on one form-factor ratio: P_1. The new relation becomes independent of P_1 and reduces to the one derived in Ref. [27] in the limit that the asymmetries A_7, A_8 and A_9 are all zero.

As mentioned repeatedly the inclusion of lepton mass contribution is trivial in our approach; the effect on all the observables is directly obtained in terms of asymmetries given in Eqs. (4.3.5) and (4.3.6) that can be measured as shown in Sec. 4.3. The new relation

obtained is generalized to include the lepton mass effects in Eq. (4.3.27). It is important to note that it involves only observables and the form-factor ratio P_1 and is free from any assumption within the SM framework. This relation also implies three inequalities given in Eqs. (4.3.29a)–(4.3.29c) which impose constraints on the parameter space of observables. We also presented three new relations between the observables that are exact at the zero crossings of angular asymmetries $A_{\rm FB}^{\rm o}$, $A_5^{\rm o}$ and $A_{\rm FB}^{\rm o} + \sqrt{2}A_5^{\rm o}$. These are particularly interesting if the mass effect and the imaginary contributions to the Wilson coefficients $\widehat{C}_7$ and $\widehat{C}_9$ are ignored, as they reduce to simple form presented in Eq. (4.3.31). Another interesting aspect is that the form-factor ratios P_1, P_2 and P_3 can each be written in terms of observables and P_1. In the limit of vanishing A_7, A_8 and A_9 (i.e negligible imaginary contributions), the form-factor ratios can be measured purely in terms of helicity fractions.

The limiting values of the observables at the minimum and maximum values of q^2 are discussed in Sec. 4.4 based on very general arguments. It is interesting to note that at $q^2 = 4m^2$ all angular asymmetries vanish and each of the helicity fraction approaches $1/3$. At the maximum value of $q^2_{\rm max}$ similar results can be obtained.

In Sec. 4.5, we have highlighted the possible ways to check the consistency of the measured observables using the SM relation derived. It was noted that the inclusion of nonzero ε_λ indicating complex contributions to the amplitudes invariably reduces the allowed parameter space of the observables. Hence, in order to check the consistency of measured observables we take a conservative approach and set all the ε_λ's to be equal to zero for the analysis. This was necessary since A_7, A_8 and A_9 are all consistent with zero. The relation among the observables, hence, reduces to Eq. (4.2.46) which is in terms of six observables F_L, $F_\parallel$, $F_\perp$, $A_{\rm FB}$, A_4, A_5 and is completely free from any form-factor dependence. The χ^2 function in Eq. (4.5.1) was minimized in the 4-dimensional parameter space of the observables F_L, $F_\perp$, $A_{\rm FB}$ and A_5 to check the consistency between the experimentally measured values by varying each of them simultaneously within the permissible domain and $A_4^{\rm pred}$ was evaluated using the relation in Eq. (4.2.46). The projections of the mini-

mized χ^2 function are studied for the various pairs of observables as shown in the contour plots of Figs. 4.1–4.3. In most of the contour plots the best fit (green) points lie at the edge of the boundaries except for the third bin. The experimental measured central values (black squares) generally lie within the contours except for the fourth and sixth bin. It is interesting to note that the best fits are always in the 1σ region perhaps validating the LHCb data set.

We compared the two distributions generated by experimental measurement and theoretical prediction of the observable A_4, assuming that A_7, A_8 and A_9 are all zero in Fig. 4.4. The number of events for the "Theory" histogram are chosen to be consistent statistically with the number of events observed by LHCb in the 1 fb^{-1} [41] data set for each of the bins. The mean values together with 1σ error bands are shown in Fig. 4.5 with a comparison between the massless and massive lepton case. It is found that lepton mass can be ignored except for the first q^2 bin. The fifth bin shows a large discrepancy whereas the other bins are in reasonable agreement. Since the A_4 distributions in Fig. 4.4 carry much more information than the mean and averages, we compare the two simulated distributions shown in the histograms using the Mathematica routine "DistributionFitTest" [50]. The P-values obtained by comparing the two are found to be less than 10^{-9} for each of the bins, except the second and fourth bins, where the P-values obtained are 2.54×10^{-5} and 6.47×10^{-6} respectively.

In order to understand better the role of the imaginary contributions that were earlier ignored, we have also preformed a simulation of all observables including A_7 A_8 and A_9. The solutions for $\varepsilon_\perp$, $\varepsilon_\parallel$ and ε_0 shown in Fig. 4.6 indicate that all the ε_λ's are consistent with zero and even the tails of $\varepsilon_\lambda^2/\Gamma_f$ do not cross 0.2. A comparison of the measured and predicted A_4 values for the six q^2 bins considering all the measured observables (including A_7, A_8 and A_9) are shown in Fig. 4.7. Interestingly, $A_4^{\rm pred}$ now fits better to a Gaussian distribution than the $\varepsilon_\lambda = 0$ case as indicated by a Kolmogorov-Smirnov test [51, 52], implying possible imaginary contributions to the transversity amplitudes. The P-values

still continue to be smaller than 10^{-9} for all the bins, except the second bin where the P-value is 6.78×10^{-3}, indicating that we reject the hypothesis that all observables are consistent with the exact SM relation of Eq. (4.3.27). Since the discrepancy seems to be the largest for the fifth bin ($14.18 \leq q^2 \leq 16.0$ GeV^2), we have performed a detailed comparison of the PDF curves for both the theoretically predicted values using $\varepsilon_\lambda = 0$ and $\varepsilon_\lambda \neq 0$ with the measured value of A_4 as shown in Fig. 4.8.

In this chapter we have derived a relation among the observables by taking into account all possible effects within the SM by restricting ourselves to rely only on one hadronic input. The violation of this relation will provide a smoking gun signal of NP. We have explicitly shown how the relation can be used to test SM, and confirm our understanding of the hadronic effects. We used the 1 fb^{-1} LHCb measured values of the observables to highlight the possible ways for the search of NP that might contribute to this decay with the derived relations.

5 Hadronic parameter extraction and right-handed currents

In this chapter the formalism for $B \to K^* \ell^+ \ell^-$, discussed in the preceding chapters, has been used in a different way. Instead of comparing the observables with the experimental measurements, we use data to extract out the hadronic parameters assuming the gauge structure of the SM only. The theory has been modified in such a way that the combinations of hadronic parameters, estimated from data, are independent of the non local contributions arising from resonance contributions.

The material of this chapter is based on the work done with Rahul Sinha [6].

I cannot believe God is a weak left-hander. - Wolfgang Pauli

5.1 Introduction

The rare decay $B \to K^* \ell^+ \ell^-$ involves a $b \to s$ flavor changing loop induced transition at the quark level making it attractive mode to search for physics beyond the SM. Indirect searches for NP involving loop processes require a comparison of theoretical estimates with experimental observations. The theoretical estimates thus need to be extremely reliable in order to make a conclusive claim on the existence or non-existence of NP. Fortunately, significant progress has been made in understanding the hadronic effects involved in the decay $B \to K^* \ell^+ \ell^-$. The mode $B \to K^* \ell^+ \ell^-$ is also of special interest as it allows for the measurement of several observables using the angular distribution [1]. The large number of observables depend on theoretical parameters that describe this decay. In this chapter we show how some of the parameters can be extracted directly from LHCb measurements allowing us to verify our theoretical understanding. Any discrepancy observed must be attributed either to a failure of our understanding of hadronic effects or to the existence of NP. We also test the relation between observables that provides another clean test for NP.

The differential decay distribution [1, 5, 27] of $B \to K^* \ell^+ \ell^-$ results in the measurement of at least nine observables using the angular distribution, as a function of q^2 the dilepton invariant mass squared. These observables are commonly chosen to be the differential decay rate with respect to q^2, two independent helicity fractions that describe the decay, the three asymmetries that describe the real part of the interference between different helicity amplitudes and three asymmetries that describe the imaginary part of the interference.

Recently LHCb [2] has reported measurements of all these observables that have been averaged in eight q^2 bins. We use the LHCb data to obtain estimates of hadronic form factors that describe the decay. Previously some of the form factors have been determined [53] using 1 fb^{-1} of LHCb data. We emphasize that our approach does not involve evaluating the decay amplitude in terms of theoretically estimated parameters. Instead we start with

the most general parametric form of the amplitude without any hadronic approximations within the SM (see Eq. (4.2.2)). Experimental data alone is used to fit the theoretical parameters introduced in the parametric amplitude. These experimentally fitted theoretical parameters are simply compared to the estimates by other authors [8, 9] which are widely regarded as the state of the art. The values of form factors obtained from experimental data show significant discrepancy when compared with theoretical expectations in several q^2 bins.

In addition to extracting form factors from data, this mode also allows a relation among observables that can provide a clean signal [5, 27] of NP. We find that the measurements do not satisfy the expected relation between the observables in the same q^2 domains where the fitted form factors also show a large discrepancy with the theoretical estimates. The simultaneous observation of these discrepancies points to possible evidence of NP.

The chapter is organized as follows. In Sec. 5.2 we briefly remind the theoretical framework developed to write the most general parametric form of the amplitude and cast the observables in a form where hadronic parameters can be obtainable from data. The relation among observables are also written here. A numerical analysis is presented in Sec. 5.3 which contains two subsections. The Sub-sec. 5.3.1 gives elaborate description of extraction of form factors using LHCb measurements, whereas, the validity of the relations derived assuming SM are examined in Sub-sec. 5.3.3 with experimental data. In Sec. 5.4 we summarize the important results obtained in this chapter. appendix. B and C estimate the complex part the amplitude and the systematic uncertainty arising mainly due to bin average effect of the observables, respectively.

5.2 Observables and parameters

In this section we use the theoretical framework derived in Chapter 3 to take into account all possible contributions within SM for the decay $B \to K^* \ell^+ \ell^-$. We start with the observ-

ables $F_\perp$, A_4, A_5, $A_{\rm FB}$, A_7, A_8 and A_9 are related to the CP averaged observables S_3, S_4, S_5, $A_{\rm FB}^{\rm LHCb}$, S_7, S_8 and S_9 measured by LHCb [2, 41] as given in Eq. (3.3.21). It may be remarked that LHCb collaboration observes a local tension with some observables based on the hadronic estimates of Refs. [8, 54].

We begin by assuming the massless lepton limit but generalize to include the lepton mass. The corrections due to the mass of the leptons are easily taken into account as discussed in Sec. 4.3. In the massless lepton limit the decay is described in terms of six transversity amplitudes which can be written in the most general form shown in Eq. (3.3.5). This form of the amplitude is the most general parametric form of SM amplitude for $B \to K^* \ell^+ \ell^-$ decay that comprehensively takes into account all contributions up to $O(G_F)$ within it. The form includes all short-distance and long-distance effects, factorizable and nonfactorizable contributions and resonance contributions. In Eq. (3.3.5) C_9 and C_{10} are Wilson coefficients with $\widetilde{C}_9^\lambda$ being the redefined "effective" Wilson coefficient such that where $\Delta C_9^{\rm (fac)}(q^2)$, $\Delta C_9^{\lambda,{\rm (non\text{-}fac)}}(q^2)$ correspond to factorizable and soft gluon non-factorizable contributions. Strong interaction effects coming from electromagnetic corrections to hadronic operators do not affect C_{10}.

The form factors $\mathcal{F}_\lambda$ and $\widetilde{\mathcal{G}}_\lambda$ introduced in Eq. (3.3.5) can be related to the conventional form factors describing the decay as shown in appendix. A.1. The form-factors $\mathcal{F}_\lambda$ are of particular interest here as we show that they can be extracted directly from data. The $\mathcal{F}_\lambda$ can be related to the well known form-factors V, A_1 and A_{12} by comparing with [8]:

$$\mathcal{F}_\perp = N\sqrt{2}\sqrt{\lambda(m_B^2, m_{K^*}^2, q^2)}\frac{V(q^2)}{m_B + m_{K^*}}, \tag{5.2.1a}$$

$$\mathcal{F}_\parallel = -N\sqrt{2}(m_B + m_{K^*})A_1(q^2), \tag{5.2.1b}$$

$$\mathcal{F}_0 = \frac{-N}{\sqrt{q^2}}\,8 m_B m_{K^*} A_{12}(q^2). \tag{5.2.1c}$$

It should be noted that $\mathcal{F}_\lambda$'s and C_{10} are completely real in the SM, with all imaginary contributions to the amplitude arising only from the imaginary part of complex $\widetilde{C}_9^\lambda$ and

$\widetilde{\mathcal{G}}_\lambda$ terms. Thus with the introduction of two variables r_λ and ε_λ the amplitude $\mathcal{A}_\lambda^{L,R}$ in Eq. (3.3.5) can be rewritten as Eq. (4.2.2) where r_λ and ε_λ contain the real and imaginary part of the amplitude, respectively. The imaginary contributions arise mostly from resonant long-distance contributions, which can be removed by studying only those q^2 regions where no resonances can contribute. In practice this means the removal of charmonium resonance regions from the whole q^2 range. LHCb $3\,\text{fb}^{-1}$ measurements [2] conservatively exclude the resonance region. Moreover, the contributions from imaginary parts are bounded directly from the LHCb measurements and the bin average values of the ε_λ's are found to be very small as shown in appendix. B. Hence for now we are neglecting the ε_λ's and will address it's contribution in the numerical analysis.

Reminding the definition of following parameters

$$\mathsf{P}_1 = \frac{\mathcal{F}_\perp}{\mathcal{F}_\parallel}, \qquad \mathsf{P}_2 = \frac{\mathcal{F}_\perp}{\mathcal{F}_0}, \tag{5.2.2}$$

we write the observables $F_\perp$, F_L, A_{FB}, A_5 and A_4 as

$$F_\perp = u_\perp^2 + 2\zeta \tag{5.2.3}$$

$$F_L\mathsf{P}_2^2 = u_0^2 + 2\zeta \tag{5.2.4}$$

$$A_{\text{FB}}^2 = \frac{9\zeta}{2\mathsf{P}_1^2}(u_\parallel \pm u_\perp)^2 \tag{5.2.5}$$

$$A_5^2 = \frac{9\zeta}{4\mathsf{P}_2^2}(u_0 \pm u_\perp)^2 \tag{5.2.6}$$

$$A_4 = \frac{\sqrt{2}}{\pi\mathsf{P}_1\mathsf{P}_2}(2\zeta \pm u_0 u_\parallel) \tag{5.2.7}$$

where,

$$\zeta = \frac{\mathcal{F}_\perp^2 C_{10}^2}{\Gamma_f}, \text{ (dropping the '}\widehat{\ }\text{' from } \mathrm{C}_{10} \text{ for simplicity)} \tag{5.2.8}$$

$$u_\lambda^2 = \frac{2\mathcal{F}_\perp^2 r_\lambda^2}{\Gamma_f} = \frac{2}{\Gamma_f}\frac{\mathcal{F}_\perp^2}{\mathcal{F}_\lambda^2}\Big(\text{Re}(\widetilde{\mathcal{G}}_\lambda) - \text{Re}(\widetilde{C}_9^\lambda)\mathcal{F}_\lambda\Big)^2. \tag{5.2.9}$$

u_λ is always taken to be positive and the sign ambiguities introduced in Eqs. (5.2.5)-(5.2.7) ensure that we can make this assumption. The five observables $F_\perp$, F_L, $A_{\rm FB}$, A_5 and A_4 have been expressed above in terms of five parameters P_1, P_2, ζ, u_0 and $u_\perp$. The other three observables A_7, A_8 and A_9 have already been used to solve for the three ε_λ values which are presented in Sec 4.2. It may be noted that since $F_\parallel = 1-F_L-F_\perp$, $u_\parallel$ is not independent and is related to the other parameters by, $u_\parallel^2 = \mathsf{P}_1^2(1-\mathsf{P}_2^{-2}(u_0^2+2\zeta)-(u_\perp^2+2\zeta))-2\zeta$.

In Sec 4.2 a relation depending on observables including all possible effects within SM which was derived and in the real amplitude limit it is written as,

$$\sqrt{4\Big(F_L+F_\parallel+\sqrt{2}\pi A_4\Big)F_\perp-\frac{16}{9}\Big(A_{\rm FB}+\sqrt{2}A_5\Big)^2}\;=\;\sqrt{4F_\parallel F_\perp-\frac{16}{9}A_{\rm FB}^2}\;+\;\sqrt{4F_LF_\perp-\frac{32}{9}A_5^2}. \tag{5.2.10}$$

This equation can be used to express any of the observables in terms of the others. A solution for A_4 [27] is

$$A_4=\frac{8A_5A_{\rm FB}}{9\pi F_\perp}+\frac{\sqrt{4F_\parallel F_\perp-\frac{16}{9}A_{\rm FB}^2}\,\sqrt{4F_LF_\perp-\frac{32}{9}A_5^2}}{2\sqrt{2}\pi F_\perp}. \tag{5.2.11}$$

Whereas, the solution for A_5 and $A_{\rm FB}$ are given by,

$$A_5=\frac{\pi A_4A_{\rm FB}}{2F_\parallel}\pm\frac{3\sqrt{4F_\parallel F_\perp-\frac{16}{9}A_{\rm FB}^2}\sqrt{2F_\parallel F_L-\pi^2A_4^2}}{8F_\parallel}, \tag{5.2.12}$$

$$A_{\rm FB}=\frac{\pi A_4A_5}{F_L}\pm\frac{3\sqrt{4F_LF_\perp-\frac{32}{9}A_5^2}\sqrt{2F_\parallel F_L-\pi^2A_4^2}}{4\sqrt{2}F_L}. \tag{5.2.13}$$

It may noted that Eqs. (5.2.11)*,* (5.2.12) *and* (5.2.13) *depend only on observables and not on any theoretical parameters and thus provides an exact test of the gauge structure of SM with experimental measurements.*

5.3 New physics analysis

In this section we discuss the detailed numerical analysis using 3 fb^{-1} of LHCb data [2]. It contains three different parts, at first we show how the experimental data can be used to extract out the form factors which are involved in this decay mode. Secondly we show that the extracted values of some parameters hint toward a possible evidence of RH currents. Lastly we present the consistency of data to test the relation among observables derived relying only on the gauge structure of the SM.

5.3.1 Form factor extraction

We demonstrate the technique to extract out the hadronic parameters by including complex contributions of the amplitudes and considering systematic uncertainty arising mainly due to bin average effect.

As it is shown in Sec. 4.3 that ε_λ's contribute to the helicity fractions F_λ and asymmetry A_4. We refer to appendix. B for thorough details of evaluation of the complex part of the amplitudes for 3 fb^{-1} of LHCb data. Using the bin average central values of $\varepsilon_\lambda/\sqrt{\Gamma_f}$, with $\pm 1\sigma$ errors from Table. B.1 we can numerically separate out the complex contributions from experimental measured values of the observables. We calculate the central value with $\pm 1\sigma$ error of the modified observables $F_\lambda^{\mathrm{ex}\prime}$ and $A_4^{\mathrm{ex}\prime}$ given by,

$$F_\lambda^{\mathrm{ex}\prime} = F_\lambda^{\mathrm{ex}} - \frac{2\varepsilon_\lambda^2}{\Gamma_f}, \tag{5.3.1}$$

$$A_4^{\mathrm{ex}\prime} = A_4^{\mathrm{ex}} - \frac{2\sqrt{2}\varepsilon_0\varepsilon_\parallel}{\pi\Gamma_f}, \tag{5.3.2}$$

which enter in the χ^2 definition Eq. (5.3.4) below. It enables us to take into account the complex corrections in our analysis and extract out the variables P_1, P_2, ζ, u_0 and $u_\perp$

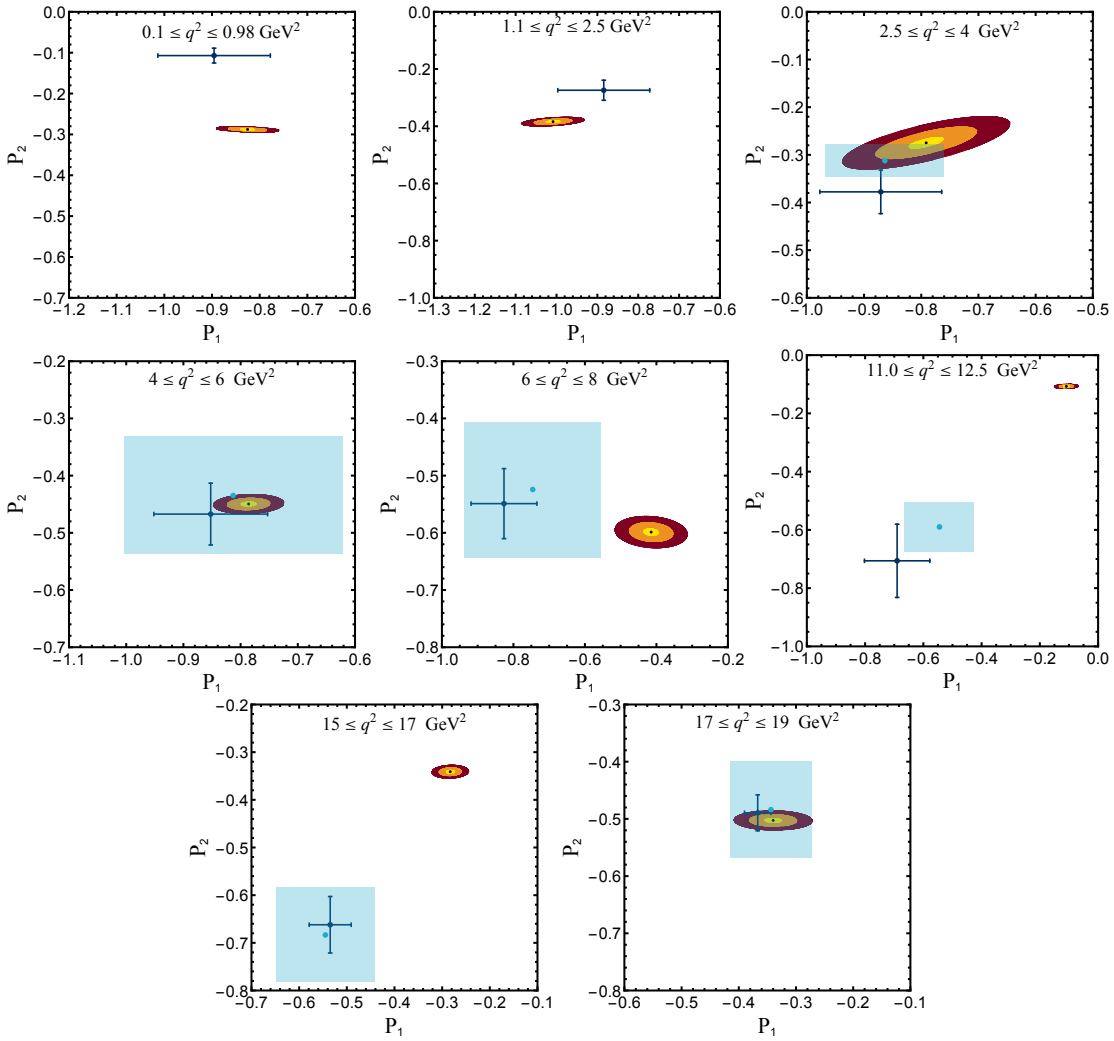

Figure 5.1. (color online). The allowed region for P_1 versus P_2 plane. The innermost yellow (lightest), the middle one orange (light) and outer most red (dark) contours represent 1σ, 3σ and 5σ regions, respectively. The theoretically estimated values using Ref. [8] for $q^2 \leq 8$ GeV^2 and Ref. [9] for $q^2 \geq 11$ GeV^2 are shown as points with error bars. The light blue bands denote exact solutions for the SM observables including charmonium resonances from Ref. [7] parametrization and are shown only for the relevant q^2 bins. In most cases, there is reasonable agreement between the theoretical values and those obtained from data. However, for the ranges $0.1 \leq q^2 \leq 0.98$GeV^2, $6 \leq q^2 \leq 8$GeV^2, $11.0 \leq q^2 \leq 12.5$ GeV^2 and $15 \leq q^2 \leq 17$ GeV^2 there are significant disagreements.

(which only deal with the real part of amplitude) from experimental measurements of the observables accurately.

It should be noted that Eqs. (5.2.3) – (5.2.7) are valid for each q^2 point. However, experiments can provide bin integrated values of observables over a certain q^2 intervals. Thus a χ^2 fit with bin average values of the observables may lead to a biased conclusion. To avoid this issue we have added systematic uncertainties for each observables due to bin average effect with the introduction of new parameter β, where the change in each observable $\mathcal{O}$ is given by,

$$\mathcal{O} \to \mathcal{O} + \beta \mathcal{O}^s. \tag{5.3.3}$$

$\mathcal{O}^s$ is the maximum shift for each observables with a best fitted q^2 function to 14 bin LHCb data [2] within the concerned bin interval. The precise determination of $\mathcal{O}^s$ is described in appendix. C. Therefore the χ^2 definition is

$$\begin{aligned}\chi^2 = \Bigg[&\left(\frac{F_\perp^{\text{ex}\prime} - F_\perp - \beta F_\perp^s}{\Delta F_\perp^{\text{ex}\prime}}\right)^2 + \left(\frac{F_L^{\text{ex}\prime} - F_L - \beta F_L^s}{\Delta F_L^{\text{ex}\prime}}\right)^2 + \left(\frac{A_4^{\text{ex}\prime} - A_4 - \beta A_4^s}{\Delta A_4^{\text{ex}\prime}}\right)^2 \\ &+ \left(\frac{A_{\text{FB}}^{2\,\text{ex}} - A_{\text{FB}}^2 - \beta A_{\text{FB}}^{2s}}{2A_{\text{FB}}^{\text{ex}}\Delta A_{\text{FB}}^{\text{ex}}}\right)^2 + \left(\frac{A_5^{2\,\text{ex}} - A_5^2 - \beta A_5^{2s}}{2A_5^{\text{ex}}\Delta A_5^{\text{ex}}}\right)^2 + \beta^2\Bigg],\end{aligned} \tag{5.3.4}$$

where $A_{\text{FB}}^{\text{ex}}$ and A_5^{ex} indicate experimental central values of the observables A_{FB} and A_5 with $\pm 1\sigma$ errors as $\Delta A_{\text{FB}}^{\text{ex}}$ and ΔA_5^{ex}, respectively. Similarly $F_\perp^{\text{ex}\prime}$, $F_L^{\text{ex}\prime}$ and $A_4^{\text{ex}\prime}$ are the central values of the modified observables defined in Eqs. (5.3.1) and (5.3.2) and $\Delta F_\perp^{\text{ex}\prime}, \Delta F_L^{\text{ex}\prime}, \Delta A_4^{\text{ex}\prime}$ are $\pm 1\sigma$ uncertainties in it. The systematic uncertainties added for each observables are denoted as $F_\perp^s$, F_L^s, A_4^s, A_{FB}^{2s}, A_5^{2s} and these values are quoted in Table. C.1 of appendix. C. The observables $F_\perp$, F_L, A_4, A_{FB}^2 and A_5^2 are evaluated in terms of the five parameters P_1, P_2, ζ, u_0 and $u_\perp$ using Eqs. (5.2.3) – (5.2.7). Considering the inverse of the covariance matrix the error ellipsoids are constructed for all the eight bins corresponding to the q^2 values in the range (0.1 – 0.98) GeV^2, (1.1 – 2.5) GeV^2, (2.5 – 4.0) GeV^2, (4 – 6) GeV^2, (6 – 8) GeV^2, (11.0 – 12.5) GeV^2, (15 – 17) GeV^2 and

$(17-19)$ GeV^2. It can be seen that β is treated as a nuisance parameter with values 0 ± 1. The χ^2 function is minimized w.r.t six parameters P_1, P_2, ζ, u_0, $u_\perp$ and β and the contours shown in Fig. 5.1 and Fig. 5.2 are the allowed regions in the corresponding planes. The minimum values of the χ^2 function for first to eighth bins are 6.9×10^{-9}, 3.4×10^{-10}, 0.055, 8.6×10^{-30}, 1.094, 0.538, 0.218 and 0.044, respectively. The best fitted values with $\pm1\sigma$ errors of the parameter β for all eight bins are $7.4\times10^{-5}\pm0.015$, $1.6\times10^{-5}\pm0.020$, 0.153 ± 0.011, $1.0\times10^{-17}\pm0.005$, 0.736 ± 0.020, 0.251 ± 0.003, 0.261 ± 0.001 and 0.161 ± 0.012, respectively.

The contours corresponding to 1σ, 3σ and 5σ permitted regions for P_1 versus P_2 plane are presented in Fig. 5.1. These contours are compared with the estimated values of P_1 and P_2 using Ref. [8] for $q^2 \leq 8$ GeV^2 and Ref. [9] for $q^2 \geq 11$ GeV^2. The center black point denotes the best fit point by minimizing the chi-square function defined in Eq. (5.3.4). In most cases reasonable agreement is found between theoretical values of P_1 and P_2 and their values obtained from data. However, there are some significant disagreements. The values of form factor ratio P_2 differ by 9σ in the $0.1 \leq q^2 \leq 0.98$ GeV^2 bin. It may be noted that this region in q^2 is highly affected by finite lepton mass and hence the large discrepancy may not accurately reflect the significance due to the unaccounted lepton mass correction systematics. Significant deviations are also found for the three bins $6 \leq q^2 \leq 8$ GeV^2, $11.0 \leq q^2 \leq 12.5$ GeV^2 and $15 \leq q^2 \leq 17$ GeV^2 where P_1 (P_2) differ by 4.2σ (0.8σ), 5.2σ (4.8σ) and 5.5σ (5.3σ), respectively. The light blue bands denote exact solutions for the SM observables including charmonium resonances from Ref. [7] parametrization and are shown only for the relevant q^2 bins. The detailed analysis of resonance effect will be discussed later in this section.

In Fig. 5.2 contours similar to Fig. 5.1, but corresponding to P_1 versus ζ permitted regions are presented for 1σ, 3σ and 5σ confidence level regions. These contours are similarly compared with the estimated values of P_1 and ζ using Refs. [8, 9] and assuming the theoretical estimate of C_{10} [30]. Data shows consistency with theoretical values of P_1 and ζ

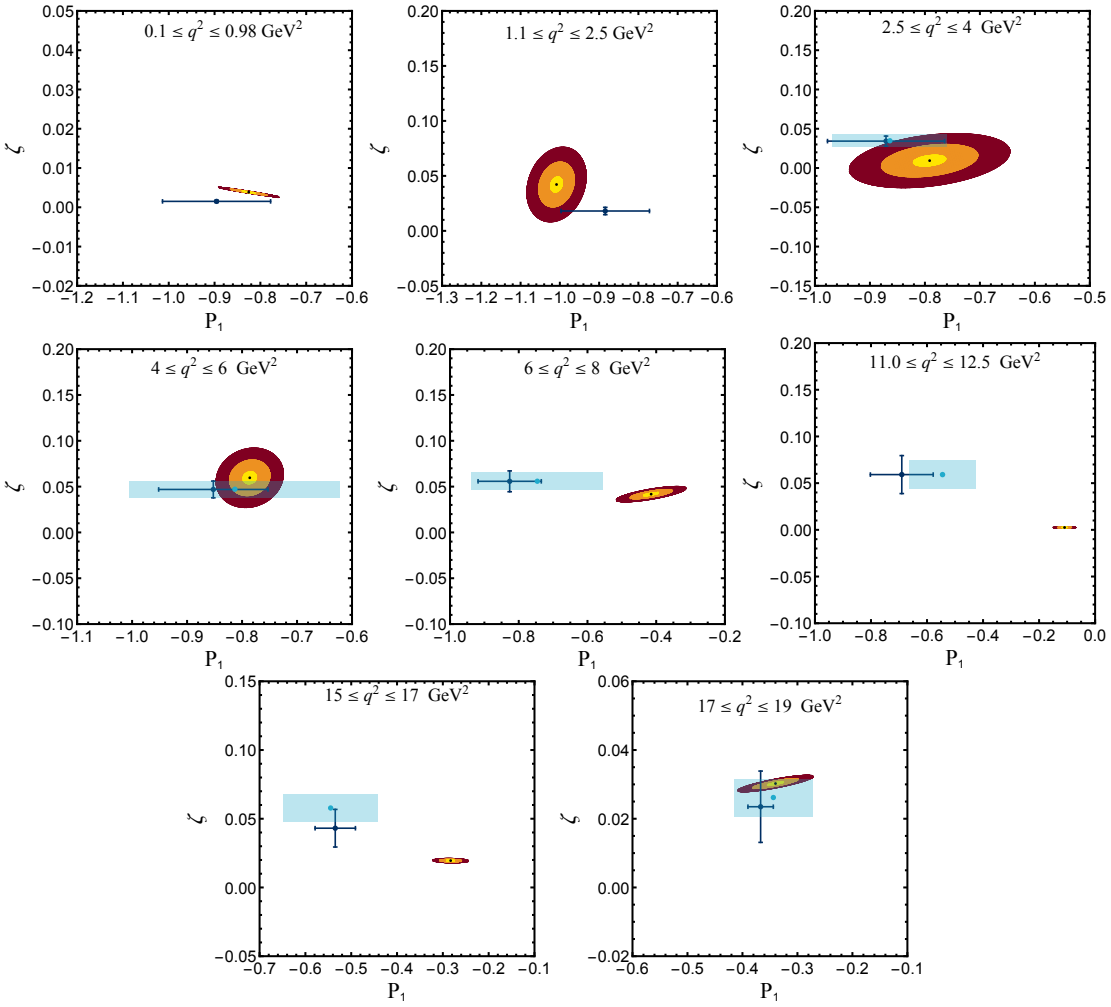

Figure 5.2. (color online). The allowed region for P_1 versus ı plane. The color code is same as Fig. 5.1. The theoretically estimated values from Ref. [8,9] are shown as points with error bars. The P_1 and ζ values significantly disagree for ranges $6 \leq q^2 \leq 8\text{GeV}^2$, $11.0 \leq q^2 \leq 12.5$ GeV^2 and $15 \leq q^2 \leq 17$ GeV^2, similar to the values of P_1 and P_2 shown in Fig. 5.1.

in most cases except for the two bins $11.0 \leq q^2 \leq 12.5$ GeV^2 and $15 \leq q^2 \leq 17$ GeV^2 where ζ disagrees by 2.8σ and 1.7σ respectively. The best fit value of ζ with $\pm 1\sigma$ error obtained from the fit can be used to calculate the form factor $\mathcal{F}_\perp$ using Eq. (5.2.8).

q^2 range in GeV^2	$V(q^2)$	$A_1(q^2)$	$A_{12}(q^2)$
$0.1 \leq q^2 \leq 0.98$	0.677 ± 0.092 (3.05σ)	0.570 ± 0.077 (3.40σ)	0.246 ± 0.034 (0.88σ)
$1.1 \leq q^2 \leq 2.5$	0.625 ± 0.071 (2.78σ)	0.409 ± 0.046 (2.00σ)	0.326 ± 0.047 (0.69σ)
$2.5 \leq q^2 \leq 4.0$	0.230 ± 0.150 (1.36σ)	0.180 ± 0.118 (1.09σ)	0.214 ± 0.149 (0.81σ)
$4.0 \leq q^2 \leq 6.0$	0.552 ± 0.043 (1.07σ)	0.400 ± 0.032 (1.69σ)	0.359 ± 0.041 (1.09σ)
$6.0 \leq q^2 \leq 8.0$	0.485 ± 0.045 (1.27σ)	0.598 ± 0.073 (3.18σ)	0.252 ± 0.025 (1.78σ)
$11.0 \leq q^2 \leq 12.5$	0.166 ± 0.018 (5.64σ)	0.560 ± 0.065 (1.76σ)	0.450 ± 0.054 (1.81σ)
$15.0 \leq q^2 \leq 17.0$	0.828 ± 0.120 (2.79σ)	0.649 ± 0.098 (1.38σ)	0.496 ± 0.074 (1.51σ)
$17.0 \leq q^2 \leq 19.0$	1.813 ± 0.436 (0.78σ)	0.698 ± 0.171 (0.80σ)	0.461 ± 0.112 (0.91σ)

Table 5.1. The form factor values obtained from fit to 3 fb^{-1} of LHCb data [2]. Round brackets indicate the standard deviation between fitted values and theoretical estimates [8, 9]. Significant discrepancies are found for V and A_1 in several q^2 region.

Finally the form factor V can be evaluated using Eq. (5.2.1a) and the value of $\mathcal{F}_\perp$ obtained. Since the recent 3 fb^{-1} of LHCb result [2] does not provide branching fraction measurement for the entire q^2 region we assume the theoretical values of I_f [8, 9] in addition to C_{10} [30]. The form factors $\mathcal{F}_\parallel$ and $\mathcal{F}_0$ can then be determined from the fits to P_1 and P_2 respectively, using Eq. (5.2.2). Thus the conventional form factors A_1 and A_{12} can easily be estimated with the relation given in Eqs. (5.2.1b) and (5.2.1c). In Table. 5.1 we list the best

fit values with the 1σ uncertainties for the three form factors $V(q^2)$, $A_1(q^2)$ and $A_{12}(q^2)$ for all the eight q^2 intervals. We also present the standard deviation of the fit compared to the theoretical estimate from Refs. [8, 9]. While sizable discrepancy is seen for all the form factors especially in the regions $q^2 < 2.5$ GeV^2 and $q^2 > 6$ GeV^2. It is interesting to note the very significant discrepancy is observed in the values of form factors V and A_1 in bins $0.1 \leq q^2 \leq 0.98$ GeV^2, $1.1 \leq q^2 \leq 2.5$ GeV^2, $6 \leq q^2 \leq 8$ GeV^2, $11.0 \leq q^2 \leq 12.5$ GeV^2 and $15 \leq q^2 \leq 17$ GeV^2. The lattice estimate of the form factors currently does not include finite K^* width. This implies, that the significance of the deviations can be lower if one includes the unaccounted systematics due to the finite K^* width. We point out that previous attempts to incorporate resonance contributions in theory has been done by parametrically taking it's effect in the Wilson coefficient C_9 [7, 55]. However the accuracy of the form of resonance parametrization does not alter our determination of form factors since, our analysis is independent of $\widetilde{C}_9^\lambda$ estimates. $\widetilde{C}_9^\lambda$ contributes only to u_λ's and *the ratios of form factors* P_1 *and* P_2 *do not get affected by resonances.* This is easily seen if we consider a situation where NP is absent and all the parameters for resonances (strength, phase etc.) are known, the observables calculated using Eqs. (5.2.3)–(5.2.7) should agree with the experimental measured observables. Thus the consistent set of Eqs. (5.2.3)–(5.2.7) must provide the same set of parameters that we would have started with, as best fit solutions. In the absence of NP the measured observables should result in the solutions for parameters matching with SM values. Since P_1 and P_2 are unaffected by resonances their best fit solutions also remain unaffected by it. Our best fit values of P_1 and P_2 differ from the SM estimates and this discrepancy cannot be accounted for by resonances.

To establish the above arguments we further undertake an extensive study illustrated in Fig. 5.3. We choose the region $q^2 > 11$ GeV^2 as resonance effects can be dominant here and assume SM form factor values of the observables from lattice calculations [9]. The solutions for P_1 and P_2 are obtained using Eqs. (5.2.3)–(5.2.7) for seven different q^2 points; 11 GeV^2, 12 GeV^2, 15 GeV^2, 16 GeV^2, 17 GeV^2, 18 GeV^2 and 19 GeV^2. The observables

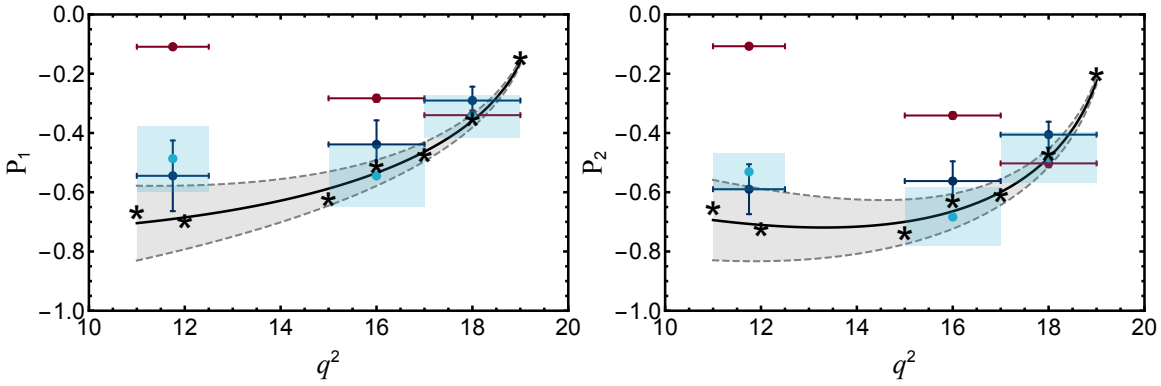

Figure 5.3. (color online) Illustrative plots for bin average and resonance effects in the solutions for P_1 (left panel) and P_2 (right panel). The SM observables are assumed from lattice form factors [9]. The black 'stars' denote the solutions obtained at seven different points in q^2 for the corresponding parameters in each plot. The black central curve with gray band is the form factor estimate (mean with $\pm 1\sigma$ error) of P_1 and P_2. The blue error bars are the solutions for P_1 and P_2 using the bin average values of SM observables whereas the light blue bands denote the solutions considering resonances in observables from Ref. [7] parametrization. The red error bars denote the solutions obtained using data (as highlighted in contours is Fig. 5.1). Including the resonances with the parametrization used in Ref. [7], the solutions for P_1 and P_2 are unaltered and superimpose with the 'stars' completely. (see text for details)

$F_\perp$, F_L, A_4, $A_{\rm FB}^2$ and A_5^2 are SM estimates calculated using lattice form factors. These seven solutions of P_1 and P_2 are denoted by 'star' symbols in the corresponding plots. The black central line with gray band is the form factor estimate (mean with $\pm 1\sigma$ error) of P_1 and P_2. It can be seen that the set of Eqs. (5.2.3)–(5.2.7) are completely consistent with SM structure and produces expected solutions. In case the solutions were completely analytically obtained, the 'stars' should sit on the black curves. However the solutions for hadronic parameters are very complicated and has been evaluated numerically, resulting in small shifts that are visible. The blue error bars are the solutions for P_1 and P_2 using the bin average values of SM observables. It can be seen that as the Eqs. (5.2.3)–(5.2.7) are valid at each q^2 point, bin averaging has induced some shifts in the solutions. However the results are in agreement within $\pm 1\sigma$ confidence level region. To illustrate the effect of resonances we have considered the parametrization from Ref. [7]. The charmonium bound states $J/\psi(1S)$, $\psi(2S)$, $\psi(3770)$, $\psi(4040)$, $\psi(4160)$ and $\psi(4415)$ are included in the mentioned five observables. Interestingly, the change in the value of observables including the resonances affected the solutions for ζ, $u_\perp$ and $u_\parallel$, however, solutions to P_1

and P_2 remained unaltered (upto second decimal place), hence, the solutions completely superimpose with the 'stars' obtained without resonance contributions. We have also investigated the effect of resonances in the bin average where the observables are evaluated with lattice form factors including the above mentioned resonances and the solutions to P_1 and P_2 are shown in light blue bands for the three q^2 bins $11.0 \leq q^2 \leq 12.5$ GeV^2, $15 \leq q^2 \leq 17$ GeV^2 and $17 \leq q^2 \leq 19$ GeV^2. In this case the results with and without resonances do not completely superimpose however are quite consistent within $\pm 1\sigma$ error bars. These solutions are also shown in Fig. 5.1 and 5.2, in same light blue bands, for the relevant bins where resonance effect may in principle be significant. The red error bars are the solutions for P_1 and P_2 obtained from data (as discussed and highlighted in contours is Fig. 5.1) that have been shown here again for convenience. We reiterate that effect of resonances in P_1, P_2 solutions is independent of the parametrization choice as the solutions do not depend on Wilson coefficient $\widetilde{C}_9^{\lambda}$ and our conclusions derived for P_1 and P_2 parameters are unaffected by resonance effect. It is justified that bin average can induce some errors in the solutions. However, we have allowed a shift in the observable values (in Eq. 5.3.4 and Table. C.1) of more than the 1σ error for each observable which hopefully is sufficient to compensate such effects.

It is important to note that in our analysis no hadronic estimates are used to solve for the five parameters from exactly five measurements. Whereas, in other approaches, when considering the same $B \to K^* \ell\ell$ mode all six form factors, Wilson coefficients and non-factorizable corrections based on conservative estimations are needed. We compare P_1 and P_2 obtained from experimental data alone, with the three form factor V, A_1 and A_{12} to which they are related as theoretical inputs. The form-factors T_1, T_2 and T_{23} are not used in this comparison. Thus, our comparisons are different in nature and have reduced uncertainties, in terms of number of theoretical estimates. This may result in higher significance level of deviation observed here.

q^2 range in GeV^2	u_0	$u_\parallel$	$u_\perp$
$15 \leq q^2 \leq 17$	0.000 ± 0.016	0.013 ± 0.153	0.367 ± 0.025
$17 \leq q^2 \leq 19$	0.166 ± 0.014	0.000 ± 4.579	0.260 ± 0.048
$15 \leq q^2 \leq 19$	0.120 ± 0.007	0.004 ± 0.441	0.244 ± 0.026

Table 5.2. The values of u_0, $u_\parallel$ and $u_\perp$ obtained from fit to 3 fb^{-1} of LHCb data [2]. In large q^2 region [10, 11] the equality $u_0 = u_\parallel = u_\perp$ is expected to hold if non-factorizable charm loop contributions are negligible. The errors in the value of $u_\parallel$ for the larger q^2 bin is unexpectedly large to draw any conclusions. Significant discrepancies which are too large to be solely due to non-factorizable charm loop corrections are observed between the values of $u_\perp$ and u_0 in both bins.

5.3.2 Hint of right-handed currents

The large q^2 region where the K^* has low-recoil energy has also been studied [10, 11] in a modified HQET framework which is a model independent approach. In this limit the number of independent hadronic form factors reduces to only three and one finds [27] that $r_0 = r_\parallel = r_\perp \equiv r$ or equivalently $u_0 = u_\parallel = u_\perp$ must hold as long as non-factorizable charm loop contributions are negligible. We find that this relation does not hold for either of the bins $15 \leq q^2 \leq 17$ GeV^2 or $17 \leq q^2 \leq 19$ GeV^2. The values of u_0, $u_\parallel$ and $u_\perp$ obtained from the fit with $\pm 1\sigma$ errors are listed in Table 5.2. We note that u_λ's receive problematic resonance contribution coming from $\widetilde{C}_9^\lambda$. To address this issue we have introduced more sytematics in measured observable than the one arising only from bin average effect. We have checked our analysis by doubling the systematics of the observables given in Table. C.1 of appendix. C for the q^2 range $11 \leq q^2 \leq 12.5$ GeV^2 and $15 \leq q^2 \leq 17$ GeV^2 and our results are stable with it. The actual significance of the deviations observed here can be obtained with the detailed study of resonance systematics which is a subject of an independent work. However the significance level is evaluated by conservatively adding systematics varying between 10% – 100% in the observables. The large discrepancies observed are equally hard to explain solely due to non-factorizable charm loop corrections

and may be additional evidence of physics beyond the SM.

The mentioned relation among u_λ is exact at a special point in the q^2 i.e., the kinematic endpoint $q^2_{\rm max}$. The heavy quark symmetry breaking corrections are negligible and the non-factorizable contributions are polarization independent at $q^2_{\rm max}$ [13]. We implement the formalism at $q^2_{\rm max}$ to study extensively. However, the explicit derivation of the work is beyond the scope of this thesis and we refer the reader to Ref. [12] for detailed description. Here we mention the important findings as follows.

We notice that an alternation in the relation among u_λ is possible in presence of RH current operators O'_9 and O'_{10} [12]. With respective couplings C'_9 and C'_{10}, the amplitudes modify as

$$\mathcal{A}^{L,R}_{\perp} = ((\widetilde{C}^{\perp}_9 + C'_9) \mp (C_{10} + C'_{10}))\mathcal{F}_{\perp} - \widetilde{\mathcal{G}}_{\perp}, \tag{5.3.5}$$

$$\mathcal{A}^{L,R}_{\parallel,0} = ((\widetilde{C}^{\parallel,0}_9 - C'_9) \mp (C_{10} - C'_{10}))\mathcal{F}_{\parallel,0} - \widetilde{\mathcal{G}}_{\parallel,0}\,. \tag{5.3.6}$$

Due to difference in contributions for different helicities, in the presence of RH currents one expects $u_0 = u_\parallel \neq u_\perp$ at $q^2 = q^2_{\rm max}$ without any approximation. To test the relation among u_λ in light of LHCb data, we expand the observables F_L, $F_\perp$, $A_{\rm FB}$ and A_5 around $q^2_{\rm max}$ assuming a 3rd order polynomial form. The zeroth order coefficients of the observable expansions are assumed from the constraints arising from Lorentz invariance and decay kinematics derived in Ref. [13], whereas all the higher order coefficients are extracted by fitting the polynomials with 14 bin LHCb data.

We calculate the limiting analytic expressions for $u_\lambda/\sqrt{2\zeta}$ at $q^2 = q^2_{\rm max}$, which is completely in terms of the coefficients of the polynomials used to expand the observables and hence are evaluated completely from data. On the other hand by construction,

$$\frac{u_\perp}{\sqrt{2\zeta}}(q^2_{\rm max}) = \frac{r - C'_9}{C_{10} + C'_{10}}, \quad \frac{u_{\parallel,0}}{\sqrt{2\zeta}}(q^2_{\rm max}) = \frac{r + C'_9}{C_{10} - C'_{10}}. \tag{5.3.7}$$

which depend explicitly on the RH couplings C'_9, C'_{10} and one hadronic parameter r/C_{10}. This enables us to predict the allowed region in C'_{10}/C_{10} – C'_9/C_{10} plane as shown in Fig. 5.4. The yellow, orange and red bands denote 1σ, 3σ and 5σ confidence level regions, respectively. The SM estimate of r/C_{10} can have uncertainties that cannot easily be accounted for. These could range from errors in Wilson coefficients, contributions from other kinds of NP or even the contributions from resonances. In order to ascertain the accuracy of our conclusion to these uncertainties, we considered the input r/C_{10} as a nuisance parameter. The bestfit value with $\pm 1\sigma$ error for the parameters C'_{10}/C_{10}, C'_9/C_{10} and r/C_{10} are -0.63 ± 0.43, -0.92 ± 0.14 and 0.84 ± 0.10, respectively. The SM prediction (the origin) remains on a 3σ significance level contour providing evidence of RH currents.

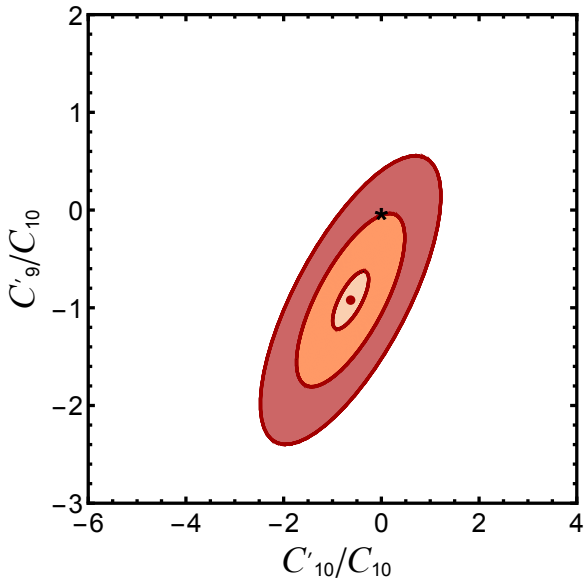

Figure 5.4. In C'_{10}/C_{10} – C'_9/C_{10} plane, the yellow, orange and red regions correspond to 1σ, 3σ and 5σ significance level, respectively. The only one SM input r/C_{10} is varied as a nuisance parameter. The SM predictions is indicated by the stars. Strong evidence of RH current is pronounced from the plot.

5.3.3 Testing relation between observables

The relation between the observables for asymmetries A_4, A_5 and $A_{\rm FB}$ given in Eqs. (5.2.11) – (5.2.13) can also be tested using LHCb data [2]. In Fig. 5.5, top left panel, we compare

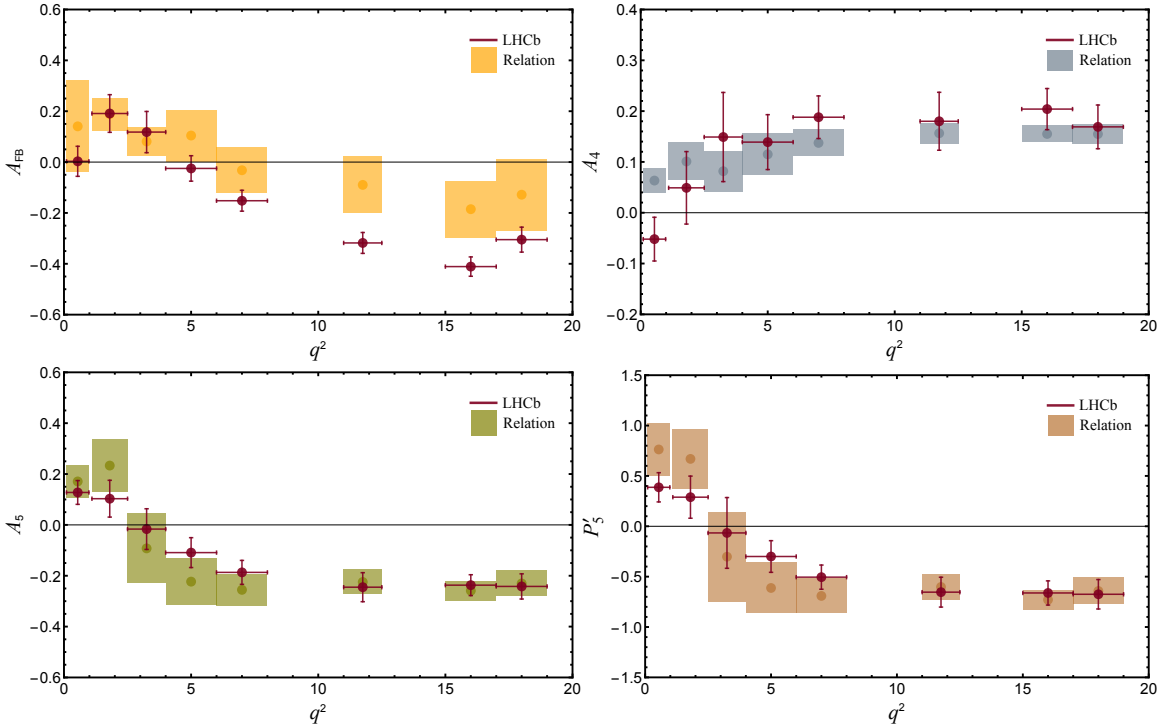

Figure 5.5. (color online) The mean values and $\pm 1\sigma$ uncertainty bands for asymmetries $A_{\rm FB}$, A_4, A_5 and P_5' calculated using Eqs. (5.2.11) – (5.2.13) are shown in yellow, gray, green and brown bands, respectively. The error bars in red (dark) correspond to the LHCb measured [2] central values and errors for each observable for the respective q^2 bins. The predictions for the asymmetries are obtained using the relations among observables which are independent of any hadronic parameters and depend on experimental measurements of the other observables remaining in the corresponding relations. Sizable discrepancies are shown for $A_{\rm FB}$ in $11.0 \leq q^2 \leq 12.5$ GeV^2 and $15 \leq q^2 \leq 17$ GeV^2 bins and for A_4 in the range $0.1 \leq q^2 \leq 0.98$ GeV^2. We note that the relations (Eqs. (5.2.11) – (5.2.13)) remain valid except in the presence of NP operators that result in modified angular distribution. Hence the presence of right-handed currents and any extra vector current such as Z' the relations will remain valid.

theoretically calculated $A_{\rm FB}$ mean values and $\pm 1\sigma$ errors (in yellow bands) with experimental measurements (red error bars) for the respective q^2 bins. All observables in the r.h.s of Eq. (5.2.13) ('relation') are assumed to be Gaussian distributions in data and the predictions for $A_{\rm FB}$ in yellow bands are obtained using the expression of the 'relation'. A very good agreement is evident for most q^2 regions, however, for the ranges $11.0 \leq q^2 \leq 12.5$ GeV^2 and $15 \leq q^2 \leq 17$ GeV^2 a deviation of 2.1σ and 1.8σ is observed. Similarly 'relation' for A_4 in Eq. (5.2.11) results in a very good agreement except for showing a discrepancy of 2.3σ only in the $0.1 \leq q^2 \leq 0.98$ GeV^2 bin, in right top panel of Fig. 5.5. The disagreement in the value of $A_{\rm FB}$ and A_4 in some q^2 bins indicates that there

is no set of form factors and Wilson coefficients which can explain $A_{\rm FB}$ and A_4 completely. Observables A_5 or equivalently P_5' [56] are found to be in complete agreement i.e. within about $\pm 1\sigma$ deviation for all q^2 bins as shown in the two lower panels of Fig. 5.5. The solutions for A_5 and $A_{\rm FB}$ have ambiguities. We chose the ambiguity for which the chi-squared deviations are the least. Our conclusions have no bearing on and do not rule out the observation made by LHCb in observable P_5' in Refs. [2, 57]. The predictions of observable P_5' derived from the relation is a signal of consistency of LHCb results. We note that the relation remains valid except in the presence of NP operators that result in modified new angular distribution. Hence we do not expect to see the discrepancy observed by LHCb [57] if right-handed currents or extra vector current such as Z' contributes to the decay. The discrepancy observed by LHCb depends on the comparison with model based calculation of form factors. Whereas, the predictions of these asymmetries made in this chapter, are independent of any form factor values and depend purely on the gauge structure of SM. If the model dependent calculations of form factors are correct, signal of NP may well be indicated in the bins suggested by Ref. [57]. We find that LHCb data indicates yet another independent discrepancy.

5.4 Summary

In summary, we have used the $3\,\text{fb}^{-1}$ of LHCb data to determine some hadronic parameters governing the decay $B \to K^* \ell^+ \ell^-$ assuming contributions from SM alone. We obtain the values of the form factors $V(q^2)$, $A_1(q^2)$ and $A_{12}(q^2)$ that are used to describe the matrix element $\langle K^* | \bar{s} \gamma^\mu P_L b | B \rangle$ directly from data. Very significant deviations are seen for the form factors V and A_1 especially in the regions $q^2 < 2.5\ \text{GeV}^2$ and $q^2 > 6\ \text{GeV}^2$. We point out that the presence of resonances in data can induce more systematic uncertainties in the fits. However in the view of absence of such a existence of resonances in $B \to K^* \ell^+ \ell^-$ data, we emphasize that the significant deviations observed in the form factor values can not be completely explained by resonances and non-factorizable contributions. We would

like to point out that there exist major differences between the global fit approaches [58] to study the anomalies in $b \to s$ transitions and the approach adopted in our work. Our work relies only on $B \to K^* \ell\ell$ decay mode, whereas, global fit techniques incorporate various decay modes and hence either use LCSR, Lattice based estimates of form factors or treat form-factors as parameters in the fit procedure. The number of inputs and fitted parameters differ making a number by number comparison of the different approaches difficult. Furthermore due to the absence of accurate estimates of nonfactorizable corrections, the global fit techniques rely on some conservative estimations of these corrections. However, the formalism we have developed parametrizes such corrections and the conclusions drawn here are independent of nonfactorizable estimates. These are perhaps the reasons why we find larger significance. However, qualitatively we don't see a significant disagreement with the other approaches as we do observe $\sim 3\sigma$ discrepancy in $\mathsf{P}_1 - \mathsf{P}_2$ plane in q^2 region $[6 - 8]\text{GeV}^2$ where observable P_5' also deviates by 2.7σ from its SM prediction.

Further, a relation between form factors expected to hold in the large q^2 region as long as non-factorizable charm loop contributions are negligible, seems to fail. This observation then leads to establish the evidence of RH currents, based on the analysis at kinematic endpoint, in a later study. Finally, the relation between observables also indicates some deviations in the same regions where the form factors were found to disagree. The forward-backward asymmetry A_{FB} deviates in the $q^2 > 11$ GeV^2 region, where as A_4 differs in the region $q^2 \leq 0.98$ GeV^2. As the systematic error arises from the experimental measurements of observables in terms of binned dilepton invariant mass are accounted, the magnitude of discrepancies observed would be hard to accommodate either as systematics from long distance resonance contributions or possible corrections to theoretical estimates. All these features can be understood if there are other unaccounted for operators contributing to the decay mode. In view of this, we speculate that these deviations are likely to be a signature of physics beyond SM.

6 Lepton flavor non-universality

In this chapter we scrutinize the hint of lepton flavor non-universality observed in both charged current and neutral current transitions of B mesons by several experimental collaborations. In an effective theory approach a possible explanation to all these observed anomalies are presented while being consistent with other measurements.

The content of this chapter is based on work done with Debajyoti Choudhury, Anirban Kundu and Rahul Sinha [17].

Everything should be made as simple as possible, but not simpler. - Albert Einstein

6.1 Introduction

The last few years have seen some intriguing hints of discrepancies in a few charged- as well as neutral-current decays of B-mesons, when compared to the expectations within the SM. While the fully hadronic decay modes are subject to large (and, in cases, not-so-well understood) strong interaction corrections, the situation is much more under control for semileptonic decays, where the dominant uncertainties come from the form factors and quark mass values. Even these uncertainties are removed to a large extent if one considers ratios of similar observables. Thus, the modes $b \to c\ell\bar{\nu}_\ell$ and $b \to s\ell^+\ell^-$ are of great interest. While, individually, none of these immediately calls for the inclusion of NP effects (given the current significance levels of the discrepancies), viewed together, they strongly suggest that some NP is lurking around the corner. Most interestingly, the pattern also argues convincingly for some NP that violates lepton-flavour universality (LFU), a cornerstone of the SM, especially to a level that cannot be simply explained by the inclusion of right-handed neutrino fields and the consequent neutrino masses.

As we have just mentioned, relative partial widths (or, equivalently, the ratios of branching ratios (BR)) are particularly clean probes of physics beyond the SM, on account of the cancellation of the leading uncertainties inherent in individual BR predictions. Of particular interest to us are the ratios $R(D)$ and $R(D^*)$ pertaining to charged-current decays, defined as

$$R(D^{(*)}) \equiv \frac{\mathrm{BR}(B \to D^{(*)}\tau\nu)}{\mathrm{BR}(B \to D^{(*)}\ell\nu)}\,, \tag{6.1.1}$$

with $\ell = e$ or μ, and an analogous ratio for the neutral-current sector

$$R_{K^{(*)}} \equiv \frac{\mathrm{BR}(B \to K^{(*)}\mu^+\mu^-)}{\mathrm{BR}(B \to K^{(*)}e^+e^-)}\,. \tag{6.1.2}$$

For the K^* mode, the discrepancy is visible not only in the ratios of binned differential distribution for muon and electron mode, but also in some angular asymmetries in $B \to$

$K^*\mu\mu$ which we have already discuss in previous chapters.

The SM estimates for these decays are already quite robust. With the major source of uncertainty being the form factors, they cancel out in ratios like $R(D^{(*)})$ or $R_{K^{(*)}}$. The values of $R(D)$ and $R(D^*)$ as measured by *BABAR* [18], when taken together, exceed SM expectations by more than 3σ. While the Belle measurements lie in between the SM expectations and the *BABAR* measurements and are consistent with both [19], their result on $R(D^*)$ [20], with the τ decaying semileptonically, agrees with the SM expectations only at the 1.6σ level[1]. Similarly, the first measurement by LHCb [21] is also 2.1σ above the SM prediction. Considering the myriad results together, and including the correlations, the tension between data and SM is at the level of 3.9σ [16].

While the data on $R(D)$ and $R(D^*)$ lie above the SM predictions, that on R_K and R_{K^*} are systematically below the expectations. A similar shortfall has been observed in the same q^2-bin for the decay $B_s \to \phi\mu\mu$, which is again mediated by the process $b \to s\mu\mu$. However, the purely leptonic decay $B_s \to \mu^+\mu^-$ and the radiative decay $B \to X_s\gamma$ do not show any appreciable discrepancy with the SM expectations. The same is true for the mass difference ΔM_s and mixing phase ϕ_s measurements for the B_s system. The pattern of deviations is thus a complicated one and, naively at least, seemingly contradictory. These, thus pose an interesting challenge to the model builders: how to incorporate all the anomalies in a model with the least number of free parameters?

While both model-dependent and model-independent search strategies for NP based on R_K and/or $R(D^{(*)})$ data have drawn lot of attention, the subject has recently received a further impetus from the announcement of the apparent deficit in R_{K^*} [15]. In this chapter we present a minimal extension of the SM operator basis which can explain all the anomalies without jeopardizing the results that are consistent with the SM.

Rather than advocating a particular model, we shall assume a very phenomenogical ap-

[1] On the other hand, the measurement of τ-polarization for the decay $B \to D^*\tau\nu$ in Belle [59] is consistent with the SM predictions, albeit with only a large uncertainty.

proach. Virtually all the data can be explained in terms of an effective Lagrangian, operative at low-energies, and different from that obtained within the SM. However, with 'minimality' being a criterion, we would like not to introduce an arbitrarily large number of new parameters, as would be the case with a truly anarchic effective theory. Instead, we investigate the situation in terms of the minimum number of such operators. The best fit for the Wilson coefficients, thus obtained, would presumably pave the way for inspired model building. We will show how the relationship between the NP Wilson coefficients may hold the key for a yet unknown flavor dynamics.

The rest of the chapter is arranged as follows. In Sec. 6.2, we recount and discuss the experimental situation. This is followed, in Sec. 6.3, by a discussion of the microscopic dynamics that lead to such processes. Sec. 6.4 discusses the minimal set of NP operators which can explain the data. Sec. 6.5 contains our results, and finally we conclude in Sec. 6.6.

6.2 The data : a brief recounting

We begin by briefly reviewing the experimental measurements and theoretical predictions for the observables of interest. We also take this opportunity to review some further processes that would turn out to have important consequences in our attempt to explain the anomalies.

- As already mentioned, discrepancies in the measurements of the observables $R(D)$ and $R(D^*)$ have been seen, over the last several years, in multiple experiments such as LHCb, *BABAR* and Belle. In Table. 6.1, taken from Ref. [60], we summarize the measurements along with the corresponding SM predictions.

  While the *BABAR* measurement for $R(D)$ is only 2σ away from the SM expectations, the discrepancy increases to 2.7σ for $R(D^*)$. Combining with the LHCb data, the latter increases to $\sim 3.2\sigma$. Admittedly the full 2016 sample is much closer to

the SM than to the rest of the measurements. However, it should be realized that the hadronically tagged sample [59] (included in the 'full' sample) has its own associated theoretical uncertainties. On the other hand, the semileptonically tagged sample leads to a value not only in consonance with the other two experiments, but consistent with the SM only at the 1.6σ level. Neglecting such subtleties, and combining the results, one finds [16]

$$R(D) = (1.36 \pm 0.15) \times R(D)_{\rm SM}, \qquad R(D^*) = (1.21 \pm 0.06) \times R(D^*)_{\rm SM}\,. \tag{6.2.1}$$

While individually the discrepancies are at $\sim 2.3\sigma$ and $\sim 3.4\sigma$ respectively, on inclusion of the $R(D)$–$R(D^*)$ correlation, the combined significance is at $\sim 4\sigma$ level.

	$R(D)$	$R(D^*)$
SM prediction	0.300 ± 0.008 [61]	0.252 ± 0.003 [62]
BABAR (Isospin constrained)	$0.440 \pm 0.058 \pm 0.042$	$0.332 \pm 0.024 \pm 0.018$ [18]
Belle (2015)	$0.375 \pm 0.064 \pm 0.026$	$0.293 \pm 0.038 \pm 0.015$ [19]
Belle (2016)	-	$0.302 \pm 0.030 \pm 0.011$ [20]
Belle (2016, Full)	-	$0.270 \pm 0.035\ ^{+0.028}_{-0.025}$ [59]
LHCb (2015)	-	$0.336 \pm 0.027 \pm 0.030$ [21]
Average	$0.407 \pm 0.039 \pm 0.024$	$0.304 \pm 0.013 \pm 0.007$ [63]

Table 6.1. The SM predictions for and the data on $R(D)$ and $R(D^*)$. While *BABAR* considers both charged and neutral B decay channels, LHCb and Belle results, as quoted here, are based only on the analysis of neutral B modes. For Belle, 'Full' implies the inclusion of both semileptonically and hadronically tagged samples, the last-mentioned excluded otherwise. (Table taken from Ref. [60].)

- For the neutral current transitions (pertaining to $b \to s\ell^+\ell^-$), we have [14, 15]:

$$\begin{aligned} R_K &= 0.745^{+0.090}_{-0.074} \pm 0.036 && q^2 \in [1:6]\,\text{GeV}^2\,, \\ R^{\text{low}}_{K^*} &= 0.660^{+0.110}_{-0.070} \pm 0.024 && q^2 \in [0.045:1.1]\,\text{GeV}^2\,, \\ R^{\text{central}}_{K^*} &= 0.685^{+0.113}_{-0.069} \pm 0.047 && q^2 \in [1.1:6]\,\text{GeV}^2\,. \end{aligned} \tag{6.2.2}$$

  The SM predictions for both R_K and $R^{\text{central}}_{K^*}$ are virtually indistinguishable from unity [64, 65], whereas for $R^{\text{low}}_{K^*}$ it is ~ 0.9 (due to the finite lepton mass effect) and are very precise with negligible uncertainties associated with them. Thus the measurements of R_K, $R^{\text{low}}_{K^*}$ and $R^{\text{central}}_{K^*}$, respectively, correspond to 2.6σ, 2.1σ and 2.4σ deviations from the SM predictions.

- Another hint of deviation (at a level of more than 3σ), for a particular neutral-current decay mode is evinced by $B_s \to \phi\mu\mu$ [8, 66, 67].

$$\Phi \equiv \frac{d}{dq^2}\text{BR}(B_s \to \phi\mu\mu)\Big|_{q^2\in[1:6]\,\text{GeV}^2} = \begin{cases} \left(2.58^{+0.33}_{-0.31} \pm 0.08 \pm 0.19\right) \times 10^{-8}\ \text{GeV}^{-2} & \text{(exp.)} \\ (4.81 \pm 0.56) \times 10^{-8}\ \text{GeV}^{-2} & \text{(SM)}\,. \end{cases} \tag{6.2.3}$$

  where $q^2 = m^2_{\mu\mu}$. Intriguingly, the q^2 region where this measurement has relatively low error (and data is quoted) is virtually the same as that for R_K and $R^{\text{central}}_{K^*}$. This measurement, thus, suggests that one possibility of the discrepancies in R_K and R_{K^*} is caused by a depletion of the $b \to s\mu^+\mu^-$ channel, rather than an enhancement in $b \to se^+e^-$. This is further vindicated by the long-standing P'_5 anomaly [66] in the angular distribution of $B \to K^*\mu\mu$, which again occurs in the central q^2 region, with the mismatch between data and SM prediction being more than 3σ.

- Such a conclusion, though, has to be tempered with the data for the corresponding two-body decay, *viz.* $B_s \to \mu\mu$. The theory predictions are quite robust now, taking into account possible corrections from large $\Delta\Gamma_s$, as well as next-to-leading order

(NLO) electroweak and next-to-next-to-leading order QCD corrections. The small uncertainty essentially arises from the corresponding CKM matrix elements and the decay constant of B_s. The recent measurement of LHCb at a significance of 7.8σ [68,69] shows an excellent agreement between the data and the SM prediction:

$$\mathrm{BR}(B_s^0 \to \mu^+\mu^-) = \begin{cases} \left(3.0 \pm 0.6^{+0.3}_{-0.2}\right) \times 10^{-9} & \text{(exp.)}, \\ (3.65 \pm 0.23) \times 10^{-9} & \text{(SM)}\,, \end{cases} \tag{6.2.4}$$

and hence puts very strong constraints on NP models, in particular on those incorporating (pseudo-)scalar currents. Of course, as the data shows, a small depletion $\sim 20\%$ in the rates is still allowed, and, indeed, to be welcomed. NP operators involving only vector currents do not affect this channel, but scalar, pseudoscalar, and axial vector operators do. Also note that (pseudo)scalar operators are disfavored by constraints from $B_s \to \mu^+\mu^-$ [70].

For future reference, we list here three further rare decay modes.

- Within the SM, the decay modes $b \to s\nu_i\bar{\nu}_i$ are naturally suppressed, owing to the fact that these are generated by either an off-shell Z-mediated diagram[2] coupling to a flavor-changing quark-vertex, or through box-diagrams. Interestingly, the current upper bounds (summed over all three neutrinos) as obtained by the Belle collaboration [71], *viz.*

$$\mathrm{BR}(B \to K\nu\bar{\nu}) < 1.6 \times 10^{-5}\,, \qquad \mathrm{BR}(B \to K^*\nu\bar{\nu}) < 2.7 \times 10^{-5} \tag{6.2.5}$$

(both at 90% C.L) are not much weaker than what is expected within the SM,

[2]The charged lepton modes, in contrast, are primarily mediated by off-shell photons.

namely [72]

$$\begin{aligned} \mathrm{BR}(B^+ \to K^+ \nu\bar{\nu})_{\mathrm{SM}} &= (3.98 \pm 0.43 \pm 0.19) \times 10^{-6} \,, \\ \mathrm{BR}(B^+ \to K^{*0} \nu\bar{\nu})_{\mathrm{SM}} &= (9.19 \pm 0.86 \pm 0.50) \times 10^{-6} \,. \end{aligned} \tag{6.2.6}$$

In other words, we have

$$\frac{\mathrm{BR}_K^{\mathrm{exp}}}{\mathrm{BR}_K^{\mathrm{SM}}} < 3.9 \,, \qquad \frac{\mathrm{BR}_{K^*}^{\mathrm{exp}}}{\mathrm{BR}_K^{\mathrm{SM}}} < 2.7 \,.$$

We may recast this in terms of δ_{NP} and δ^*_{NP}, that encompass all the NP contributions to such decays and are defined through

$$\frac{\mathrm{BR}(B \to K \nu\bar{\nu})_{\mathrm{NP}}}{\mathrm{BR}(B \to K \nu_\ell \bar{\nu}_\ell)_{\mathrm{SM}}} = 3 + \delta_{\mathrm{NP}} \,, \,, \qquad \frac{\mathrm{BR}(B \to K^* \nu\bar{\nu})_{\mathrm{NP}}}{\mathrm{BR}(B \to K^* \nu_\ell \bar{\nu}_\ell)_{\mathrm{SM}}} = 3 + \delta^*_{\mathrm{NP}} \,. \tag{6.2.7}$$

where the denominators are for a specific flavor ν_ℓ and not summed over flavors. Thus,

$$\delta_{\mathrm{NP}} < 8.7 \,, \qquad \delta^*_{\mathrm{NP}} < 5.1 \,. \tag{6.2.8}$$

- The purely leptonic mode $B_s \to \tau\tau$ is yet to be observed but LHCb put a 90% confidence level bound on the BR [73]:

$$\mathrm{BR}(B_s \to \tau\tau) < 6.8 \times 10^{-3} \,. \tag{6.2.9}$$

The SM prediction, of course, is way too small, at $(7.73 \pm 0.49) \times 10^{-7}$ [69].

- And, finally, the limits on the rare lepton flavor violating modes $B \to K\mu\tau$ [74] are

$$\mathrm{BR}(B^+ \to K^+ \mu^+ \tau^-) < 4.5 \times 10^{-5} \,, \quad \mathrm{BR}(B^+ \to K^+ \mu^- \tau^+) < 2.8 \times 10^{-5} \,. \tag{6.2.10}$$

6.3 Operators relevant to the observables

Having delineated, in the preceding section, the observables of interest, we now proceed to the identification of the operators, within the SM and beyond, responsible for effecting the transitions. As the scale of NP surely is above the electroweak scale, we will talk in terms of effective current-current operators that, presumably, are obtained by integrating out the heavy degrees of freedom, and not confine ourselves within any particular model. To be precise, the genesis of these operators will be left to the model builders.

Given the fact that, even within the SM, the neutral-current decays under consideration occur only as loop effects, several current-current operators would, in general, be expected to contribute to a given four-fermion amplitude. However, as we shall soon see, certain structures have a special role. To this end, we introduce a shorthand notation:

$$(x, y) \equiv \bar{x}_L \gamma^\mu y_L \quad \forall \;\; x, y \,. \tag{6.3.1}$$

6.3.1 The $b \to c\tau\bar{\nu}_\tau$ transition

This proceeds through a tree-level W-exchange in the SM. If the NP adds coherently to the SM, one can write the effective Hamiltonian as

$$\mathcal{H}^{\text{eff}} = \frac{4G_F}{\sqrt{2}} V_{cb} \left(1 + C^{\text{NP}}\right) \left[(c, b)(\tau, \nu_\tau)\right] \,, \tag{6.3.2}$$

where the NP contribution, parametrized by C^{NP} , vanishes in the SM limit. Using Eq. (6.1.1), we can write

$$\frac{R(D^{(*)})_{\text{SM+NP}}}{R(D^{(*)})_{\text{SM}}} = \left|1 + C^{\text{NP}}\right|^2 . \tag{6.3.3}$$

Thus, to explain the data, one needs either small positive values, or large negative values, of C^{NP} . If the NP involves an operator with different Lorentz structures, or with different

field content (like $b \to c\tau\bar{\nu}_\mu$), the addition would be incoherent in nature, thereby altering the functional form of the differential width.

6.3.2 The $b \to s\mu^+\mu^-$ transition

Responsible for the FCNC decays $B \to K^{(*)}\mu^+\mu^-$ and $B_s \to \phi\mu^+\mu^-$, within the SM, this transition proceeds, primarily, through two sets of diagrams, viz. the "penguin-like" one (driven essentially by the top quark) and the "box" (once again, dominated by the top) as is already being discussed in details in this thesis. Reminding the effective Hamiltonian

$$\mathcal{H}^{\text{eff}} = \frac{-4G_F}{\sqrt{2}} V_{tb} V_{ts}^* \sum_i C_i(\mu) O_i(\mu) , \tag{6.3.4}$$

where the relevant operators are

$$\begin{aligned} O_7 &= \frac{e}{16\pi^2} m_b \left(\bar{s}\sigma_{\mu\nu} P_R b\right) F^{\mu\nu}, \\ O_9 &= \frac{e^2}{16\pi^2} \left(\bar{s}\gamma_\mu P_L b\right) (\bar{\mu}\gamma^\mu \mu) , \\ O_{10} &= \frac{e^2}{16\pi^2} \left(\bar{s}\gamma_\mu P_L b\right) (\bar{\mu}\gamma^\mu \gamma_5 \mu) . \end{aligned}$$

The Wilson coefficients, matched with the full theory at m_W and then run down to m_b with the renormalization group equations at the next-to-next-to-leading logarithmic (NNLL) accuracy [30], are given in the SM as $C_7 = -0.304$, $C_9 = 4.211$, $C_{10} = -4.103$. If the NP operators are made only with (axial)vector currents, one can denote the modified Wilson coefficients as

$$C_9 \to C_9 + C_9^{\text{NP}} = 4.211 + C_9^{\text{NP}} \quad \text{and} \quad C_{10} \to C_{10} + C_{10}^{\text{NP}} = -4.103 + C_{10}^{\text{NP}} . \tag{6.3.5}$$

The consequent normalized differential branching fraction for the $B \to K\mu^+\mu^-$ decay in terms of the dimuon invariant mass squared, q^2, is given by

$$\frac{1}{\Gamma_0}\frac{d\Gamma(B\to K\mu^+\mu^-)}{dq^2} = 2\lambda^{1/2}(m_B^2, m_K^2, q^2)\sqrt{1-\frac{4m_\mu^2}{q^2}}\left\{\frac{1}{6}\lambda(m_B^2, m_K^2, q^2)\left(1+\frac{2m_\mu^2}{q^2}\right)\right.$$
$$\left.\times\left(|F_A|^2+|F_V|^2\right)+q^2|F_P|^2+4m_\mu^2 m_B^2|F_A|^2+2m_\mu\left(m_B^2-m_K^2+q^2\right)\mathrm{Re}(F_P F_A^*)\right\}, \quad (6.3.6)$$

where

$$\Gamma_0 = \frac{G_F^2\alpha^2}{2^9\pi^5 m_B^3}|V_{tb}V_{ts}^*|^2, \text{ and } \lambda(a,b,c) \equiv a^2+b^2+c^2-2(ab+bc+ac)$$

is the famed phase-space factor. The functions F_i depend on the Wilson coefficients and q^2 dependent form factors $f_{0,+,T}$ of the $B \to K$ transition [36], namely

$$\begin{aligned} F_P &= -m_\mu\left(C_{10}+C_{10}^{\rm NP}\right)\left[f_+(q^2)-\frac{m_B^2-m_K^2}{q^2}\left(f_0(q^2)-f_+(q^2)\right)\right], \\ F_A &= \left(C_{10}+C_{10}^{\rm NP}\right)f_+(q^2), \\ F_V &= \left(C_9+C_9^{\rm NP}\right)f_+(q^2)+2C_7\, m_b\,\frac{f_T(q^2)}{m_B+m_K}. \end{aligned} \quad (6.3.7)$$

The differential distribution for $B \to V\ell\ell$ mode, where V stands for a K^* or ϕ meson, can be expressed in terms of certain angular coefficients I_i [1] as

$$\frac{d\Gamma(B\to V\mu^+\mu^-)}{dq^2} = \frac{1}{4}\left[3I_1^c(q^2)+6I_1^s(q^2)-I_2^c(q^2)-2I_2^s(q^2)\right] \quad (6.3.8)$$

The coefficients I_i are functions of the transversity amplitudes $\mathcal{A}_{\lambda,t}^{L,R}$ where λ denotes the three states of polarizations of the meson V, and L and R denote the left and right chirality of the lepton current, respectively. The detailed expressions of I_i and $\mathcal{A}_{\lambda,t}^{L,R}$ can be found in [30].

6.3.3 The $b \to s\nu\bar{\nu}$ transition

Quite akin to the preceding case, this transition (which governs the $B \to K^{(*)}\nu\bar{\nu}$ decay) proceeds through both penguin (only Z though) and box-diagrams. Unless NP introduces right-handed neutrino fields, the low energy effective Hamiltonian may be well-parametrized by [72]

$$\mathcal{H}^{\text{eff}} = -\frac{4G_F}{\sqrt{2}} V_{tb} V_{ts}^* \frac{\alpha_{\text{em}}}{4\pi} C_L^{\text{SM}} \left(1 + C_\nu^{\text{NP}}\right) \times 2\,(s,b)(\nu,\nu), \tag{6.3.9}$$

where α_{em} is the fine structure constant and C_ν^{NP} denotes the NP contribution. Including NLO QCD correction and the two loop electroweak contribution, the SM Wilson coefficient is given by $C_L^{\text{SM}} = -X_t/s_w^2$ where $X_t = 1.469 \pm 0.017$ [75–77].

6.3.4 The two-body decay rates

The branching fraction for $B_s^0 \to \ell^+\ell^-$, where ℓ is any charged lepton, can be written, at the leading order, as

$$\text{BR}(B_s^0 \to \ell^+\ell^-) = \frac{G_F^2 \alpha^2 m_{B_s} \tau_{B_s} f_{B_s}^2 m_\ell^2}{16\pi^3} |V_{tb} V_{ts}^*|^2 \sqrt{1 - \frac{4m_\ell^2}{m_{B_s}^2}} \left| C_{10} + C_{10}^{\text{NP}} \right|^2 , \tag{6.3.10}$$

while that for $B_c^- \to \tau^- \nu_\tau$ is given by

$$\text{BR}(B_c^- \to \tau^- \nu_\tau) = \frac{G_F^2 m_{B_c} \tau_{B_c^-} f_{B_c}^2 m_\tau^2}{8\pi} |V_{cb}|^2 \left(1 - \frac{m_\tau^2}{m_{B_c}^2}\right)^2 \left| 1 + C^{\text{NP}} \right|^2 , \tag{6.3.11}$$

where m_B, τ_B and f_B are the mass, lifetime and decay constant of the relevant B meson respectively. We assume an identical operator structure leading to coherent addition of the amplitudes.

6.4 Model

In view of this, we adopt a very phenomenological approach, rather than advocate a particular model. Assuming an effective Lagrangian, with the minimal number of new parameters, in the guise of the unknown Wilson coefficients, we seek the best fit. While not an entirely new idea, our analysis takes into account not only the anomalous channels but also the existing limits on several other channels; as we will show, they provide the tightest constraints on the parameter space. This approach hopefully will pave the way to unraveling the as yet unknown flavor dynamics.

In view of the aforementioned constraints, we consider only a combination of two 4-Fermi operators, characterized by a single Wilson coefficient (assumed to be real to avoid new sources of CP violation). Since we do not claim to obtain the ultraviolet completion thereof, we do not speculate on the (flavor) symmetry that would have led to such a structure, which could have arisen from a plethora of NP scenarios, such as models of (gauged) flavor, leptoquarks (or, within the supersymmetric paradigm, a breaking of R-parity) etc. To wit, we propose a model involving two four-Fermi operators in terms of the second and third generation (weak-eigenstate) fields

$$\mathcal{H}^{\rm NP} = A_1 \left(\bar{Q}_{2L}\gamma_\mu L_{3L}\right)\left(\bar{L}_{3L}\gamma^\mu Q_{3L}\right) + A_2 \left(\bar{Q}_{2L}\gamma_\mu Q_{3L}\right)\left(\bar{\tau}_R\gamma^\mu \tau_R\right) \tag{6.4.1}$$

where the overall Clebsch-Gordan coefficients have been subsumed and we demand $A_2 = A_1$.

This operator, seemingly, contributes to $R(D^{(*)})$ but not to the other anomalous processes. This, though, is true only above the electroweak scale. Below this scale, the Hamiltonian needs to be rediagonalized[3] In the quark sector, this is determined by the quark masses and

[3] With NP only modifying the Wilson coefficients of certain SM operators to a small extent, the QCD corrections (as well as hadronic uncertainties) are analogous. Additional effects due to operator mixings are too small to be of any concern.

the small non-alignment due to $A_{1,2}$ can be neglected. In the leptonic sector, though, the extreme smallness of the neutrino masses implies that the nonuniversal term $\mathcal{H}^{\rm NP}$ plays a major role [78]. To this end, we consider the simplest of field rotations for the left-handed leptons from the unprimed (flavor) to the primed (mass) basis, namely

$$\tau = \cos\theta\,\tau' + \sin\theta\,\mu' \,, \qquad \nu_\tau = \cos\theta\,\nu'_\tau + \sin\theta\,\nu'_\mu \,. \tag{6.4.2}$$

This, immediately, generates a term with the potential to explain the $b \to s\mu\mu$ anomalies.

6.5 Results

The scenario is, thus, characterized by two parameters, namely A_1 and $\sin\theta$. The best fit values for these can be obtained by effecting a χ^2-test defined through

$$\chi^2 = \sum_{i=1}^{7} \frac{\left(O_i^{\rm exp} - O_i^{\rm th}\right)^2}{\left(\Delta O_i^{\rm exp}\right)^2 + \left(\Delta O_i^{\rm th}\right)^2} \tag{6.5.1}$$

where $O_i^{\rm exp}$ ($O_i^{\rm th}$) denote the experimental (theoretical) mean and $\Delta O_i^{\rm exp}$ ($\Delta O_i^{\rm th}$) the corresponding 1σ uncertainty, with the theoretical values depending on the model parameters. We include a total of seven measurements for the evaluation of χ^2, namely, $R(D)$, $R(D^*)$, R_K, $R_{K^*}^{\rm low}$, $R_{K^*}^{\rm cntr}$, Φ, and BR($B_s \to \mu\mu$) (while not affected by the NP interactions in Eq. (6.4.1), is relevant for the scenario considered later). The uncertainty in observables from theory side is considered in $\Delta O_i^{\rm th}$, can be seen from Table. 6.1 for $R(D^{(*)})$, Refs. [64, 65] for $R_{K^{(*)}}$, Eq. (6.2.3) for Φ and Eq. (6.2.4) for BR($B_s \to \mu\mu$). For our numerical analysis, we use $V_{cb} = 0.0416$, $V_{tb}V_{ts}^* = -0.0409$, and find, for the SM, $\chi^2_{\rm SM} \simeq 46$ or $\chi^2_{\rm SM}/{\rm d.o.f.} \simeq 6.7$. It should be noted that in the χ^2 definition (Eq. (6.5.1)), the CKM element V_{cb} completely cancels even after including the NP operators we are considering, and the dependency on $V_{tb}V_{ts}^*$ only enters through one observable namely, Φ.

Within the new model, where two NP parameters are introduced, the best fit corresponds

to $\chi^2_{\rm min} \simeq 9$ or $\chi^2_{\rm min}/\text{d.o.f.} \simeq 2$ (denoting a marked improvement) with the NP contributions being $C_9^{\rm NP} = -1.7$ and $C^{\rm NP} = -2.12$. In terms of the model parameters, this corresponds to (note that there is a $\theta \to -\theta$ degeneracy)

$$A_1(=A_2) = -2.92\ \text{TeV}^{-2}\,, \qquad \sin\theta = \pm 0.022\,, \tag{6.5.2}$$

Even this low value of $\chi^2_{\rm min}$ is largely dominated by a single measurement, namely, $R^{\rm low}_{K^*}$. This is not unexpected, as an agreement to this experimental value to better than 1σ is not possible if the NP contribution can be expressed just as a modification of the SM Wilson coefficients, rather than through the introduction of a new and small dynamical scale, which affects only the low-q^2 region. Note that the small value of $\sin\theta$ can only partially explain the atmospheric neutrino oscillation, while the full explanation needs additional dynamics.

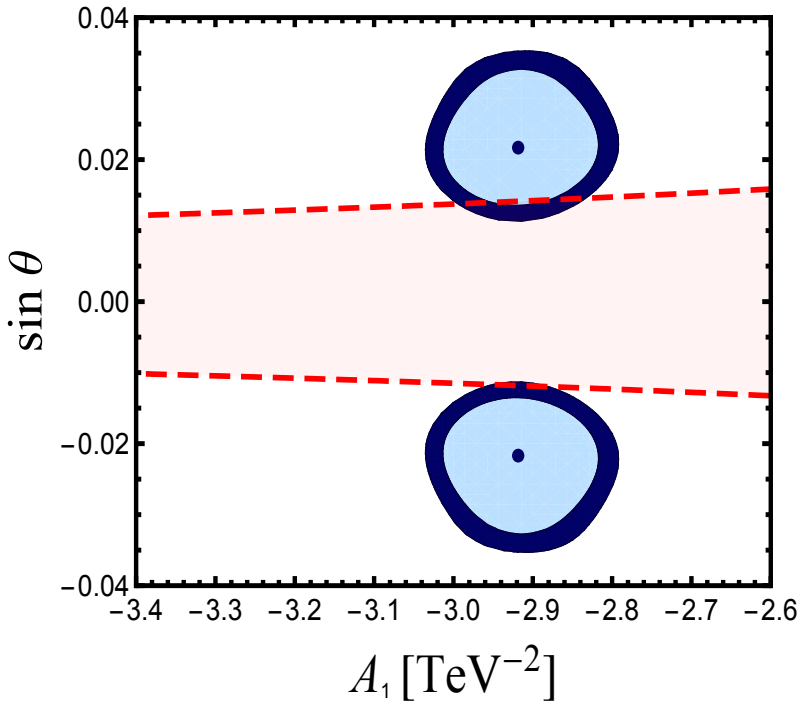

Figure 6.1. The light and dark blue regions denote 95% and 99% C.L. bands around the best-fit points. The red shaded region is allowed by bounds from $\text{BR}(B^+ \to K^+\mu^-\tau^+)$.

More importantly, in effecting the field rotation of Eq. (6.4.2) in $\mathcal{H}^{\rm NP}$, we generate terms of the form $(s,b)(\mu,\tau)$, leading to potential lepton-flavor violating (LFV) decays. The

current limits on the relevant ones are [74]

$$\mathrm{BR}(B^+ \to K^+\mu^\pm\tau^\mp) < 4.5\,(2.8) \times 10^{-5}\,. \tag{6.5.3}$$

In Fig. 6.1, we display the constraints from this particular mode. While the best-fit point is summarily ruled out, clearly solutions can be found if a slight worsening of the χ^2 (to $\simeq 15$ or $\chi^2/\mathrm{d.o.f.} \simeq 3$) is acceptable. This would still represent a much better agreement than is possible within the SM. The corresponding values of the observables are: $R_K = 0.86$, $R_{K^*}^{\mathrm{cntr}} = 0.88$, $R_{K^*}^{\mathrm{low}} = 0.90$, $R(D^{(*)}) = 1.25 \times R(D^{(*)})_{\mathrm{SM}}$ and $\Phi = 4.1 \times 10^{-8}\,\mathrm{GeV}^{-2}$, representing quite a reasonable fit to all but $R_{K^*}^{\mathrm{low}}$. It should be noted here that the $\theta \to -\theta$ degeneracy is broken by the LFV constraint, with $\theta > 0$ being slightly preferable.

Further improving the fit to $R_{K^{(*)}}$ requires the introduction of a small bit of C_{10}^{NP}. Postponing the discussion of $B_s \to \tau\tau$, this is most easily achieved if we choose to destroy, to a small degree, the relation $A_2 = A_1$. As an illustrative example, we consider $A_2 = 4A_1/5$. The consequent best fit values for A_1 and $\sin\theta$ remain virtually the same but, now, $\chi^2_{\mathrm{min}} = 7$ or $\chi^2/\mathrm{d.o.f.} \simeq 1.4$ with NP contributions being $C_9^{\mathrm{NP}} = -1.51$, $C_{10}^{\mathrm{NP}} = 0.17$ and $C^{\mathrm{NP}} = -2.12$. The result is depicted in Fig. 6.2. Once the LFV constraint is imposed, the observables at the overlap region are $R_K \simeq 0.80$, $R_{K^*}^{\mathrm{cntr}} \simeq 0.83$, $R_{K^*}^{\mathrm{low}} \simeq 0.88$, $R(D^{(*)}) = 1.24 \times R(D^{(*)})_{\mathrm{SM}}$ and $\Phi \simeq 3.8 \times 10^{-8}\,\mathrm{GeV}^{-2}$, showing marked improvement in the fit to all but $R_{K^*}^{\mathrm{low}}$ and corresponds to $\chi^2 \simeq 10$ or $\chi^2/\mathrm{d.o.f.} \simeq 2$. While the finite contribution to C_{10}^{NP} does enhance $B_s \to \tau\tau$, the latter (gray shaded region in Fig. 6.2) does not have a major impact. It should be realized, though, that a stronger breaking of the $A_2 = A_1$ relation would have led to a better (worse) agreement with the LFV ($B_s \to \tau\tau$) constraints.

It is interesting to speculate on the origin of this split between the A_i. A naive explanation would be to attribute the difference to the quantum numbers of the leptonic fields under an as yet unidentified gauge symmetry, with the attendant anomaly cancellation being effected by either invoking heavier fermionic fields or through other means. Care must be

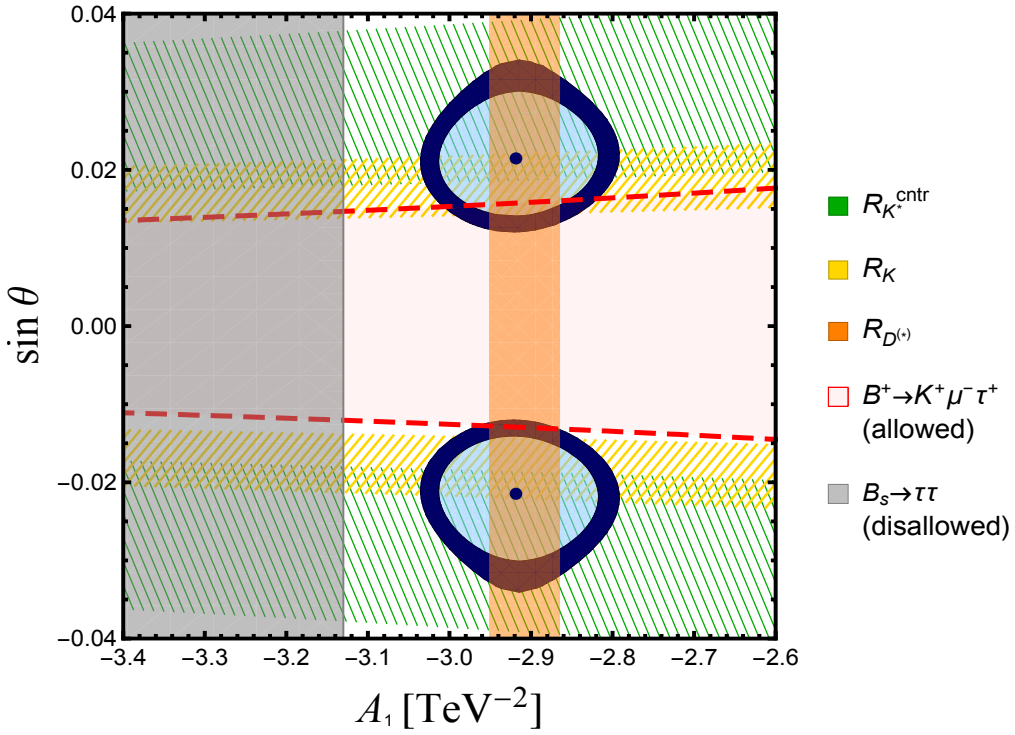

Figure 6.2. The fit for $A_2 = 4A_1/5$, with the bands around the best-fit points corresponding to 95% and 99% C.L. Also shown are the 1σ bands from $R_{K^{(*)}}$ and $R(D)$, and the 95% upper limits from $B_s \to \tau\tau$ and $B^+ \to K^+\mu^-\tau^+$.

taken, however, not to induce undesirable phenomenology. An alternative is to attribute the difference to quantum corrections, although the aforementioned shift is somewhat larger than that expected from a naive renormalization group flow perspective, namely $\sim (\alpha_{\rm wk.}/4\pi)\ln(\Lambda_{\rm NP}^2/m_b^2)$, where $\Lambda_{\rm NP}$ ~1 TeV is the putative scale of NP. It should be noted here, though, that the 20% shift is only illustrative and not really needed. Indeed, once the electroweak symmetry is broken, the various pieces in $\mathcal{H}^{\rm eff}$ suffer differing RG flow down to the m_b scale, and the consequent breaking of the degeneracy is, putatively, of the right magnitude to explain the remaining discrepancies.

It is worthwhile, at this stage, to explore the consequences of introducing other operators in $\mathcal{H}^{\rm NP}$. While operators constructed out of $SU(2)_L$-triplet currents (denoted by the subscript '3') such as $(\bar{Q}_{2L}\gamma^\mu Q_{3L})_3\,(\bar{L}_{3L}\gamma_\mu L_{3L})_3$, $(\bar{Q}_{2L}\gamma^\mu L_{3L})_3\,(\bar{L}_{3L}\gamma_\mu Q_{3L})_3$ etc. would also have admitted solutions to the anomalies, they, typically, would also result in unsuppressed $b \to s\nu\bar{\nu}$ transitions. Circumventing the bounds would, then, require the introduction of

multiple operators and cancellations between them. Such possibilities can be discussed in detail elsewhere.

This would, typically, still leave behind too large a rate for $B_s \to \tau\tau$ [79] and, hence needs the further introduction of yet another operator such as the second one in $\mathcal{H}^{\rm NP}$. Apart from enhancing $B_s \to \tau\tau$ ($B \to X_s\tau\tau$ and $\Lambda_b \to \Lambda\tau\tau$ are affected too, but bounds from these sectors are not too serious), this would also affect the other modes to varying degrees. Consequently, the best fit values will change. Indeed a lower χ^2 ($\simeq 5.4$) is achievable for virtually the same A_1, but slightly smaller $|\sin\theta|$ ($\simeq 0.018$). Understandably, if both the $B_s \to \tau\tau$ bound as well that in Eq. (6.5.3) are to be satisfied, the χ^2 can be reduced to at most $\simeq 11$. Similarly, BR($B \to X_s\tau\tau$), as well as BR($\Lambda_b \to \Lambda\tau\tau$) will also be increased and should be close to observation at the LHCb. However, processes like $b \to s\gamma$ or $\tau \to \mu\gamma$ will remain under control, as we have checked. Similarly, while we do not "explain" $(g-2)_\mu$, the agreement is marginally better than within the SM. The new operators also generate, through renormalization group running, operators involving four leptons [80], and thus may lead to effects like $\tau \to 3\mu$. They are, however, well within control, mostly because of the small value of $\sin\theta$.

6.6 Summary

To summarize, we have identified the minimal modification to the SM in terms of an effective theory that can explain the anomalies in both the charged– and the neutral-current decays of bottom-mesons, a task that has been challenging on account of the seemingly contradictory requirements that the data demands. We circumvent this by postulating just two four-Fermi operators with Wilson coefficients related by a symmetry and taking advantage of the possibility of a small but non-trivial rotation of the charged lepton fields that a flavor-nonuniversal operator entails. Taking all the data into account, we find that with just two new parameters, the χ^2/d.o.f. can be reduced from 6.7 (in the SM) to below

3 while being consistent with all other data. For the best fit point, most observables are consistent within $\sim 1\sigma$, while R_{K^*} and BR($B \to \phi\mu\mu$) in the low-q^2 bins, are consistent to only within $\sim 2\sigma$.

The scale of NP that such an explanation demands is a few TeVs at best, rendering searches at the LHC to be very interesting. An even stronger preference is that at least one of $B \to K^{(*)}\mu\tau$ and $B_s \to \tau\tau$ should be close to discovery. The mode $B \to K^{(*)}\mu\tau$ will show up both in the case of equal coefficient of the two operators namely $A_1 = A_2$ and also when A_1 and A_2 are allowed to vary to the extent that the explanation of the anomalies allow. However an enhancement in $B_s \to \tau\tau$ is possible in the later case only. A more precise determination of the ratios that we have discussed in this chapter is, therefore, of prime importance, as this can open the door to new flavor dynamics and hence the world beyond the SM.

7 Conclusions & outlook

The compelling indications of the incompleteness of the SM has enforced us to extend the theory further to incorporate all observed phenomena in nature. In absence of any salient hint of the existence of new particle at the collider experiments we are at a verge of the era where precision measurements can play a major role. Among these, flavor physics is an important subject. The loop induced decay processes are very sensitive to the SM as well as BSM physics. In this thesis we have studied the rare decay modes of B meson. To disentangle to effect of physics beyond the SM, the precise knowledge of SM contributions are essential. A very intense research work is devoted to improve the accuracy of SM contributions especially the hadronic effects from long past. While these efforts are paramount, in this thesis we try to establish an alternative way out by evading the ignorance of hadronic effects.

In the first part of this thesis, we consider the decay $B \to K^* \ell^+ \ell^-$. Unlike the case for fully hadronic decay modes that suffer from large and in cases, not-so-well understood, strong interaction corrections, the theoretical uncertainties in semileptonic decays are much better controlled.

- Starting with the general parametrization of the hadronic matrix elements especially including the contributions arising from non local effects, in chapter 3 we write the most general form of the amplitude based only on Lorentz invariance and gauge invariance.

- The form of the amplitude for the mode notionally includes all short-distance and long-distance effects, the effect of factorisable as well as nonfactorizable contributions and resonance contributions. It comprehensively takes into account all contributions up to $O(G_F)$ within the SM.

- We show the complex part of the amplitude can be estimated from data and find the values are consistent with zero within 1σ uncertainty for $3\,\text{fb}^{-1}$ of LHCb data.

- Using the advantage of the mentioned form of the amplitude, in chapter 4 we derive a relation among nine CP averaged observables for this decay mode valid for the entire kinematically allowed region. The relation is exact in the SM limit and thus allows us to check the consistency of data with the SM gauge structure. We use both $1\,\text{fb}^{-1}$ and $3\,\text{fb}^{-1}$ of LHCb data and find reasonable agreement between the measured value of the observables and the predictions from the relation except for small deviations at few q^2 bins. We note that the relation remains invariant in presence of RH current operators and any new vector current contribution to the decay mode.

In the next part of this thesis, in chapter 5, we scrutinize the hadronic parameters which are involved in this mode using LHCb data.

- Implementing the same formalism developed in the chapter 3, we construct certain combinations of hadronic parameters which can directly be estimated using measurements of observables only. We find that the extracted values for some parameters namely, P_1 and P_2 are not affected by contamination (if any) of data with the $c\bar{c}$ bound states present in the region of interest.

- The extracted values of form factors show significant disagreements when compared with the available estimates in literature calculated in LCSR and Lattice theory.

- Further a relation among form factors expected to hold in heavy quark symmetry limit is violated significantly for the latest LHCb data. In a later study, this particular observation in turn leads to provide unambiguous signal of RH currents. The analysis is derived at the kinematic endpoint limit and is free from any hadronic estimates.

We emphasize that our approach differs from what is usually done in literature as we make no attempt to evaluate hadronic parameters but eliminate them in favor of measured observables to the extent possible. Hence, our conclusions are not limited in general by the order of accuracy up to which the calculations are done.

Universality of weak interactions is one of the key predictions of the SM. However, observations of neutrino oscillation are clear indications of new non-universal interactions beyond the SM. Recently few anomalies such as $R_{K^{(*)}}$ and $R(D^{(*)})$ have been observed by various experimental groups with a deviation around $2\sigma - 4\sigma$ confidence level from the SM prediction. Finally in the last part of this thesis, in chapter 6, we explore the possibilities to explain the anomalies hinting towards lepton non-universality.

- In an effective theory approach we provide a simultaneous explanation to all these anomalies observed in $b \to c$ and $b \to s$ transitions, with only two new model parameters. The new operators evade the constraints arising from the measurements of other decay modes. We present a simplistic scenario with two operators and some unknown symmetry relates them. It is illustrated that a possible breaking of that symmetry due to quantum corrections improves the NP parameter space significantly.

- The scale of NP that such an explanation demands is found to be a few TeVs at best and thus makes the searches at the LHC to be very interesting.

- A strong prediction of our analysis is that either $B \to K\mu\tau$ and $B_s \to \tau\tau$ will be close to discovery, and such channels should be looked at in LHCb as well as

Belle-II.

There are several directions to which one can make progress. In this thesis we observe evidence of BSM physics in some specific decay modes. However, it is necessary that NP should show up in all possible channels having the same dynamics as of the modes studied here.

- Hence, in this context, one can extend the study to other decay modes having the same quark level transition. An immediate example is the decay $B_s \to \phi\ell^+\ell^-$ which is less studied in literature compared to the mode $B \to K^*\ell^+\ell^-$. By implementing the approach developed in this thesis, where the conclusions have no/minimal dependency on hadronic estimates one can constrain and/or confirm the existence of BSM scenarios.

- Similarly, the approach can be implemented to study the mesons having higher spin *e.g.* spin two mesons and also to the baryons. LHCb has observed the decay $\Lambda_b \to \Lambda\ell^+\ell^-$ and will continue to improve the analysis to measure various observables in this mode and other baryonic transitions also in near future.

- We do not attempt to probe the origin of the new operators which can explain the anomalies in context of lepton non-universality; while a Z' or a leptoquark may do the job and can be investigated in future study.

- Eventually, in the long run, if data persists to show the nature of deviations discussed here, the study in this thesis will guide for various possibilities to construct an UV complete theory beyond the SM or, in other case, the techniques used here will be useful to identify and/or disentangle the NP effects from the SM scenario.

A Some useful tricks & results

Here we list some useful techniques and expressions in the context of the results in chapters 3 and 4.

A.1 Form factors

In this appendix we write the explicit form of the combination of form factors $\mathcal{F}_\lambda$ and $\widetilde{\mathcal{G}}_\lambda$ in terms of the parameters used to parametrize the most general form of the hadronic matrix elements of $B \to K^*$ transition. The form factors $\mathcal{F}_\lambda$ and $\widetilde{\mathcal{G}}_\lambda$ can be related to the form factors $\mathcal{X}_i$ and $\mathcal{Y}_i$ introduced in Eqs. (3.2.3) and (3.2.4) by comparing the expressions for $\mathcal{A}_\lambda^{L,R}$ in Eqs. (3.3.3a) – (3.3.3c) with Eq. (3.3.5) as follows:

$$\mathcal{F}_\perp = N\sqrt{2}\sqrt{\lambda(m_B^2, m_{K^*}^2, q^2)}\mathcal{X}_3, \tag{A.1.1a}$$

$$\widetilde{\mathcal{G}}_\perp = N\sqrt{2}\sqrt{\lambda(m_B^2, m_{K^*}^2, q^2)}\,\frac{2(m_b + m_s)}{q^2}\widehat{C}_7\mathcal{Y}_3 + \cdots,$$

$$\mathcal{F}_\parallel = 2\sqrt{2}N\mathcal{X}_1, \tag{A.1.1b}$$

$$\widetilde{\mathcal{G}}_\parallel = 2\sqrt{2}N\,\frac{2(m_b - m_s)}{q^2}\widehat{C}_7\mathcal{Y}_1 + \cdots, \tag{A.1.1c}$$

$$\mathcal{F}_0 = \frac{N}{2m_{K^*}\sqrt{q^2}}[4k.q\mathcal{X}_1 + \lambda(m_B^2, m_{K^*}^2, q^2)\mathcal{X}_2], \tag{A.1.1d}$$

$$\widetilde{\mathcal{G}}_0 = \frac{N}{2m_{K^*}\sqrt{q^2}}\,\frac{2(m_b - m_s)}{q^2}\widehat{C}_7[4k.q\mathcal{Y}_1 + \lambda(m_B^2, m_{K^*}^2, q^2)\mathcal{Y}_2] + \cdots, \tag{A.1.1e}$$

where these $\mathcal{X}_i$'s and $\mathcal{Y}_i$'s can be related to the well-known form factors V, $A_{0,1,2}$ and $T_{1,2,3}$ by comparing with Ref. [4] which are known up to next-to-next-to-leading order in HQET.

$$\mathcal{X}_0 = -\frac{2m_{K^*}}{q^2}A_0(q^2), \tag{A.1.2a}$$

$$\mathcal{X}_1 = -\frac{1}{2}(m_B + m_{K^*})A_1(q^2), \tag{A.1.2b}$$

$$\mathcal{X}_2 = \frac{A_2(q^2)}{m_B + m_{K^*}}, \tag{A.1.2c}$$

$$\mathcal{X}_3 = \frac{V(q^2)}{m_B + m_{K^*}}, \tag{A.1.2d}$$

$$\mathcal{Y}_1 = \frac{1}{2}(m_B^2 - m_{K^*}^2)T_2(q^2), \tag{A.1.2e}$$

$$\mathcal{Y}_2 = -T_2(q^2) - \frac{q^2}{m_B^2 - m_{K^*}^2}T_3(q^2), \tag{A.1.2f}$$

$$\mathcal{Y}_3 = -T_1(q^2). \tag{A.1.2g}$$

Here a point to be noted that as the form factors A_1 and A_2 are always positive the ratio

$$\frac{2k.q(m_B + m_{K^*})^2}{\lambda(m_B^2, m_{K^*}^2, q^2)}\frac{A_1}{A_2} \geq 0 \tag{A.1.3}$$

giving rise to the fact that $\mathcal{F}_\parallel$ and $\mathcal{F}_0$ always have the same sign which is negative.

A.2 Derivation of r_λ solutions

In this appendix we present the derivation of $r_\parallel$, $r_\perp$ and r_0 solutions defined in Eq. (4.2.1). Starting with the first set of equations (Set-I) involving $r_\parallel$ and $r_\perp$ in terms of the observables given in Eqs. (4.2.20), (4.2.21) and (4.2.22) we have

$$r_\parallel^2 + \widehat{C}_{10}^2 = \frac{F_\parallel' I_f \mathsf{P}_1^2}{2\mathcal{F}_\perp^2}, \tag{A.2.1}$$

$$r_\perp^2 + \widehat{C}_{10}^2 = \frac{F'_\perp \Gamma_f}{2\mathcal{F}_\perp^2}, \tag{A.2.2}$$

$$\widehat{C}_{10}(r_\parallel + r_\perp) = \frac{A_{\rm FB}\Gamma_f \mathsf{P}_1}{3\mathcal{F}_\perp^2}. \tag{A.2.3}$$

Multiplying Eq. (A.2.1) and (A.2.2) we can write

$$\begin{aligned}\frac{F'_\parallel F'_\perp \Gamma_f^2 \mathsf{P}_1^2}{4\mathcal{F}_\perp^4} &= (r_\parallel r_\perp - \widehat{C}_{10}^2)^2 + \widehat{C}_{10}^2(r_\parallel + r_\perp)^2 \\ &= (r_\parallel r_\perp - \widehat{C}_{10}^2)^2 + \frac{A_{\rm FB}^2 \Gamma_f^2 \mathsf{P}_1^2}{9\mathcal{F}_\perp^4}\end{aligned}$$

hence,

$$r_\parallel r_\perp - \widehat{C}_{10}^2 = \pm\frac{\Gamma_f \mathsf{P}_1}{2\mathcal{F}_\perp^2}\sqrt{F'_\parallel F'_\perp - \frac{4A_{\rm FB}^2}{9}}. \tag{A.2.4}$$

Now expressing $\widehat{C}_{10}^2$ in terms of $r_\parallel^2$ using Eq. (A.2.1) and in terms of $r_\perp^2$ using Eq. (A.2.2) we can write

$$\begin{aligned}2r_\parallel r_\perp - 2\widehat{C}_{10}^2 &= 2r_\parallel r_\perp - \Big(\frac{F'_\parallel \Gamma_f \mathsf{P}_1^2}{2\mathcal{F}_\perp^2} - r_\parallel^2\Big) - \Big(\frac{F'_\perp \Gamma_f}{2\mathcal{F}_\perp^2} - r_\perp^2\Big) \\ &= \Big[(r_\parallel + r_\perp)^2 - \frac{F'_\parallel \Gamma_f \mathsf{P}_1^2}{2\mathcal{F}_\perp^2} - \frac{F'_\perp \Gamma_f}{2\mathcal{F}_\perp^2}\Big]\end{aligned} \tag{A.2.5}$$

Equating Eqs. (A.2.4) and (A.2.5) we get

$$\begin{aligned}r_\parallel + r_\perp &= \pm\Big[\frac{F'_\parallel \Gamma_f \mathsf{P}_1^2}{2\mathcal{F}_\perp^2} + \frac{F'_\perp \Gamma_f}{2\mathcal{F}_\perp^2} \pm \frac{\Gamma_f \mathsf{P}_1}{2\mathcal{F}_\perp^2} Z'_1\Big]^{1/2} \\ &= \frac{\pm\sqrt{\Gamma_f}}{\sqrt{2}\mathcal{F}_\perp}\Big[\mathsf{P}_1^2 F'_\parallel + F'_\perp \pm \mathsf{P}_1 Z'_1\Big]^{1/2}\end{aligned} \tag{A.2.6}$$

where $Z'_1 = \sqrt{4F'_\parallel F'_\perp - \frac{16}{9}A_{\rm FB}^2}$. Now, Eqs. (A.2.1) and (A.2.2) imply:

$$r_\parallel^2 - r_\perp^2 = \frac{F'_\parallel \Gamma_f \mathsf{P}_1^2}{2\mathcal{F}_\perp^2} - \frac{F'_\perp \Gamma_f}{2\mathcal{F}_\perp^2}, \tag{A.2.7}$$

which gives $r_\parallel - r_\perp$ to be,

$$r_\parallel - r_\perp = \frac{\pm\sqrt{\Gamma_f}}{\sqrt{2}\mathcal{F}_\perp}\frac{\mathsf{P}_1^2 F'_\parallel - F'_\perp}{\left[\mathsf{P}_1^2 F'_\parallel + F'_\perp \pm \mathsf{P}_1 Z'_1\right]^{1/2}}. \tag{A.2.8}$$

To fix the sign ambiguity of the radical let us consider the zero crossing point of the observable $A_{\rm FB}$ where,

$$r_\parallel + r_\perp\big|_{A_{\rm FB}=0} = \pm\frac{\sqrt{\Gamma_f}}{\sqrt{2}\mathcal{F}_\perp}\left(\sqrt{F'_\perp} \pm \mathsf{P}_1\sqrt{F'_\parallel}\right) = 0. \tag{A.2.9}$$

It can be easily seen from appendix. A.1 that P_1 is always negative and thus the positive sign ambiguity has to be chosen within the radical. Solving Eqs. (A.2.6) and (A.2.8) we get the expressions for $r_\parallel$ and $r_\perp$ given in Eqs. (4.2.30) and (4.2.31). Similarly, following all the steps stated above for the other two sets of equations (Set-II and Set-III) we get the solutions for r_0 (in Eq. (4.2.33)) and two more expressions for the variable $r_\perp$ (Eqs. (4.2.34) and (4.2.38)).

Generalization of Eqs. (A.2.6) and (A.2.8) for the massive case in Sec.4.3 is trivial from here. Below we present the explicit expressions for both massless and massive cases.

$$r_\parallel + r_\perp = \begin{cases} \dfrac{\pm\sqrt{\Gamma_f}}{\sqrt{2}\mathcal{F}_\perp}\left[\mathsf{P}_1^2\left(F_\parallel - \dfrac{2\varepsilon_\parallel^2}{\Gamma_f}\right) + \left(F_\perp - \dfrac{2\varepsilon_\perp^2}{\Gamma_f}\right) + \mathsf{P}_1 Z'_1\right]^{1/2} & \text{massless case} \\ \dfrac{\pm\sqrt{\Gamma_f^{\rm o}}}{\sqrt{2}\mathcal{F}_\perp\beta}\left[\mathsf{P}_1^2\left(F_\parallel^{\rm o} - \dfrac{\mathcal{T}_\parallel}{\Gamma_f^{\rm o}}\right) + \left(F_\perp^{\rm o} - \dfrac{\mathcal{T}_\perp}{\Gamma_f^{\rm o}}\right) + \mathsf{P}_1 Z_1^{\rm o}\right]^{1/2} & \text{massive case} \end{cases} \tag{A.2.10}$$

$$r_\parallel - r_\perp = \begin{cases} \dfrac{\pm\sqrt{\Gamma_f}}{\sqrt{2}\mathcal{F}_\perp} \dfrac{\mathsf{P}_1^2\left(F_\parallel - \dfrac{2\varepsilon_\parallel^2}{\Gamma_f}\right) - \left(F_\perp - \dfrac{2\varepsilon_\perp^2}{\Gamma_f}\right)}{\left[\mathsf{P}_1^2\left(F_\parallel - \dfrac{2\varepsilon_\parallel^2}{\Gamma_f}\right) + \left(F_\perp - \dfrac{2\varepsilon_\perp^2}{\Gamma_f}\right) + \mathsf{P}_1 Z_1'\right]^{1/2}} & \text{massless case} \\ \dfrac{\pm\sqrt{\Gamma_f^{\mathrm{o}}}}{\sqrt{2}\mathcal{F}_\perp\beta} \dfrac{\mathsf{P}_1^2\left(F_\parallel^{\mathrm{o}} - \dfrac{\mathcal{T}_\parallel}{\Gamma_f^{\mathrm{o}}}\right) - \left(F_\perp^{\mathrm{o}} - \dfrac{\mathcal{T}_\perp}{\Gamma_f^{\mathrm{o}}}\right)}{\left[\mathsf{P}_1^2\left(F_\parallel^{\mathrm{o}} - \dfrac{\mathcal{T}_\parallel}{\Gamma_f^{\mathrm{o}}}\right) + \left(F_\perp^{\mathrm{o}} - \dfrac{\mathcal{T}_\perp}{\Gamma_f^{\mathrm{o}}}\right) + \mathsf{P}_1 Z_1^{\mathrm{o}}\right]^{1/2}} & \text{massive case} \end{cases} \tag{A.2.11}$$

Using Eqs. (A.2.3) and (A.2.10) we can write

$$\widehat{C}_{10} = \begin{cases} \dfrac{\pm A_{\mathrm{FB}}\sqrt{2\Gamma_f}\mathsf{P}_1}{3\mathcal{F}_\perp\left[\mathsf{P}_1^2\left(F_\parallel - \dfrac{2\varepsilon_\parallel^2}{\Gamma_f}\right) + \left(F_\perp - \dfrac{2\varepsilon_\perp^2}{\Gamma_f}\right) + \mathsf{P}_1 Z_1'\right]^{1/2}} & \text{massless case} \\ \dfrac{\pm A_{\mathrm{FB}}^{\mathrm{o}}\sqrt{2\Gamma_f^{\mathrm{o}}}\mathsf{P}_1}{3\mathcal{F}_\perp\left[\mathsf{P}_1^2\left(F_\parallel^{\mathrm{o}} - \dfrac{\mathcal{T}_\parallel}{\Gamma_f^{\mathrm{o}}}\right) + \left(F_\perp^{\mathrm{o}} - \dfrac{\mathcal{T}_\perp}{\Gamma_f^{\mathrm{o}}}\right) + \mathsf{P}_1 Z_1^{\mathrm{o}}\right]^{1/2}} & \text{massive case} \end{cases} \tag{A.2.12}$$

B Estimation of complex part of the amplitude from data

In this appendix we estimate the complex contributions of the amplitude for $B \to K^*\ell^+\ell^-$ mode using 3fb^{-1} of LHCb data. It is shown in chapter 4 that the complex contributions ε_λ to the amplitude of the decay mode $B \to K^*\ell^+\ell^-$, can be taken into consideration.The ε_λ's are solved in terms of iterative solutions proportional to the observables A_7, A_8, A_9 and a form factor ratio P_1. The expressions for all the three ε_λ's are shown in Eqs. (4.2.42)–(4.2.44). They are reproduced here for convenience.

$$\varepsilon_\perp = \frac{\sqrt{2}\pi\Gamma_f}{(r_0 - r_\parallel)\mathcal{F}_\perp}\left[\frac{A_9\mathsf{P}_1}{3\sqrt{2}} + \frac{A_8\mathsf{P}_2}{4} - \frac{A_7\mathsf{P}_1\mathsf{P}_2 r_\perp}{3\pi C_{10}}\right], \tag{B.0.1}$$

$$\varepsilon_\parallel = \frac{\sqrt{2}\pi\Gamma_f}{(r_0 - r_\parallel)\mathcal{F}_\perp}\left[\frac{A_9 r_0}{3\sqrt{2}r_\perp} + \frac{A_8\mathsf{P}_2 r_\parallel}{4\mathsf{P}_1 r_\perp} - \frac{A_7\mathsf{P}_2 r_\parallel}{3\pi C_{10}}\right], \tag{B.0.2}$$

$$\varepsilon_0 = \frac{\sqrt{2}\pi\Gamma_f}{(r_0 - r_\parallel)\mathcal{F}_\perp}\left[\frac{A_9\mathsf{P}_1 r_0}{3\sqrt{2}\mathsf{P}_2 r_\perp} + \frac{A_8 r_\parallel}{4r_\perp} - \frac{A_7\mathsf{P}_1 r_0}{3\pi C_{10}}\right]. \tag{B.0.3}$$

A point to be noted as explained in detail in Sec. 4.2, is that the $(\varepsilon_\lambda/\Gamma_f^{1/2})$'s are completely expressed in terms of observables and the form factor ratio P_1. However, these solutions are essentially iterative, since the r_λ's and C_{10} are derived in terms of the primed observables that depend on ε_λ. If $(\varepsilon_\lambda/\Gamma_f^{1/2})$ are small as should be expected, accurate solutions for them can be found with a few iterations. In Sec. 4.5 the variation of ε_λ with P_1 was studied for 1 fb^{-1} LHC data and it was found that the solutions are not sensitive to the

value of P_1.

We generate a set of events for every bin, with each event consisting of randomly chosen values drawn from Gaussian distributions generated for each of the observables F_L, $F_\perp$, A_4, A_5, $A_{\rm FB}$, A_7, A_8 and A_9. The distributions are generated using experimental results from Ref. [2], with the experimentally measured value as mean and the uncertainty as standard deviation.

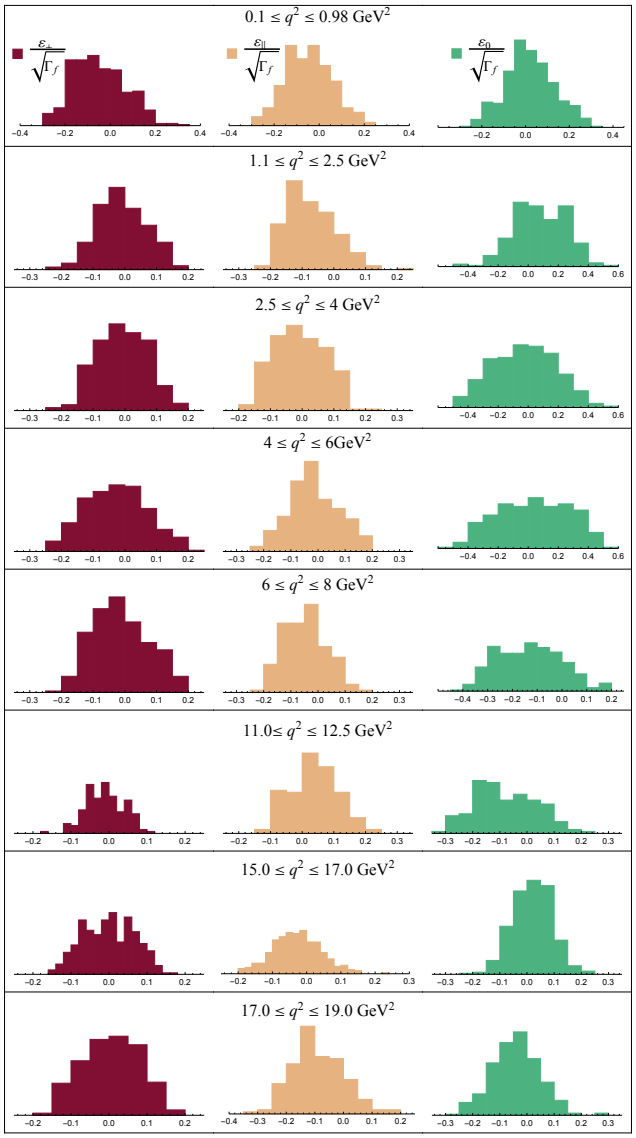

Figure B.1. (color online) The solutions for $\varepsilon_\perp/\sqrt{\Gamma_f}$, $\varepsilon_\parallel/\sqrt{\Gamma_f}$ and $\varepsilon_0/\sqrt{\Gamma_f}$ using distributions for first through eighth q^2 bins are depicted in red (dark), light brown (lightest) and green respectively. All the $\varepsilon_\lambda/\sqrt{\Gamma_f}$'s are consistent with zero.

q^2 in GeV^2	$\varepsilon_\perp/\sqrt{\Gamma_f}$	$\varepsilon_\parallel/\sqrt{\Gamma_f}$	$\varepsilon_0/\sqrt{\Gamma_f}$
$0.1 \leq q^2 \leq 0.98$	-0.048 ± 0.116	-0.047 ± 0.103	0.020 ± 0.111
$1.1 \leq q^2 \leq 2.5$	-0.010 ± 0.078	-0.010 ± 0.078	0.078 ± 0.172
$2.5 \leq q^2 \leq 4.0$	-0.009 ± 0.079	-0.008 ± 0.080	-0.025 ± 0.212
$4.0 \leq q^2 \leq 6.0$	-0.026 ± 0.097	0.014 ± 0.093	0.032 ± 0.234
$6.0 \leq q^2 \leq 8.0$	-0.011 ± 0.088	-0.046 ± 0.078	-0.132 ± 0.129
$11.0 \leq q^2 \leq 12.5$	-0.011 ± 0.050	0.038 ± 0.074	-0.078 ± 0.114
$15.0 \leq q^2 \leq 17.0$	-0.000 ± 0.067	-0.027 ± 0.071	0.020 ± 0.072
$17.0 \leq q^2 \leq 19.0$	0.006 ± 0.076	-0.090 ± 0.090	-0.040 ± 0.088

Table B.1. The $\varepsilon_\lambda/\sqrt{\Gamma_f}$ mean values with $\pm 1\sigma$ errors from Fig. B.1

ε_λ are solved iteratively for every set of observables. We find converged iterative solutions for $\varepsilon_\lambda/\sqrt{\Gamma_f}$ for each set of observables with the histograms shown in Fig. B.1. The red (dark), light brown (lightest) and green histograms denote the solutions for $\varepsilon_\perp/\sqrt{\Gamma_f}$, $\varepsilon_\parallel/\sqrt{\Gamma_f}$ and $\varepsilon_0/\sqrt{\Gamma_f}$ respectively for all the eight bins with q^2 range $(0.1 - 0.98)$ GeV^2, $(1.1 - 2.5)$ GeV^2, $(2.5 - 4.0)$ GeV^2, $(4 - 6)$ GeV^2, $(6 - 8)$ GeV^2, $(11.0 - 12.5)$ GeV^2, $(15 - 17)$ GeV^2 and $(17 - 19)$ GeV^2.

We have also quoted the mean and $\pm 1\sigma$ errors for each $\varepsilon_\lambda/\sqrt{\Gamma_f}$ in Table. B.1 calculated from the distributions shown in Fig. B.1. It can be easily seen that the $\varepsilon_\lambda/\sqrt{\Gamma_f}$ are consistent with zero within 1σ error uncertainties. From Eqs. (4.2.3)–(4.2.6), the contributions from imaginary part of the amplitude to the observables F_L, $F_\parallel$, $F_\perp$ and A_4 are quadratic in the corresponding $\varepsilon_\lambda/\sqrt{\Gamma_f}$ and thus are negligible.

C Systematic uncertainty evaluation for bin bias

In this appendix we discuss about the bin average effect of observables in the analysis presented in chapter 5. We illustrate the evaluation of systematic uncertainties used in the numerical analysis in Sec. 5.3.

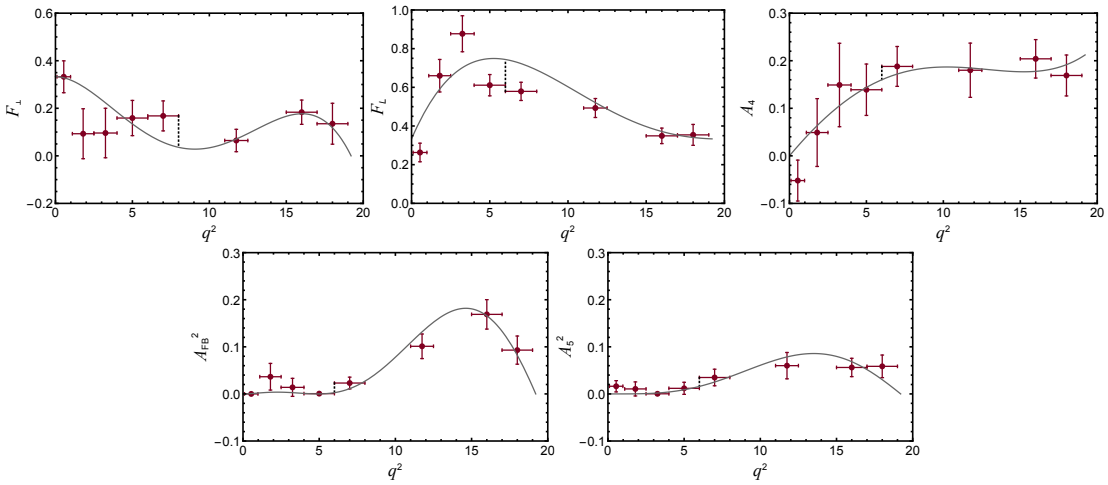

Figure C.1. (color online). The procedure to calculate systematic errors are shown for observables $F_\perp$, F_L, A_4, $A_{\rm FB}^2$ and A_5^2, respectively. The red error bars are LHCb measurements and gray curves represent best fitted polynomial in q^2 for 14 bin LHCb data [2]. The black dashed lines denote the maximum deviation of bin average central value of the observables with the q^2 function for bin $6 \leq q^2 \leq 8$ GeV^2. The length of these black lines are denoted by $F_\perp^s$, F_L^s, A_4^s, $A_{\rm FB}^{2s}$ and A_5^{2s}, respectively. Similar lines can be drawn for other q^2 bins also and the values of systematic errors are given in Table. C.1 for all observables.

As written in Eq. (5.3.3), the shift $\mathcal{O}^s$ in each observable is calculated for each q^2 bin, by considering the maximum deviation of the bin average value of the observable $\mathcal{O}$ from

q^2 range in GeV^2	$F_\perp^s$	F_L^s	A_4^s	$A_{\rm FB}^{2s}$	A_5^{2s}
$0.1 \leq q^2 \leq 0.98$	0.014	0.230	0.088	0.002	0.016
$1.1 \leq q^2 \leq 2.5$	0.223	0.151	0.036	0.034	0.010
$2.5 \leq q^2 \leq 4.0$	0.164	0.223	0.064	0.013	0.004
$4.0 \leq q^2 \leq 6.0$	0.069	0.138	0.021	0.002	0.008
$6.0 \leq q^2 \leq 8.0$	0.132	0.165	0.028	0.020	0.019
$11.0 \leq q^2 \leq 12.5$	0.029	0.063	0.006	0.051	0.023
$15.0 \leq q^2 \leq 17.0$	0.019	0.048	0.027	0.036	0.023
$17.0 \leq q^2 \leq 19.0$	0.109	0.020	0.039	0.077	0.053

Table C.1. The systematic uncertainties for each observables $F_\perp$, F_L, A_4, $A_{\rm FB}^2$ and A_5^2 are shown. The values denote magnitude of maximum deviation of the bin average central value with the fitted q^2 polynomial within every q^2 bin.

a fitted q^2 polynomial of entire range. It is highlighted in Fig. C.1 where red error bars are LHCb measurements and gray curves represent best fitted polynomial in q^2 for 14 bin LHCb data. We use 14 bin measurement (based on the method of moments [81]) from LHCb to fit the polynomial in q^2, rather than the 8 bin data set as it provides more information to determine the shape of the polynomial for entire q^2 region. The black dashed line denotes the maximum deviation of bin average central value of the observable with the q^2 function for the region $6 \leq q^2 \leq 8$ GeV^2 and $\mathcal{O}^s$ is the length of the line for observable $\mathcal{O}$. Similar technique is applied for other q^2 bins also and the values of systematic errors are given in Table. C.1 for all observables.

It should be noted that as discussed in Sec. 5.3 finite lepton mass can affect the analysis in the first two q^2 region namely $q^2 \leq 2.5$ GeV^2 and in the absence of a measurement of asymmetries A_{10} and A_{11} (defined in Eqs. (4.3.5)–(4.3.6)) we have to rely on some hadronic estimates. This in principle may cause more uncertainties and we took a conservative approach by considering two times the $\mathcal{O}^s$ values for all observables given in

Table. C.1 for the two bins $0.1 \leq q^2 \leq 0.98$ GeV^2 and $1.1 \leq q^2 \leq 2.5$ GeV^2.

We emphasize that resonances in our analysis will only affect the fitted function in q^2, which in turn will induce more systematic uncertainties to the observables. We have checked the χ^2 fit (in Sub-sec. 5.3.1) by increasing the systematic uncertainties two times of the values given in Table. C.1 for the regions $11 \leq q^2 \leq 12.5$ GeV^2 and $15 \leq q^2 \leq 17$ GeV^2 and our results are stable with it. However a detailed study of resonance systematics on this decay mode is currently going on and will be a subject of an independent work itself.

Bibliography

[1] F. Kruger, L. M. Sehgal, N. Sinha, and R. Sinha, *Angular distribution and CP asymmetries in the decays* $\bar{B} \to K^- \pi^+ e^- e^+$ *and* $\bar{B} \to \pi^- \pi^+ e^- e^+$, *Phys. Rev.* **D61** (2000) 114028, arXiv:hep-ph/9907386 [hep-ph]. [Erratum: Phys. Rev.D63,019901(2001)].

[2] **LHCb** Collaboration, R. Aaij *et al.*, *Angular analysis of the* $B^0 \to K^{*0} \mu^+ \mu^-$ *decay using* $3\,fb^{-1}$ *of integrated luminosity*, *JHEP* **02** (2016) 104, arXiv:1512.04442 [hep-ex].

[3] A. Khodjamirian, T. Mannel, A. A. Pivovarov, and Y. M. Wang, *Charm-loop effect in* $B \to K^{(*)} \ell^+ \ell^-$ *and* $B \to K^* \gamma$, *JHEP* **09** (2010) 089, arXiv:1006.4945 [hep-ph].

[4] M. Beneke, T. Feldmann, and D. Seidel, *Systematic approach to exclusive* $B \to V l^+ l^-$, $V\gamma$ *decays*, *Nucl. Phys.* **B612** (2001) 25–58, arXiv:hep-ph/0106067 [hep-ph].

[5] R. Mandal, R. Sinha, and D. Das, *Testing New Physics Effects in* $B \to K^* \ell^+ \ell^-$, *Phys. Rev.* **D90** no. 9, (2014) 096006, arXiv:1409.3088 [hep-ph].

[6] R. Mandal and R. Sinha, *Implications from* $B \to K^* \ell^+ \ell^-$ *observables using* $3 fb^{-1}$ *of LHCb data*, *Phys. Rev.* **D95** no. 1, (2017) 014026, arXiv:1506.04535 [hep-ph].

[7] F. Kruger and L. M. Sehgal, *Lepton polarization in the decays b —> X(s) mu+ mu- and B —> X(s) tau+ tau-*, *Phys. Lett.* **B380** (1996) 199–204, arXiv:hep-ph/9603237 [hep-ph].

[8] A. Bharucha, D. M. Straub, and R. Zwicky, $B \to V\ell^+\ell^-$ *in the Standard Model from light-cone sum rules*, *JHEP* **08** (2016) 098, arXiv:1503.05534 [hep-ph].

[9] R. R. Horgan, Z. Liu, S. Meinel, and M. Wingate, *Calculation of* $B^0 \to K^{*0}\mu^+\mu^-$ *and* $B_s^0 \to \phi\mu^+\mu^-$ *observables using form factors from lattice QCD*, *Phys. Rev. Lett.* **112** (2014) 212003, arXiv:1310.3887 [hep-ph].

[10] B. Grinstein and D. Pirjol, *Exclusive rare* $B \to K^*\ell^+\ell^-$ *decays at low recoil: Controlling the long-distance effects*, *Phys. Rev.* **D70** (2004) 114005, arXiv:hep-ph/0404250 [hep-ph].

[11] C. Bobeth, G. Hiller, and D. van Dyk, *The Benefits of* $\bar{B}- > \bar{K}^* l^+ l^-$ *Decays at Low Recoil*, *JHEP* **07** (2010) 098, arXiv:1006.5013 [hep-ph].

[12] A. Karan, R. Mandal, A. K. Nayak, R. Sinha, and T. E. Browder, *Signal of right-handed currents using* $B \to K^*\ell^+\ell^-$ *observables at the kinematic endpoint*, *Phys. Rev.* **D95** no. 11, (2017) 114006, arXiv:1603.04355 [hep-ph].

[13] G. Hiller and R. Zwicky, *(A)symmetries of weak decays at and near the kinematic endpoint*, *JHEP* **03** (2014) 042, arXiv:1312.1923 [hep-ph].

[14] **LHCb** Collaboration, R. Aaij *et al.*, *Test of lepton universality using* $B^+ \to K^+\ell^+\ell^-$ *decays*, *Phys. Rev. Lett.* **113** (2014) 151601, arXiv:1406.6482 [hep-ex].

[15] **LHCb** Collaboration, R. Aaij *et al.*, *Test of lepton universality with* $B^0 \to K^{*0}\ell^+\ell^-$ *decays*, arXiv:1705.05802 [hep-ex].

[16] Y. Amhis *et al.*, *Averages of b-hadron, c-hadron, and* τ*-lepton properties as of summer 2016*, arXiv:1612.07233 [hep-ex].

[17] D. Choudhury, A. Kundu, R. Mandal, and R. Sinha, *Minimal unified resolution to $R_{K^{(*)}}$ and $R(D^{(*)})$ anomalies with lepton mixing*, arXiv:1706.08437 [hep-ph].

[18] **BaBar** Collaboration, J. P. Lees *et al.*, *Measurement of an Excess of $\bar{B} \to D^{(*)}\tau^-\bar{\nu}_\tau$ Decays and Implications for Charged Higgs Bosons*, *Phys. Rev.* **D88** no. 7, (2013) 072012, arXiv:1303.0571 [hep-ex].

[19] **Belle** Collaboration, M. Huschle *et al.*, *Measurement of the branching ratio of $\bar{B} \to D^{(*)}\tau^-\bar{\nu}_\tau$ relative to $\bar{B} \to D^{(*)}\ell^-\bar{\nu}_\ell$ decays with hadronic tagging at Belle*, *Phys. Rev.* **D92** no. 7, (2015) 072014, arXiv:1507.03233 [hep-ex].

[20] **Belle** Collaboration, A. Abdesselam *et al.*, *Measurement of the branching ratio of $\bar{B}^0 \to D^{*+}\tau^-\bar{\nu}_\tau$ relative to $\bar{B}^0 \to D^{*+}\ell^-\bar{\nu}_\ell$ decays with a semileptonic tagging method*, in *Proceedings, 51st Rencontres de Moriond on Electroweak Interactions and Unified Theories: La Thuile, Italy, March 12-19, 2016*. 2016. arXiv:1603.06711 [hep-ex]. https://inspirehep.net/record/1431982/files/arXiv:1603.06711.pdf.

[21] **LHCb** Collaboration, R. Aaij *et al.*, *Measurement of the ratio of branching fractions $\mathcal{B}(\bar{B}^0 \to D^{*+}\tau^-\bar{\nu}_\tau)/\mathcal{B}(\bar{B}^0 \to D^{*+}\mu^-\bar{\nu}_\mu)$*, *Phys. Rev. Lett.* **115** no. 11, (2015) 111803, arXiv:1506.08614 [hep-ex]. [Erratum: Phys. Rev. Lett.115,no.15,159901(2015)].

[22] Y. Nir, *Flavor Physics*, *Lectures given at "GGI lectures on the theory of fundamental interactions 2016* .

[23] Y. Grossman, *Just a Taste: Lectures on Flavor Physics*, .

[24] B. Grinstein, *TASI-2013 Lectures on Flavor Physics*, in *Theoretical Advanced Study Institute in Elementary Particle Physics: Particle Physics: The Higgs Boson and Beyond (TASI 2013) Boulder, Colorado, June 3-28, 2013*. 2015. arXiv:1501.05283 [hep-ph]. https://inspirehep.net/record/1340469/files/arXiv:1501.05283.pdf.

[25] Z. Ligeti, *TASI Lectures on Flavor Physics*, in *Proceedings, Theoretical Advanced Study Institute in Elementary Particle Physics: Journeys Through the Precision Frontier: Amplitudes for Colliders (TASI 2014): Boulder, Colorado, June 2-27, 2014*, pp. 297–340. 2015. arXiv:1502.01372 [hep-ph]. https://inspirehep.net/record/1343118/files/arXiv:1502.01372.pdf.

[26] S. J. Lee and H. SerÃť dio, *A Short Guide to Flavour Physics and CP Violation*, arXiv:1504.07549 [hep-ph].

[27] D. Das and R. Sinha, *New Physics Effects and Hadronic Form Factor Uncertainties in $B \to K^* \ell^+ \ell^-$*, *Phys. Rev.* **D86** (2012) 056006, arXiv:1205.1438 [hep-ph].

[28] R. Sinha, *CP violation in B mesons using Dalitz plot asymmetries*, arXiv:hep-ph/9608314 [hep-ph].

[29] C. Bobeth, M. Misiak, and J. Urban, *Photonic penguins at two loops and m_t dependence of $BR[B \to X_s l^+ l^-]$*, *Nucl. Phys.* **B574** (2000) 291–330, arXiv:hep-ph/9910220 [hep-ph].

[30] W. Altmannshofer, P. Ball, A. Bharucha, A. J. Buras, D. M. Straub, and M. Wick, *Symmetries and Asymmetries of $B \to K^* \mu^+ \mu^-$ Decays in the Standard Model and Beyond*, *JHEP* **01** (2009) 019, arXiv:0811.1214 [hep-ph].

[31] G. Buchalla, A. J. Buras, and M. E. Lautenbacher, *Weak decays beyond leading logarithms*, *Rev. Mod. Phys.* **68** (1996) 1125–1144, arXiv:hep-ph/9512380 [hep-ph].

[32] T. Hurth and M. Nakao, *Radiative and Electroweak Penguin Decays of B Mesons*, *Ann. Rev. Nucl. Part. Sci.* **60** (2010) 645–677, arXiv:1005.1224 [hep-ph].

[33] A. J. Buras, *Climbing NLO and NNLO Summits of Weak Decays*, arXiv:1102.5650 [hep-ph].

[34] A. J. Buras and M. Munz, *Effective Hamiltonian for B —> X(s) e+ e- beyond leading logarithms in the NDR and HV schemes*, *Phys. Rev.* **D52** (1995) 186–195, arXiv:hep-ph/9501281 [hep-ph].

[35] P. Ball and V. M. Braun, *Exclusive semileptonic and rare B meson decays in QCD*, *Phys. Rev.* **D58** (1998) 094016, arXiv:hep-ph/9805422 [hep-ph].

[36] P. Ball and R. Zwicky, $B_{d,s} \to \rho, \omega, K^*, \phi$ *decay form-factors from light-cone sum rules revisited*, *Phys. Rev.* **D71** (2005) 014029, arXiv:hep-ph/0412079 [hep-ph].

[37] **LHCb** Collaboration, R. Aaij *et al.*, *Observation of a resonance in* $B^+ \to K^+\mu^+\mu^-$ *decays at low recoil*, *Phys. Rev. Lett.* **111** no. 11, (2013) 112003, arXiv:1307.7595 [hep-ex].

[38] J. Lyon and R. Zwicky, *Resonances gone topsy turvy - the charm of QCD or new physics in* $b \to s\ell^+\ell^-$*?*, arXiv:1406.0566 [hep-ph].

[39] B. Grinstein, M. J. Savage, and M. B. Wise, *B —> X(s) e+ e- in the Six Quark Model*, *Nucl. Phys.* **B319** (1989) 271–290.

[40] M. Beneke and T. Feldmann, *Symmetry breaking corrections to heavy to light B meson form-factors at large recoil*, *Nucl. Phys.* **B592** (2001) 3–34, arXiv:hep-ph/0008255 [hep-ph].

[41] **LHCb** Collaboration, R. Aaij *et al.*, *Differential branching fraction and angular analysis of the decay* $B^0 \to K^{*0}\mu^+\mu^-$, *JHEP* **08** (2013) 131, arXiv:1304.6325 [hep-ex].

[42] **LHCb** Collaboration, R. Aaij *et al.*, *Differential branching fraction and angular analysis of the decay* $B^0 \to K^{*0}\mu^+\mu^-$, *Phys. Rev. Lett.* **108** (2012) 181806, arXiv:1112.3515 [hep-ex].

[43] **BaBar** Collaboration, B. Aubert *et al.*, *Measurements of branching fractions, rate asymmetries, and angular distributions in the rare decays $B \to K\ell^+\ell^-$ and $B \to K^*\ell^+\ell^-$*, *Phys. Rev.* **D73** (2006) 092001, arXiv:hep-ex/0604007 [hep-ex].

[44] **CMS** Collaboration, S. Chatrchyan *et al.*, *Angular analysis and branching fraction measurement of the decay $B^0 \to K^{*0}\mu^+\mu^-$*, *Phys. Lett.* **B727** (2013) 77–100, arXiv:1308.3409 [hep-ex].

[45] **CDF** Collaboration, T. Aaltonen *et al.*, *Observation of the Baryonic Flavor-Changing Neutral Current Decay $\Lambda_b \to \Lambda\mu^+\mu^-$*, *Phys. Rev. Lett.* **107** (2011) 201802, arXiv:1107.3753 [hep-ex].

[46] **CDF** Collaboration, T. Aaltonen *et al.*, *Measurements of the Angular Distributions in the Decays $B \to K^{(*)}\mu^+\mu^-$ at CDF*, *Phys. Rev. Lett.* **108** (2012) 081807, arXiv:1108.0695 [hep-ex].

[47] N. Isgur and M. B. Wise, *Weak Decays of Heavy Mesons in the Static Quark Approximation*, *Phys. Lett.* **B232** (1989) 113–117.

[48] N. Isgur and M. B. Wise, *WEAK TRANSITION FORM-FACTORS BETWEEN HEAVY MESONS*, *Phys. Lett.* **B237** (1990) 527–530.

[49] J. Charles, A. Le Yaouanc, L. Oliver, O. Pene, and J. C. Raynal, *Heavy to light form-factors in the heavy mass to large energy limit of QCD*, *Phys. Rev.* **D60** (1999) 014001, arXiv:hep-ph/9812358 [hep-ph].

[50] *Details of the routine can be found at*, . http://reference.wolfram.com/language/ref/DistributionFitTest.html.

[51] A. Kolmogorov, *Sulla determinazione empirica di una legge di distribuzione*, *G. Ist. Ital. Attuari. 4: 83-91 1933* .

[52] N. Smirnov, *Table for estimating the goodness of fit of empirical distributions*, *Ann. Math. Statist.* **19** no. 2, (06, 1948) 279–281. https://doi.org/10.1214/aoms/1177730256.

[53] C. Hambrock and G. Hiller, *Extracting $B \to K^*$ Form Factors from Data*, *Phys. Rev. Lett.* **109** (2012) 091802, arXiv:1204.4444 [hep-ph].

[54] S. Descotes-Genon, L. Hofer, J. Matias, and J. Virto, *On the impact of power corrections in the prediction of $B \to K^* \mu^+ \mu^-$ observables*, *JHEP* **12** (2014) 125, arXiv:1407.8526 [hep-ph].

[55] N. G. Deshpande, J. Trampetic, and K. Panose, *Resonance Background to the Decays $b \to s l^+ l^-$, $B \to K^* l^+ l^-$ and $B \to K l^+ l^-$*, *Phys. Rev.* **D39** (1989) 1461.

[56] S. Descotes-Genon, J. Matias, M. Ramon, and J. Virto, *Implications from clean observables for the binned analysis of $B- > K* \mu^+ \mu^-$ at large recoil*, *JHEP* **01** (2013) 048, arXiv:1207.2753 [hep-ph].

[57] **LHCb** Collaboration, R. Aaij *et al.*, *Measurement of Form-Factor-Independent Observables in the Decay $B^0 \to K^{*0} \mu^+ \mu^-$*, *Phys. Rev. Lett.* **111** (2013) 191801, arXiv:1308.1707 [hep-ex].

[58] S. Descotes-Genon, L. Hofer, J. Matias, and J. Virto, *Global analysis of $b \to s\ell\ell$ anomalies*, *JHEP* **06** (2016) 092, arXiv:1510.04239 [hep-ph].

[59] **Belle** Collaboration, S. Hirose *et al.*, *Measurement of the τ lepton polarization and $R(D^*)$ in the decay $\bar{B} \to D^* \tau^- \bar{\nu}_\tau$*, *Phys. Rev. Lett.* **118** no. 21, (2017) 211801, arXiv:1612.00529 [hep-ex].

[60] D. Choudhury, A. Kundu, S. Nandi, and S. K. Patra, *Unified resolution of the $R(D)$ and $R(D^*)$ anomalies and the lepton flavor violating decay $h \to \mu\tau$*, *Phys. Rev.* **D95** no. 3, (2017) 035021, arXiv:1612.03517 [hep-ph].

[61] **HPQCD** Collaboration, H. Na, C. M. Bouchard, G. P. Lepage, C. Monahan, and J. Shigemitsu, *$B \to Dlv$ form factors at nonzero recoil and extraction of $|V_{cb}|$*, *Phys. Rev.* **D92** no. 5, (2015) 054510, arXiv:1505.03925 [hep-lat]. [Erratum: Phys. Rev.D93,no.11,119906(2016)].

[62] J. F. Kamenik and F. Mescia, *$B \to D\tau\nu$ Branching Ratios: Opportunity for Lattice QCD and Hadron Colliders*, *Phys. Rev.* **D78** (2008) 014003, arXiv:0802.3790 [hep-ph].

[63] http://www.slac.stanford.edu/xorg/hflav/semi/fpcp17/RDRDs.html.

[64] G. Hiller and F. Kruger, *More model-independent analysis of $b \to s$ processes*, *Phys. Rev.* **D69** (2004) 074020, arXiv:hep-ph/0310219 [hep-ph].

[65] M. Bordone, G. Isidori, and A. Pattori, *On the Standard Model predictions for R_K and R_{K^*}*, *Eur. Phys. J.* **C76** no. 8, (2016) 440, arXiv:1605.07633 [hep-ph].

[66] **LHCb** Collaboration, R. Aaij *et al.*, *Angular analysis and differential branching fraction of the decay $B_s^0 \to \phi\mu^+\mu^-$*, *JHEP* **09** (2015) 179, arXiv:1506.08777 [hep-ex].

[67] W. Altmannshofer and D. M. Straub, *New physics in $b \to s$ transitions after LHC run 1*, *Eur. Phys. J.* **C75** no. 8, (2015) 382, arXiv:1411.3161 [hep-ph].

[68] **LHCb** Collaboration, R. Aaij *et al.*, *Measurement of the $B_s^0 \to \mu^+\mu^-$ branching fraction and effective lifetime and search for $B^0 \to \mu^+\mu^-$ decays*, *Phys. Rev. Lett.* **118** no. 19, (2017) 191801, arXiv:1703.05747 [hep-ex].

[69] C. Bobeth, M. Gorbahn, T. Hermann, M. Misiak, E. Stamou, and M. Steinhauser, *$B_{s,d} \to l^+l^-$ in the Standard Model with Reduced Theoretical Uncertainty*, *Phys. Rev. Lett.* **112** (2014) 101801, arXiv:1311.0903 [hep-ph].

[70] R. Fleischer, *Probing new physics with $B_s^0 \to \mu^+\mu^-$: Status and perspectives*, *Int. J. Mod. Phys.* **A29** (2014) 1444004, arXiv:1407.0916 [hep-ph].

[71] **Belle** Collaboration, J. Grygier *et al.*, *Search for $B \to h\nu\bar{\nu}$ decays with semileptonic tagging at Belle*, arXiv:1702.03224 [hep-ex].

[72] A. J. Buras, J. Girrbach-Noe, C. Niehoff, and D. M. Straub, *$B \to K^{(*)}\nu\bar{\nu}$ decays in the Standard Model and beyond*, *JHEP* **02** (2015) 184, arXiv:1409.4557 [hep-ph].

[73] **LHCb** Collaboration, R. Aaij *et al.*, *Search for the decays $B_s^0 \to \tau^+\tau^-$ and $B^0 \to \tau^+\tau^-$*, *Phys. Rev. Lett.* **118** no. 25, (2017) 251802, arXiv:1703.02508 [hep-ex].

[74] **Particle Data Group** Collaboration, C. Patrignani *et al.*, *Review of Particle Physics*, *Chin. Phys.* **C40** no. 10, (2016) 100001.

[75] M. Misiak and J. Urban, *QCD corrections to FCNC decays mediated by Z penguins and W boxes*, *Phys. Lett.* **B451** (1999) 161–169, arXiv:hep-ph/9901278 [hep-ph].

[76] G. Buchalla and A. J. Buras, *The rare decays $K \to \pi\nu\bar{\nu}$, $B \to X\nu\bar{\nu}$ and $B \to l^+l^-$: An Update*, *Nucl. Phys.* **B548** (1999) 309–327, arXiv:hep-ph/9901288 [hep-ph].

[77] J. Brod, M. Gorbahn, and E. Stamou, *Two-Loop Electroweak Corrections for the $K \to \pi\nu\bar{\nu}$ Decays*, *Phys. Rev.* **D83** (2011) 034030, arXiv:1009.0947 [hep-ph].

[78] S. L. Glashow, D. Guadagnoli, and K. Lane, *Lepton Flavor Violation in B Decays?*, *Phys. Rev. Lett.* **114** (2015) 091801, arXiv:1411.0565 [hep-ph].

[79] A. Crivellin, D. Müller, and T. Ota, *Simultaneous explanation of $R(D^{(*)})$ and $b \to s\mu^+\mu^-$: the last scalar leptoquarks standing*, *JHEP* **09** (2017) 040, arXiv:1703.09226 [hep-ph].

[80] F. Feruglio, P. Paradisi, and A. Pattori, *On the Importance of Electroweak Corrections for B Anomalies*, *JHEP* **09** (2017) 061, arXiv:1705.00929 [hep-ph].

[81] F. Beaujean, M. Chrzaszcz, N. Serra, and D. van Dyk, *Extracting Angular Observables without a Likelihood and Applications to Rare Decays*, *Phys. Rev.* **D91** no. 11, (2015) 114012, arXiv:1503.04100 [hep-ex].